UNIVERSITÉ DU QUÉBEC

INRS- ÉNERGIE, MATÉRIAUX ET TÉLÉCOMMUNICATIONS

Measurement of the pulsatile ocular dynamics of the human eye for glaucoma diagnosis

par

Kanwarpal Singh

Thèse présentée

pour l'obtention

du grade de Philosophiæ Doctor (Ph.D.)

en Sciences de l'Énergie et des Matériaux

Jury d'évaluation

Président du jury Et examinateur interne	Dr. François Légaré, INRS-EMT
Examinateur externe	Dr. Caroline Boudoux (École Polytechnique de Montréal)
	Dr. Pierre Blondeau (Université de Sherbrooke)
Directeur de recherche	Dr. Tsuneyuki Ozaki, INRS-EMT
Codirecteur de recherche	Dr. Mark Lesk, (Université de Montréal)
	Dr. Santiago Costantino (Université de Montréal)

i

Abstract

The objective of this thesis work is to design a non-invasive diagnostic instrument to study the biomechanical properties of the eye and test the potential of this instrument for the early diagnosis of glaucoma.

Glaucoma is an eye disease in which the vision loss is permanent. The present diagnostic methods are unable to detect glaucoma in its initial stages. It commonly takes several years following the onset of the disease in order to identify people with glaucoma. A new diagnostic instrument that could detect glaucoma at its onset is highly desirable. It has been shown in numerous studies that pulsatile ocular blood flow plays a major role in glaucoma. The ocular blood flow drives the mechanical pulsations of the eye. As both ocular blood flow and ocular biomechanics are altered in glaucoma, it can be assumed that the mechanical pulsations driven by ocular blood flow would also be altered. A device capable of measuring such pulsations could potentially be used as a new diagnostic tool for glaucoma.

In previous works, the pulsatility of the eye has been measured using tonometer-based technologies, which measure the variations in the intra ocular pressure at the cornea. These instruments do not measure mechanical displacement of ocular tissues. Furthermore, most of the tonometer-based technologies have to make contact with the eye in order to perform such measurements. As contact techniques are not preferred for the reasons such as infection and damage to the eye, technologies that require no contact with the eye were sought. Technologies such as ultrasonic transducers, laser interferometry and low-coherence interferometry have been used to measure one or the other aspect of the ocular pulsations. Ultrasonic transducers were shown to measure the corneal axial displacements, but could not be applied to measure the pulsations of the interior ocular tissues, such as the retina. In glaucoma it could be more interesting to measure the pulsatility of the retina rather than that of the cornea. Therefore

technologies such as laser interferometry and low coherence interferometry have been applied by some research groups.

In this thesis work, a device based on Fourier-domain low-coherence interferometry was developed. The device was first tested on live animals, such as rabbits and rats, and then further tested on human subjects recruited at the Research Center of the Hospital Maisonneuve-Rosemont. The developed device could measure simultaneously the pulsations of the cornea and the retina. In the later part of the thesis work, a comparative study between glaucoma and non-glaucoma subject was performed.

The results obtained suggest that the pulsations of the ocular tissues, such as the cornea and the retina, are larger in patients with glaucoma compared to normal subjects. The developed device provides for the first time an opportunity to study the pulsations of the cornea and the retina simultaneously and at video rate, with a displacement resolution as small as 400 nm. This allows the researchers and the clinicians to measure the biomechanical properties of the eye and study their role in glaucoma.

_____   _____

Student (Kanwarpal Singh)   Research Supervisor
                                      (Dr. Tsuneyuki Ozaki)

                                      _____

                                      Co-supervisor
                                      (Dr. Santiago Costantino)

                                      _____

                                      Co-supervisor
                                      (Dr. Mark Lesk)

Acknowledgement

This is an opportunity that I would not like to miss to thank all the people who have helped me during my thesis work. This work is a result of the collaboration between the INRS, MPB technologies and the Research Center of the Hospital Maisonneuve-Rosemont (HMR).

I would like to thank MPB technologies, which provided a heterodyne interferometer to test its potential in measuring the ocular dynamics. I am also thankful to the INRS, Fonds de recherche du Québec - Nature et technologies, Ministère de l'Éducation, du Loisir et du Sport and Fonds de la recherche en santé du Québec which at some point of my PhD studies, supported me financially.

I am highly obliged to the Research Center of the HMR, for providing its facilities to carry out my work. Marie-Josée and Julie at the animal research facility of the HMR were of great help during the animal experiments. The work with human subjects could not have been completed without the help of Dr. Denis Descovich, at HMR.

During the course of this work, Dr. Carolyne Dion (postdoctoral fellow) and Dr. Marcelo Wajszilber (Research associate) in our group, were constant helping hands and learning sources. They gave their expert input, from the start until the end of my PhD.

I would like to mention the support of my wife Gargi, who dared to be the first human subject, trusting me that the device is safe for her eyes. Whenever I had to test the developed system, she would happily volunteer to be a subject.

I am thankful to Dr. Leopold Schmetterer and his laboratory for extending their fullest support during my visit to Medical University of Vienna as a visiting student. Dr Schmetterer opened up all his facilities and expertise for me to learn.

My co-supervisor, Dr. Santiago Costantino has been a major source of inspiration for me. He was always a good critic and a source of improvisation in this work. My PhD would have never taken its present shape without him. Dr. Mark Lesk,

Table of figures

Table of Contents

Chapter 1

Hypothesis and objectives

1.1 Introduction

Glaucoma is the second largest cause of blindness after cataract, which is more prevalent in the older population. In Canada, more than 400,000 cases of glaucoma were reported by the year 2002, and this number is expected to increase in the coming years [1]. According to a recent study [2] there will be about 80 million people worldwide suffering from glaucoma.

In glaucoma, the optic nerve, which is responsible for carrying the vision from the eye to the brain, suffers permanent and irreversible damage. This damage can be observed as an increase in the central excavation of the optic disc, normally termed as cupping of the optic disc. Optic disc is the area at the back of the eye from where blood vessels enter and axons carrying the vision information leave the eye. One of the major difficulties with this disease is that most people who have glaucoma do not notice any symptoms until they begin to lose substantial segments of their visual field. From a clinical point of view, without years of

monitoring it is impossible to identify people with glaucoma who are in the initial stage of the disease. If glaucoma can be detected in the initial stages of its progression, then although the damage that has already been done cannot be reversed, its progression can be either stopped or slowed down. A good diagnosis method would allow clinicians to distinguish people whose eyesight is deteriorating faster from those with a more benign course. Consequently, more aggressive therapy and available treatments can be adopted for high-risk glaucoma patients, which in some cases can stabilize the progression of the diseases.

It was estimated [3] that the Canadian health system spent about 300 million Canadian dollars per year in direct cost related to glaucoma between 1990 and 2000. Driven by the country's aging population, incidences of glaucoma are soaring as baby boomers reach 50 and 60 years old. Therefore, a cost-effective method for the early detection of glaucoma would significantly help in reducing the cost needed for its treatment.

1.2 Anatomy of the human eye

Before going into the details of glaucoma, it is necessary to understand the basics of image formation and eye anatomy.

The eye is one of the most important organs of the human body, as we perceive the visual world with our eyes. The basic procedure of vision formation is outlined in Figure 1. When light falls on an object, it is scattered and reflected in all directions. Some of this light reaches the eye, where it encounters the first ocular element, which is the cornea. These light rays are refracted when they pass through the cornea, resulting from the corneal curvature as well as the difference in the refractive index between the cornea and air. These refracted rays are further refracted by the ocular lens to form an inverted image of the object on the retina, which is the tissue of the eye that senses light. The light received by the retina is

converted into the electrical signals by the cells present in the retina. These signals from the retina are then transferred to the brain via the optic nerve where they are interpreted as an image.
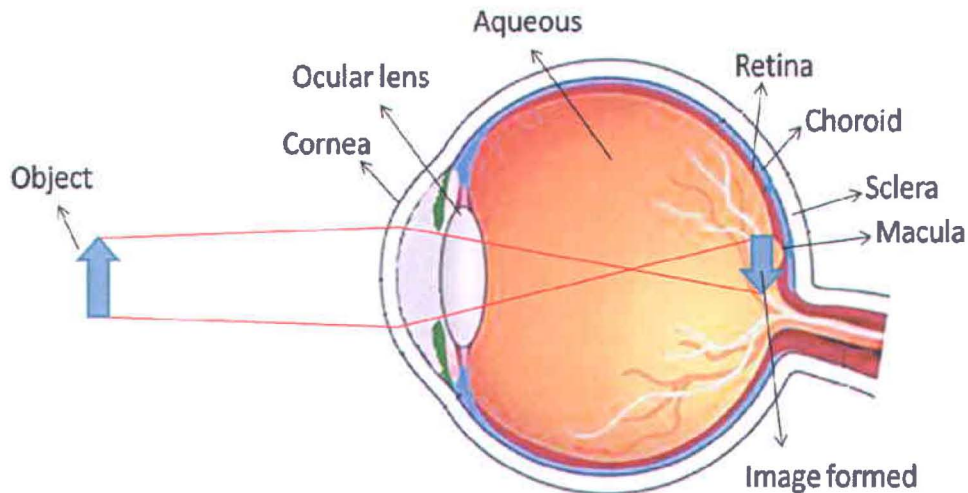
Figure 1. Basic ray diagram for image formation in the human eye. Image source: http://www.improve-vision-naturally.com

This is an extremely simplified version of image formation, but the actual procedure is highly complex. The function and structure of some of the common ocular elements is discussed further in more detail.

1.2.1 Cornea

Cornea is a transparent ocular tissue whose thickness varies between 450 to 650 μm. It is nearly spherical in shape with a radius of curvature of about 8 mm. Cornea absorbs light with wavelengths below 300 nm. Cornea is composed of different layers such as corneal epithelium, Bowman's layer, corneal stroma, Descemet's membrane and corneal endothelium.

The first layer of the cornea, the corneal epithelium is about 50 μm thick. The outer surface of the corneal epithelium is very smooth and secrete glycocalyx component that adjoins the tear film. The smooth surface of the corneal epithelium and presence of the tear film reduces the aberrations in the image formation that could have occurred due to the irregularities in the cornea surface. Under the corneal epithelium is the Bowman's layer, whose thickness varies from 8 to 14 μm in adult humans. Bowman's layer is made up of dense fibrous collagen, which makes it a relatively strong layer and resistant to the shearing, penetration and infection. It also helps the cornea in maintaining its shape.
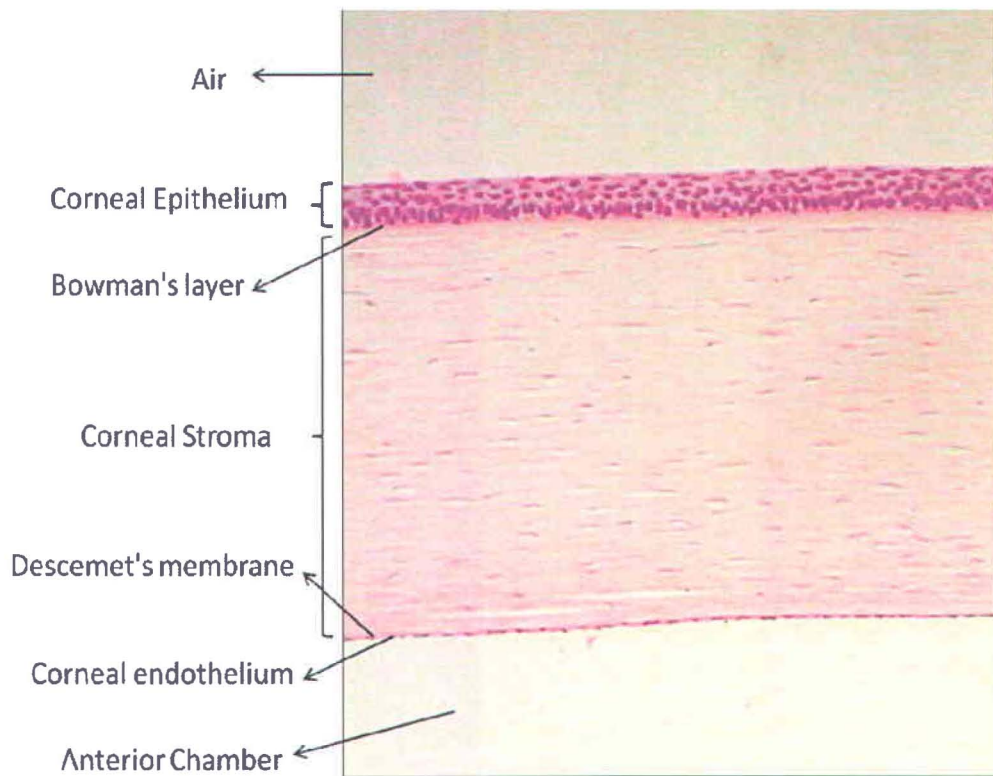
Figure 2. Corneal layers of the human eye.

The third layer of the cornea is the corneal stroma, which is also the thickest layer (approximately 500 μm) of the cornea. Corneal stroma is made up of plane sheets of collagen fibers called lamellae. About 200 to 300 lamellae are arranged parallel to each other to form the corneal stroma. The collagen fibers in each lamella are parallel to each other but at an angle in to the collagen fibers in the adjacent lamellae. This arrangement of the collagen fibers in the stroma helps to reduce the scattering of the light in the cornea.

Stroma is followed by Descemet's membrane, which is basically a basement membrane on which the endothelium cells grow. Its thickness can vary from 5 μm in children to approximately 15 μm in adults. The last layer of the cornea is corneal endothelium, which is about 5 μm thick. Corneal endothelium is a single cell layer. It is responsible for intake of the nutrients from the aqueous humor to nourish the cornea. It also regulates the hydration level of the cornea by removing the excessive water.

Cornea gives the eye its highest refractive or focusing power [4]. The total focusing power of the eye is about 60 to 65 diopters, out of which, corneal focusing power accounts for about 43 to 48 diopter. Light from the object received by the eye is refracted because of the corneal curvature and the difference in the refractive index of the tear film at the cornea and it's surrounding. The first refraction of the light occurs at the interface between the cornea and the air, which have a refractive index (n) of approximately 1.376 and 1.000, respectively. The second refraction of the light occurs at the interface between the cornea and aqueous humor (n=1.336). Besides acting as a focusing element, the cornea also serves as a filter for ultraviolet radiation.

1.2.2 Anterior Chamber
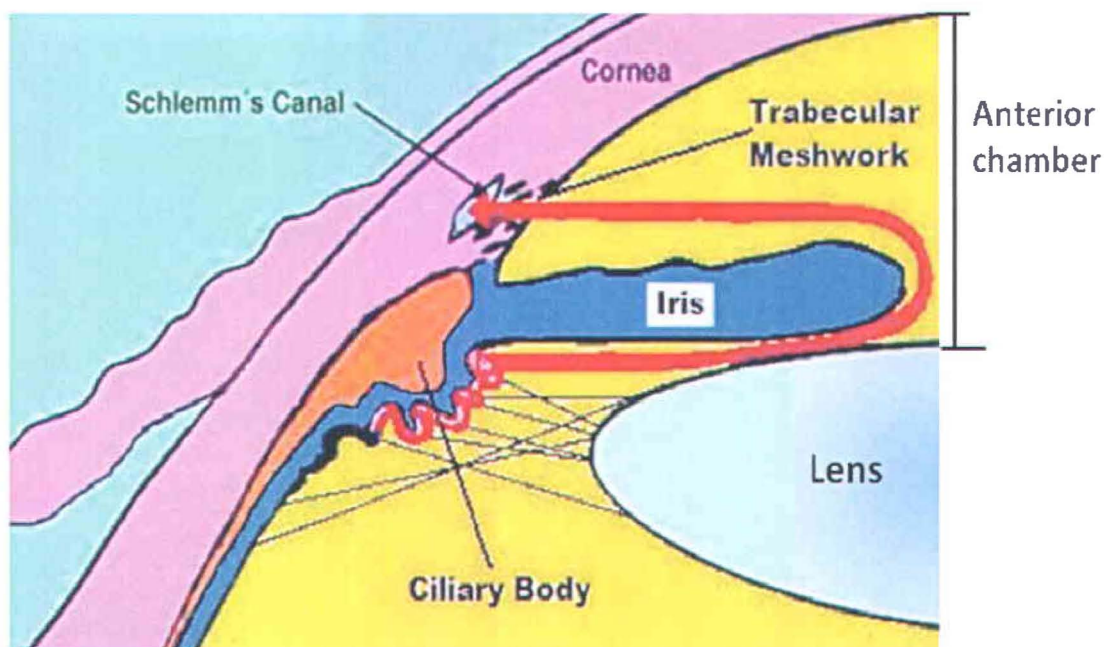
Figure 3. Flow of aqueous humor in the human eye. Image source:
http://nenaaragon.hubpages.com/hub/Open-Angle-Glaucoma

Below the cornea is the anterior chamber, a space between the corneal endothelium and the iris. The depth of the anterior chamber is approximately 3.1 mm in an adult human [5]. It is filled with a transparent liquid called aqueous humor. In order to maintain the shape of the eye, it is necessary that the pressure of the liquid inside the eye is more than the atmospheric pressure. The pressure inside the eye is maintained by the regulation of the aqueous humor, which is produced by the ciliary body. The flow of aqueous humor in the eye is depicted in Figure 3 by the red arrow. After being produced by the ciliary body, the aqueous humor flows between the iris and the ocular lens. It enters the anterior chamber through the opening of the iris called the pupil. Then, it leaves the anterior chamber through the trabecular meshwork into the Schlemm's canal.

1.2.3 Iris

After passing through the anterior chamber, light encounters the pupil, an opening in the iris that acts like a diaphragm for the light. The pupil controls the amount of light that enters the eye by changing its size. The size of the pupil in an adult human can change from 2 mm to 8 mm in diameter, depending on the condition of the light. In the presence of bright light, the size of the pupil reduces, whereas in dim light it increases, to allow more light to enter the eyes. The size of the pupil is controlled by the dilator and the sphincter muscle of the iris. We get the color of our eyes from the pigment present in the iris. This pigment is called melanin, which is produced by melanocytes, the melanin producing cells. The amount of melanin and its location in the iris defines the color of the eyes. For example, people with brown eyes have more melanin in their iris than the people with blue eyes.

1.2.4 Ocular lens

Below the iris is the ocular lens or the crystalline lens, which is an elastic structure with an oval shape. The ocular lens is attached to the ciliary body through zonule fibers. The anterior surface of the ocular lens has a radius of curvature of approximately 8 mm to 14 mm, whereas that for the posterior surface is approximately 5 mm to 8 mm. The central thickness of the ocular lens varies from 3.5 mm to 5 mm. In adults, the diameter of the ocular lens is approximately 9 mm.

The refractive index of the ocular lens has a gradient due to the change in the optical density from the surface to the center. The concentration of the proteins brings this change in the optical density, which increases from the surface to the center of the ocular lens. This variation in the refractive index gives additional refractive power to the ocular lens, besides the refractive power it gets from its shape.
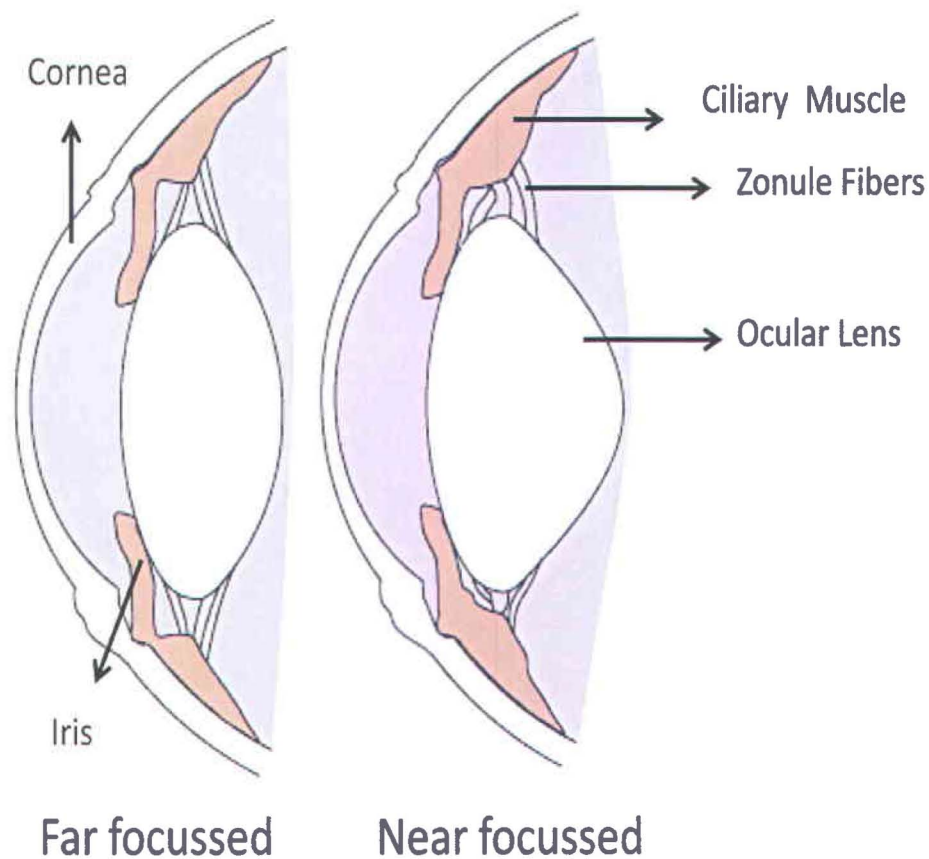
Figure 4. Accommodation of the ocular lens. Image source : http://healthy-ojas.com/eye/presbyopia.html

The ocular lens can take different shapes depending on the different focusing situations. The process of fine adjustment in the focusing properties of the ocular lens is termed as accommodation. If the ocular lens was left to take its own shape, then it would have close to a spherical shape. However, in order to focus the image of the object on to the retina, which is the light sensing tissue, the lens shape can be modified by regulating the tension on the zonule fibers through ciliary muscles. Under normal conditions, the zonule fibers are stretched, giving the lens a disc like structure to focus on the distant object. To focus on closer

8

objects, the ciliary muscle comes into action, which contracts to loosen the zonule fibers giving the lens its spherical shape (Figure 4).

The ocular lens absorbs the near ultra violet (NUV) wavelengths between 300 nm and 400 nm, and transmits the visible light spectrum. The absorption of NUV radiations by the ocular lens can cause damage to the lens proteins, increasing its opacity. NUV absorption can also lead to accumulation of yellow pigment in the center of the lens.

1.2.5 Retina

Light after being refracted by the ocular lens is focused on the retina. It is a very thin layer responsible for sensing the light. It is situated at the back of the eye between the choroid and the aqueous vitreous. Retina consists of different cell types that are arranged in a laminar structure inside the retina (Figure 5). The basic cell types found in the retina are photoreceptor cells, bipolar cells, horizontal cells, amacrine cells, muller cells and ganglion cells.

Photoreceptor cells are the light sensing cells in the retina. To reach the photoreceptors, light has to penetrate through the complete retinal thickness. This light is absorbed by the pigment in the photoreceptor cells. In a human eye, there are two types of photoreceptors; cones and rods, which derive their name due to their appearance. Cones are responsible for the color vision of the eye. A cone can have one of the three types of pigments, which are responsible for absorbing green, red or blue color of the visible light. Although the absorption spectra of the three different types of pigments found in cones overlap with each other, the maximum sensitivity for each color is different. The three types of cones have their maximum sensitivity at 420 nm (blue), 531 nm (green) and 588 nm (red). The rods have absorption spectral centered at 498 nm, which spreads over the whole visible range. This makes the rods insensitive to colors. Rods are particularly useful in low light vision.
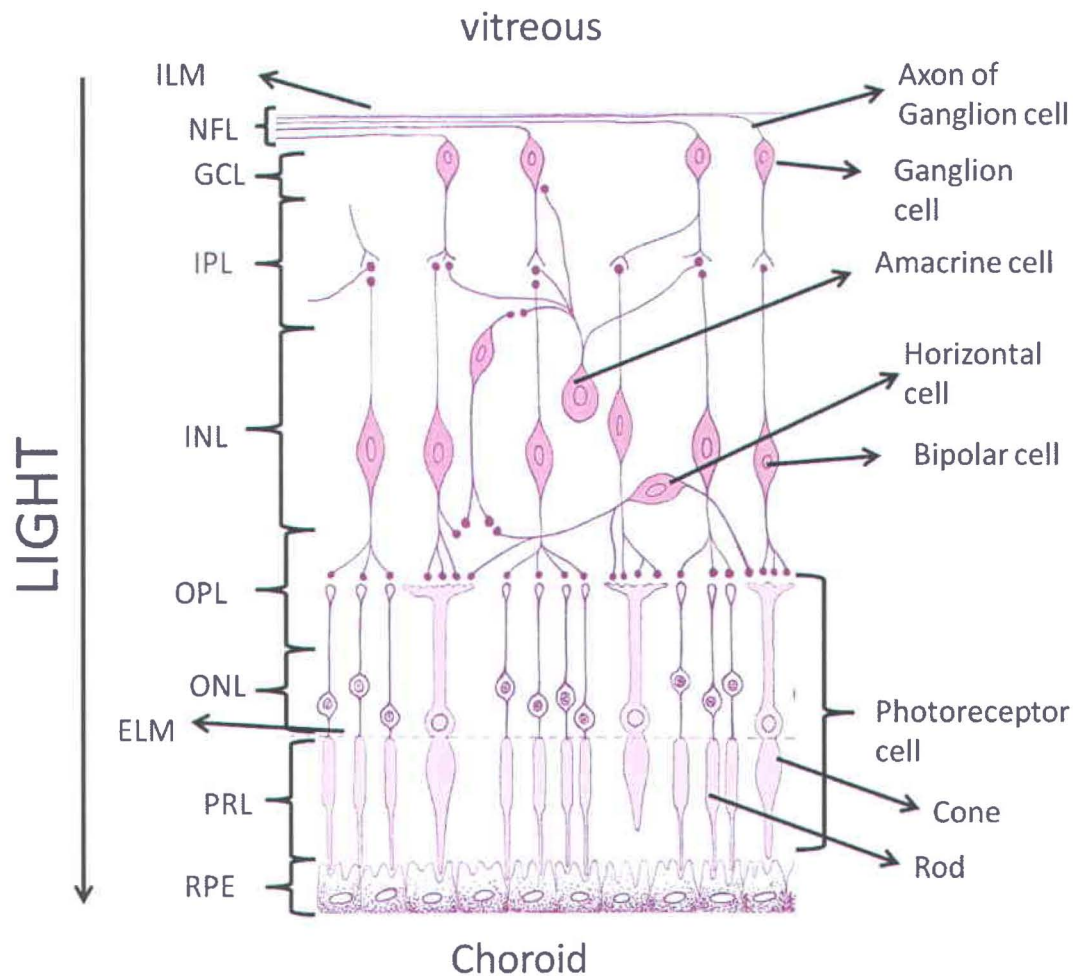
Figure 5. Schematic of the retina. Different layers of the retina are inner limiting membrane (ILM), nerve fiber layer (NFL), ganglion cell layer (GCL), inner plexiform layer (IPL), inner nuclear layer (INL), outer plexiform layer (OPL), outer nuclear layer (ONL), photo receptor layer (PRL) and retinal pigment epithelium (RPE). Image source : Reference [6]

The complete signal processing inside the retina is a highly complex phenomenon and only its basics are discussed further. The signal generated by the photoreceptor cells is regulated by the inflow and the outflow of sodium ions. In the absence of the light, there is a constant inflow of the sodium ions into the photoreceptor cells through ion channels. The ion channels are the protein-

10

assisted openings in the cell membrane that act as gates. These ion channels can be opened or closed through electrical or chemical stimulus. When the light photons are absorbed by the pigment in the photoreceptor cells, it initiates a chemical reaction that closes the ion channel, blocking the inflow of the sodium ions. This reduces the membrane potential of the photoreceptor cells, which in turn lead to decrease in the release of the neurotransmitters at the photoreceptor and bipolar cell junction.

The neurotransmitters released by the photoreceptor cell and received by bipolar cell can be inhibitory or exciter in action. When they are inhibitory, the reduction in the neurotransmitters released by the photoreceptor cell leads to an increase in the membrane potential of the bipolar cell. Due to increase in the bipolar cell membrane potential, neurotransmitters released at the bipolar cell and ganglion cell junction are increased.

The increased neurotransmitters that are received by the ganglion cells initiate an action potential in the axons of the ganglion cell. Action potential in a ganglion cell is a burst of voltage signal with maximum amplitude of approximately 40 mV that propagates along its axon. These bursts of voltage signals that leave the eye through the axons of the ganglion cells constitute the vision signals. There are some intermediate cells, such as horizontal and amacrine cells between the ganglion cells and photoreceptor cells, which help in the additional processing of the visual signals.

The axons of the ganglion cells carrying the vision signal leave the eye from a special opening called the optic disc. The bundle of the axons of the ganglion cells form the optic nerve, which carries the vision signal to the lateral geniculate nucleus of the brain. Optic nerve is considered a part of the central nervous system and an extension of the brain. After leaving the eye, the optic nerves from the two eyes meet at optic chiasm. It is the place where the axons from the nasal side of the two eyes cross over to the other side. The axons from the temporal side of one eye and the nasal side of the other eye form the optic tract which travel to

11

the visual cortex. Visual cortex is the place inside the brain where the electrical signals from the eye are interpreted as an image.
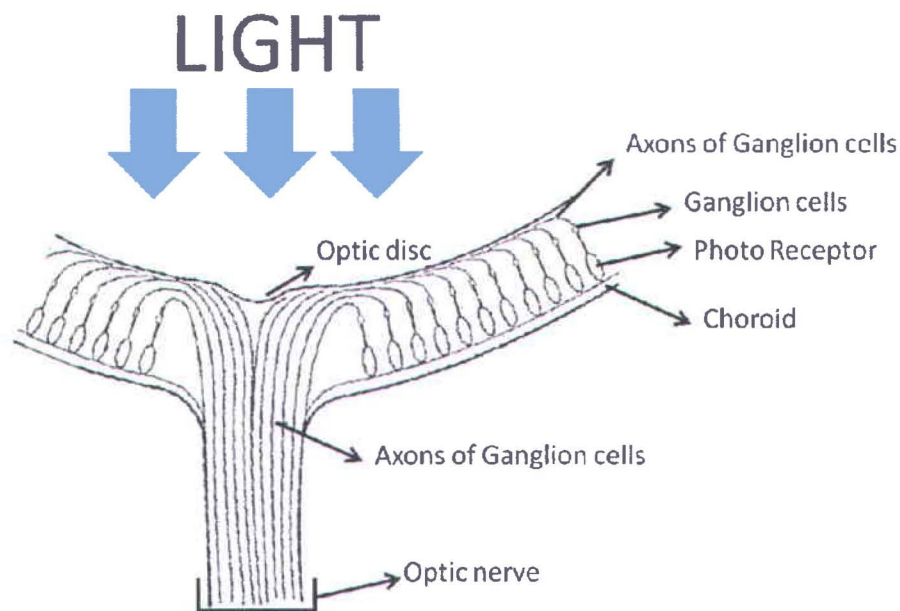
Figure 6. Sketch of the posterior eye.

1.3 Glaucoma

In glaucoma, the axons of the ganglion cells are damaged which appears as loss of NFL, thus inhibiting the vision signals to reach the brain and this kind of damage to the axons is irreversible. There are various risk factors that have been identified which might lead to glaucoma and out of these risk factors, increased intra ocular pressure (IOP) is the most widely accepted risk factor for glaucoma.

IOP is the pressure of the aqueous humor that fills the space between the cornea and the ocular lens. It is about 15 mmHg in the normal eye. A pressure higher than 21 mmHg is considered a significant risk factor that might lead to Glaucoma. Aqueous humor produced by the ciliary body enters the anterior chamber through

12

the pupil. This liquid then leaves the anterior chamber through the trabecular meshwork, which is a part of the eye's circulation system. Sometimes the pathways through which aqueous humor leaves the anterior chamber are blocked. Under these conditions the inflow of the aqueous humor is outbalanced by the outflow leading to increased pressure of the aqueous humor or the increased IOP. Although the pathophysiology of glaucoma is not fully understood, it is believed that the increased IOP exerts a force on the back of the eye. This force leads to damage of the axons of the ganglion cells, which destroys them over a period of time. Based on the anatomy and causes, glaucoma has been divided into sub categories. Some of these categories are listed in the next section.

1.3.1 Types of Glaucoma

Broadly, glaucoma can be categorized as primary open angle glaucoma (POAG), closed angle glaucoma (CAG), normal tension glaucoma (NTG), congenital glaucoma and secondary glaucoma.

Out of the above listed glaucoma categories, POAG [7] is the most common type of glaucoma. About 90 % of the glaucoma cases found in western countries belong to this category [2]. In POAG, the IOP increases over time with age. This kind of glaucoma is difficult to notice as the pressure increases over a long period of time and the vision loss initially occurs at the periphery of the retina. This vision loss is not noticed by the patients until they have already lost a substantial part of their vision. POAG derives its name from the fact that in this kind of glaucoma, the angle between the cornea and the iris is as wide as normal people. The exact cause of POAG is unknown, but it is believed to be related to the blockage of the aqueous humor drainage system, as shown in Figure 7. This can be caused by the improper functioning of the trabecular meshwork. In such cases, the aqueous humor, which is produced continuously, is not removed from the anterior chamber, leading to an increase in its pressure. Most therapies for POAG aim at reducing the IOP. These therapies cannot reverse the damage already done, but can slow down the progression. The IOP can be reduced through medication

13

or by laser trabeculoplasty. In laser trabeculoplasty, small burns are made in trabecular meshwork which increases the flow of the aqueous humor, thereby reducing IOP. People at greater risk of POAG include those with IOP larger than 21 mmHg, older than 40 years, family history of glaucoma.
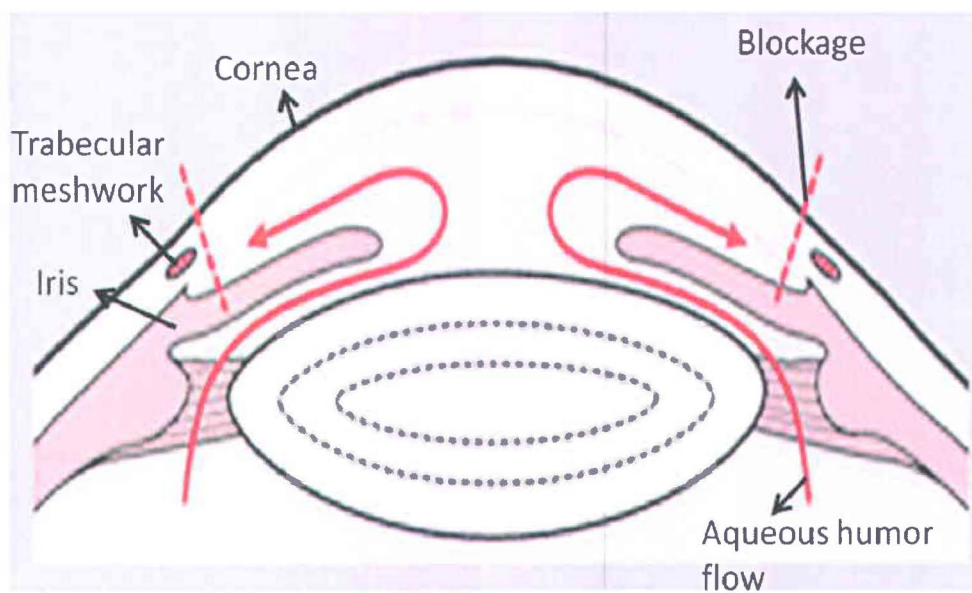
Figure 7. Primary open angle glaucoma showing the flow of aqueous humor which is blocked at the entry of the trabecular meshwork. Modified from Damjanov, 1996.

In CAG, the pressure of the eye increases suddenly over a relatively short period of time. The IOP increase can occur within few days or few weeks. Since the IOP increase is sudden, the symptoms of CAG are easily noticeable. This kind of glaucoma can have symptoms such as pain in the eye, headaches, halos around lights, dilated pupils, red eyes, nausea and vomiting. In CAG, the iris is pushed towards the cornea where it touches the trabecular meshwork. Due to the shifting of the iris, the angle between the cornea and the iris is reduced which gives it the name closed angle glaucoma. The contact between the iris and the trabecular meshwork blocks the drainage of the aqueous humor, leading to increased IOP. If the IOP is not reduced within few hours of its sudden increase, it may lead to a

permanent vision loss. The therapies adopted in CAG are usually similar to POAG and aim at reducing the IOP, but unlike POAG, theses therapies need to be more aggressive such as laser iridotomy in which a hole is drilled into the iris using a high power laser to allow for passage of aqueous humor.
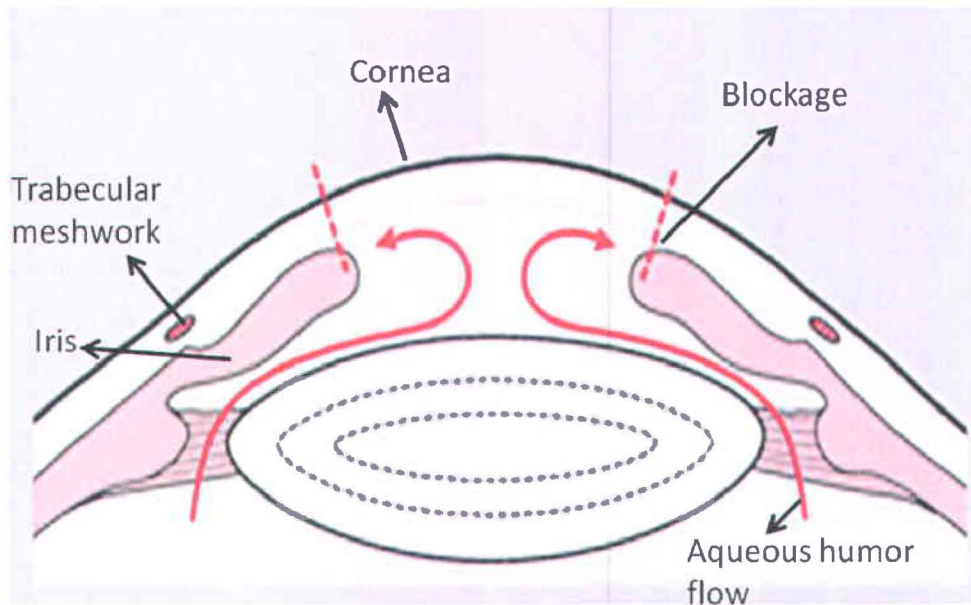
Figure 8. Closed angle glaucoma in which the iris is pushed against cornea, thereby blocking the drainage path of the aqueous humor. Modified from Damjanov, 1996.

Normal tension glaucoma is a special case of POAG where the IOP is statistically normal but still there is damage to the optic nerve. In patients with NTG, the IOP ranges between 10 mmHg to 21 mmHg, which is the normal range for IOP but still the eyes develop glaucoma. This damage can be seen as increased optic disk cupping and loss of nerve fiber layer. The cause of NTG is not yet understood, but recent studies suggest that it is related to irregularities in the ocular blood flow [8-10]. It is found that in NTG the blood supply to the optic nerve head is reduced, which might lead to ischemia, a situation where the oxygen supply to cells is reduced which leads to cell death. Although a less common case of glaucoma in

15

populations of European descent, NTG is dominant in Japanese populations and in Korea.

Congenital glaucoma is found in babies whose aqueous humor drainage system (trabecular meshwork) is not developed properly. This is usually characterized by large eye size and unclear hazy cornea. Although very rare, it can have serious affects on the child's vision. If detected in the early stage, congenital glaucoma can be treated to avoid complete vision loss.

There is another class of glaucoma called secondary glaucoma, in which the rise in IOP can be due to secondary reasons. For example it can be caused by reasons such as recent eye injury, medication, infection in the eye, diabetes or some other reason. Pigmentary glaucoma is one such kind of glaucoma in which pigmented granules released by the iris gets mixed with the aqueous humor. When these pigmented granules reach the trabecular meshwork, it causes a clog, preventing the outflow of the aqueous thus increasing the IOP. Phacomorphic glaucoma is another kind of secondary glaucoma in which the swelling of the ocular lens pushes the iris towards the anterior chamber, thereby closing the angle between the iris and the cornea leading to blockage of aqueous humor outflow.

For all types of glaucoma listed above, there is no single factor that can account for a particular type. There are several tests that need to be performed for detecting glaucoma. In the next section, some of the diagnostic techniques for glaucoma are discussed.

1.3.2 Diagnosis of Glaucoma

1.3.2.1 IOP measurement

Early glaucoma diagnosis is still a challenge for clinicians as there are no clearly defined indicators for early glaucoma. It is estimated that only half of the people who have glaucoma actually know that they have it since they do not notice the symptoms in early stage.

With current ongoing research, new possible risk factors for glaucoma are being identified. As a marker for glaucoma, earlier studies relied on increased intra ocular pressure, a condition called ocular hypertension. An IOP of greater than 21 mmHg is considered a significant risk factor for glaucoma [11]. Defining glaucoma with '21 mmHg' as a marker has some problems, as in NTG, the IOP is lower than 21 mmHg. Nevertheless, increased IOP still remains the most important risk factor for glaucoma.

IOP is measured by clinicians using a technique called tonometry. A tonometer is an instrument that measures the pressure of the liquid inside the eye. There are different variants of tonometers and can be classified as contact and non-contact tonometers.

In contact tonometry, like the Goldman tonometry, [12] which is considered as a gold standard for IOP measurement, the head of the tonometer is placed against the cornea to applanate or flatten certain area of the cornea. The IOP of the eye is measured from the pressure required to flatten the cornea. Measurements of IOP using these kinds of tonometers suffer from one drawback: the measured IOP is biased by corneal biomechanical properties including thickness. For example, the IOP of an eye with thin cornea would be underestimated, where as for thick cornea it would be overestimated [13, 14]. To circumvent this problem, a new technique called dynamic contour tonometry (DCT) [15] was introduced. In DCT, the head of the tonometer is a spherically concave shaped tip with radius of curvature of about 10 mm. At the center of the tip of the tonometer, a pressure sensor with area about 0.25 mm^2 is placed. The tonometer tip is placed on the cornea and a constant force is applied to the tip. This forces the corneal surface to touch and take the shape of the tonometer tip. Theoretically, when the contour or shape of the tip matches the shape of the cornea, the pressure on both sides of the cornea has to be equal. Thus the pressure at the pressure sensor of the tonometer tip gives an estimate of the IOP that is assumed to be less dependent on the corneal thickness and its rigidity [16].

17

In non-contact tonometry, air puffs combined with an optical system are used to measure the IOP. The optical system is made up of a light source and a detector. The air puff is used to flatten the cornea, which reflects the light from the light source. The detector receives the maximum light from the cornea when it is completely flattened. The pressure of the air required to flatten the cornea is used to calculate the IOP. In such kind of tonometers, since there is no contact with the eye, there are less chances of infection. Non-contact tonometers have been successfully applied in clinic and compared with Goldman tonometers [17, 18]. There are some variants of non-contact tonometers, such as Langham's pneumotonograph [19] that can measure the IOP variations continuously over a period of time. In Langham's pneumotonograph, a constant flow of air is used instead of air puffs to applanate the cornea. The backpressure of the air is used to measure the IOP and its variations over time. The variations in the IOP are termed as ocular pulse and have been studied in relation to glaucoma. As the IOP and its derivatives are not conclusive markers for glaucoma, other diagnostics tests are performed in parallel to verify this disease.

1.3.2.2 Optic nerve head anatomy

Structural changes to the optic nerve head (ONH) are important indicators of glaucoma. The damage to the ONH can be visualized directly by looking into the eye using an ophthalmoscope or some other imaging technique. Some of the techniques that are used to make photographs of the optic nerve head are optic disc photography [20], optical coherence tomography [21] and scanning laser ophthalmoscopy [22]. When the axons of the ganglion cells leave the eye through the optic disc, they form a cup-like structure. Even normal people usually have some cupping of the optic disc, but in glaucoma the ratio of the diameter of the cup to the diameter of the disc increases. A cup-to-disc ratio of about 1/3 and below is considered normal. An eye with a cup-to-disc ratio larger than 1/3 is considered suspicious for glaucoma [23, 24]. Doctors observe the cup-to-disc ratio over a period of time in order to monitor the progression of glaucoma. Progressive increase of cup-to-disc ratio is almost always an indicator of

glaucoma. However if there is only one visit and the cup-to-disc ratio is intermediate, then it is often hard to know if there is glaucoma. But an increase of cup-to-disc compared to the previous visit is usually diagnostic of glaucoma. The results based on structural changes of the optic nerve head needs careful analysis, as increased cup-to-disc ratio is not always an indicator of glaucoma [25].

1.3.2.3 Haemodynamic

The study of the haemodynamics of the eye is another area of research that is currently being explored for diagnosis of glaucoma [26, 27]. The blood supply to the eye termed as ocular blood flow (OBF) is pulsatile in nature and thus also called pulsatile ocular blood flow (POBF). The blood supply to the eye is responsible for the supply of oxygen and nutrients to various ocular tissues. OBF is also responsible for maintaining the temperature of the back of the eye [28], which is required for the proper functioning of the eye. Irregularities in blood flow can be over-perfusion, a condition of supply of more blood than required, or under-perfusion, a condition of supply of less blood, which can lead to cell death. The exact mechanism of the ganglion cell death due to irregularities in the ocular blood flow is not well understood yet. Some studies have related the ganglion cell death to apoptosis [29, 30], but the factors that lead to apoptosis are still unclear. Apoptosis is the phenomena by which a cell destroys itself, which sometimes is also called programmed cell death.

The OBF has been estimated by measuring the ocular pulse amplitude (OPA) of the eye. OPA is the difference between the minimum and the maximum IOP measured over a period of time and can be measured with standard tonometers, such as dynamic contour tonometer [13] and Langham's pneumotonograph [17]. In some studies, OPA has been found to be lower in patients with primary open angle glaucoma (POAG) [31], where as in other studies no statistically significant difference was found [32] between the two groups. However, in case of patients with normal tension glaucoma, a consistently lower OPA is observed as compared to the normal people [32-34].

Estimation of POBF through measurement of the ocular pulse amplitude is a topic of debate. Since this technology measures only a dependent parameter of the OBF and not the actual blood flow, the results might be biased due to other ocular properties such as corneal thickness and its rigidity. In order to overcome this limitation, attempts have been made to measure directly the blood flow inside the eye. In this direction the velocity of the blood flow was measured in patients with normal tension glaucoma using color Doppler imaging and found to be lower than normal subjects [35].

1.3.2.4 Perimetry

Perimetry [36] is another diagnostic technique for glaucoma. This is a conclusive diagnostic tool in glaucoma, as it directly measures the extent of the visual field and its light sensitivity in the patients. In a perimetry test the patient is asked to look at the center of a bowl shaped instrument that is illuminated at the center, and a light stimulus is moved to different locations in the visual field. The person is asked to press a button when he sees a light signal. To test the sensitivity of a particular location of the visual field, light stimulus of different intensities and different sizes is used. The input from the subject is recorded using a computer. This way a map of the visual field of the patient is generated. This is a common test, in the diagnosis of glaucoma and other ocular diseases. Specific patterns of visual field loss are diagnostic of glaucoma if they are corroborated by structural changes of the optic nerve head and retinal nerve fibre layer. The visual field is also used to monitor whether glaucoma has progressed in an individual.

As discussed above, a large portion of the studies has aimed at the measurement of the IOP or the blood flow in relation to glaucoma. The role of the biomechanical properties such as rigidity of the eye in glaucoma has not been investigated much. In the next section the role of biomechanical properties of the eye in glaucoma is discussed.

1.4 The Role of the biomechanical properties of the eye in glaucoma

Axons of the ganglion cells make the inner layer of the retina, which is called the nerve fiber layer. The nerve fiber layer from different locations of the retina converges at the optic disc to form the optic nerve head. These axons then exit the eye by passing through a specialized disc of sclera known as the lamina cribrosa, which is shown in Figure 9.

Figure 9 text labels:
- Fovea
- Lamina cribrosa
- Dural sheath
- Optic nerve
- Long posterior ciliary artery
- Short posterior ciliary arteries
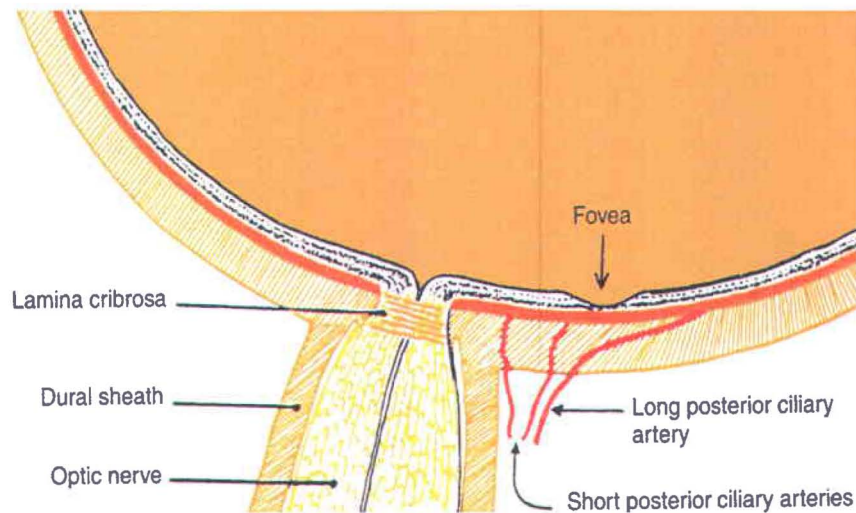
Figure 9. Posterior eye structure showing the lamina cribrosa.

The lamina cribrosa is a porous structure, which is part of the sclera that forms the outermost layer of the eye. The Lamina cribrosa is the site from where the axons leave the eye and the blood vessels enter the eye. These blood vessels are responsible for nourishing the optic nerve head and the retina. In glaucoma, the size of the optic disc cup increases and lamina cribrosa becomes more exposed at the base of the cup of the optic disc. Besides being a site for the exit of the axons and entry of the blood vessels, it also acts as a barrier between the intraocular forces such as IOP and extraocular tissues. Because of its porous structure, lamina

cribrosa has been viewed as a vulnerable site in glaucoma, but the role of the lamina cribrosa in glaucoma has been ambiguous.

Some studies suggest that in the initial stage of glaucoma the lamina cribrosa is less rigid, whereas in later or advanced stages of glaucoma it is more rigid. The rigidity of the lamina cribrosa has been studied, *ex vivo* in human [37] and monkey [38] eyes. The long term changes in the lamina cribrosa have also been studies *in vivo* in human [39, 40] and monkey eyes [41]. Although it has been postulated that a less rigid lamina cribrosa leads to development glaucoma, the exact mechanism between the progression of glaucoma and the rigidity of the lamina cribrosa is not known.

The rigidity of the lamina cribrosa can be estimated by studying its compliance with the intra ocular pressure [42]. For this, the change in the position of the lamina cribrosa with respect to the retinal surface is measured after changing the intra ocular pressure over a long period of time. The compliance of the lamina cribrosa can be studied using techniques like confocal scanning laser ophthalmoscopy (CSLO) [39]. Using CSLO, the height maps of the ocular area around the optic disc are generated. From these maps, parameters such as cup depth and cup-to-disk ratio are estimated. The parameter that is measured in glaucoma using CSLO is the mean cup depth, which is the mean distance between the base of the optic disc and the retinal surface. Some studies suggest that lamina cribrosa moves towards the retina (anteriorly) reducing the cup depth after the IOP is reduced [42, 43]. Lamina cribrosa is said to be more compliant if the change in the cup depth is larger as compared to other eyes for the same change in IOP. In one of the study [42] it was found that lamina cribrosa was more compliant in high-risk glaucoma patients than in low-risk glaucoma patients, thereby suggesting that the rigidity of the lamina cribrosa is different in different group of people. Thus, techniques such as the CSLO, indirectly study the compliance of the lamina cribrosa, but it takes months to collect data for such kind of measurements since the IOP must be changed by glaucoma therapy such as medications, laser or surgery.

22

As was discussed previously, ocular blood flow plays an important role in glaucoma. This makes the lamina cribrosa an important actor in glaucoma, since the micro blood vessels that nourish the optic nerve head enter the eye from this location. The blood vessels while passing through the lamina cribrosa are organized in parallel planes, which are parallel to the wall of the eye. This structure is depicted in Figure 10.
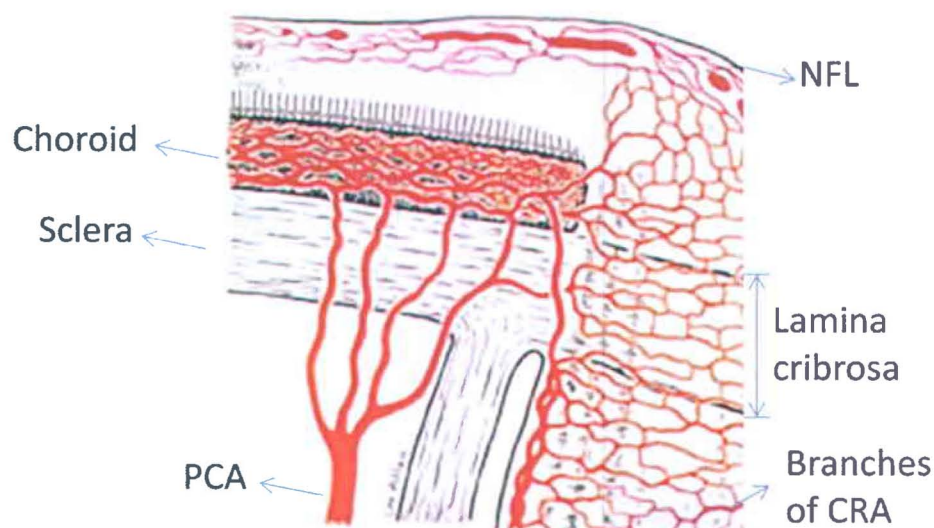
Figure 10. Blood supply to the optic nerve head and the retina. Abbreviations are nerve fiber layer (NFL), central retinal artery (CRA) and posterior ciliary artery (PCA).

During systole of the cardiac cycle, the lamina cribrosa is pushed backward [44], which suggests that the micro blood vessels would feel compression due to such movement. In fact, in a study [42] it was observed that there was a slight improvement in the optic nerve head blood flow upon reduction of the IOP. In patients whose eyes are more compliant or their lamina cribrosa less rigid, the micro blood vessels would be subjected to more compression. Considering the

23

role of blood flow in glaucoma and the role of the lamina cribrosa in blood flow, it becomes evident that biomechanical properties such as the rigidity of the lamina cribrosa could contribute to the progression of glaucoma.

In the above discussion, we have only considered the effect of long-term change of IOP on the displacement of the lamina cribrosa to estimate its biomechanical properties. From the previous work on the pulsatile ocular blood flow, it is known that the IOP of the eye is not a constant quantity; rather it is also pulsatile in nature. These pulsations in the IOP are caused by the pulsatile ocular blood flow driven by rhythmic cardiac pulsations. The choroid is a layer that is sandwiched between the sclera (the outer layer of the eye) and the retina. The blood volume inside the choroid is increased during systole, that is during the inflow of the blood. The choroid receives the highest amount of blood flow per gram of tissue in the human body. Due to the increased volume of the blood into the choroid, there is an expansion of the choroid that increases its thickness. During diastole, the blood leaves the eye reducing the blood volume in the choroid, which in turn brings the choroid back to its natural state. Thus, during systole and diastole the thickness of the choroid pulsates in synchrony with the cardiac cycle. During the expansion of the choroid, the retina being in front of it is also pushed anteriorly. Since the eye is filled with an incompressible liquid called aqueous humor, the pushing of the retina causes a pressure wave to propagate from the retina surface to the cornea surface. This wave is detected as change in the IOP measurement at the cornea surface.

This pulsating IOP, as measured with various tonometers, is found to be synchronous with the cardiac cycle. If a long-term change in IOP can displace the lamina cribrosa with reference to the retinal surface, then we cannot rule out the effect of the pulsatile change of IOP on the lamina cribrosa. Considering this fact, it is hypothesized in this thesis work that "*due to the pulsatile change in the IOP, the lamina cribrosa also pulsates synchronous with the cardiac cycle and these small displacements in the lamina cribrosa are contributing to the progression of glaucoma.*"

24

It is not only the alteration in the blood flow due to the pulsatile movement of the lamina cribrosa that might be contributing to the progression of glaucoma but there could be other mechanisms as well. Since lamina cribrosa and the peripapillary retina are supplied with blood by different arteries, there might be a delay between the axial movements of the two tissue areas. In this situation, there would be a pulsatile relative movement between the two tissues. Thus the axons of the ganglion cells being attached to the lamina cribrosa and the peripapillary retina would feel a pulsatile stretching over time due to such a relative movement. Hence, it is further hypothesized in this thesis work that *"there is a relative movement between the lamina cribrosa and the peripapillary retina during the cardiac cycle which causes a stretching into the axons of the ganglion cells and such a stretching might be causing damage to them leading to glaucoma."*

1.5 Objective

Although many studies have postulated the role of biomechanical properties of the eye and specifically of the lamina cribrosa in glaucoma, due to unavailability of clinical techniques, these properties have been investigated only partially, mostly in cadaver eyes and animal models. Furthermore, it is only the long-term changes in the lamina cribrosa topography that have been measured *in vivo*. The small displacements in the lamina cribrosa that are caused by the pulsatile ocular blood flow still remain uninvestigated.

The pulsatile nature of the eye was described by Silver *et al.* [45] as a result of an imbalance between pulsatile blood inflow and steady blood outflow into the elastic eye. Each bolus of blood entering the eye causes an increase in the volume of the contents of the globe with a consequent rise in intraocular pressure, and then a decrease in volume and pressure during the outflow process. This pulsatility also drives the displacement of the various ocular tissues. The amplitude of the movement necessarily depends on both the ocular

25

hemodynamics and on the eye's biomechanical properties. It is not yet known whether the pulsatile movements of the ocular tissues (such as the lamina cribrosa) could contribute to the pathophysiology of the glaucoma, but if they do, then their measurement could be used as an early diagnostic/prognostic test. Furthermore, as demonstrated by Hommer *et al*.[46], measurement of the pulsatile movement of the eye can be used to estimate the ocular volume change, and thus the ocular rigidity from the Friedenwald equation [47], which may lead to insights on the pathophysiology of glaucoma.

As it is believed that increased IOP leads to glaucoma through compression of the lamina cribrosa, the small movements of the lamina cribrosa could also play a role, first, by altering the blood flow to the eye and secondly by contributing to the stretching of the axons. These small movements of the lamina cribrosa can potentially be more damaging, as these movements occur about 86,000 times per day.

In order to measure the small movements of ocular tissues, such as lamina cribrosa, a new device is required. *The objective of this thesis is to develop such a device and to test its performance in human subjects as a potential glaucoma diagnostic tool.* It is required from the device that it should be able to measure the movement of ocular tissues with an accuracy of approximately 1 μm. The device should also be able to precisely locate the position of the measurement so that movements of the different regions of the retina can be made. Above all, it will be highly desirable that this device is non-invasive.

Keeping these requirements in the mind, a non-invasive optical device based on Fourier-domain low-coherence interferometry was developed. The developed system is capable of measuring the movements of the cornea and the retina simultaneously, with an axial resolution of approximately 400 nm.

Further in this thesis, some of the previous works related to the measurement of ocular tissue movements, technique used in this thesis work and the results obtained are discussed.

26

Chapter 2

Techniques to measure the ocular distances

2.1 Introduction

Various techniques for measuring pulsatile ocular movements have been reported in the literature. Application of techniques such as ultrasound transducers [48], laser and low-coherence interferometry [49-52] and spectral domain optical coherence tomography (SD-OCT) [53] have been demonstrated. The details of these techniques are discussed further briefly.

2.2 Ultrasound transducers

The use of ultrasound transducers for measuring the ocular tissue dynamics was first demonstrated by Zuckerman *et al.* [48] in 1977. Since then, ultrasound transducers have been used by various groups to study corneal dynamics [54-56].

Ultrasound transducers use high frequency sound signals to detect axial movement of the cornea. A basic scheme of the ultrasound transducer technology to measure corneal displacement is shown in Figure 11.
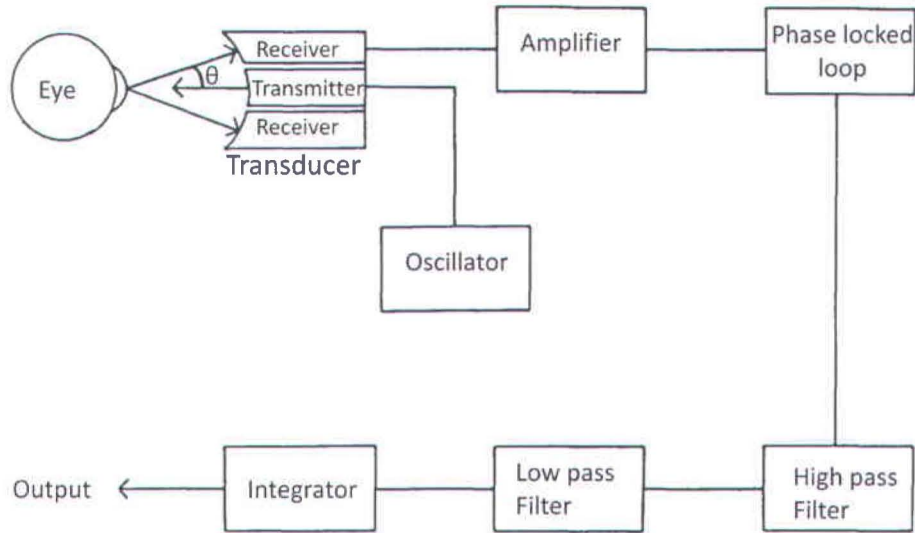
Figure 11. Schematic of the Ultrasound Transducer system to measure corneal displacement.

The oscillator produces a high frequency voltage signal of frequencies ranging from 0.5 MHz to 1 MHz, which is fed to the transmitter of the transducer. The transmitter produces close to a collimated ultrasonic beam at the cornea. The signal produced by the transmitter is sinusoidal, with a temporal waveform of $A\sin(2\pi ft)$ where A is the amplitude, f is the frequency and t is the time of the signal. Due to axial displacement of the cornea, the ultrasonic beam reflected from the cornea is frequency modulated or Doppler-shifted. The Doppler-shifted signal is given by $A\sin(2\pi(f \pm \Delta f)t)$. The change in the frequency Δf or the Doppler shift is proportional to the corneal velocity and can be represented as

$\Delta f = f \dfrac{v}{c} \cos(\theta)$, where f is the initial frequency of the signal, v is the velocity of the cornea, c is the speed of the sound in the media and θ is the angle between the receiver and the transmitter. The Doppler shifted signal received by the receiver is then amplified using an amplifier. The signal from the amplifier is fed to a phase locked loop unit whose output is proportional to the Doppler shift. If the angle between the transmitter and the receiver is kept constant, then output of the phase locked loop unit is proportional to the velocity of the cornea. In order to obtain the displacement of the cornea, the signal is integrated using an electronic integrator.
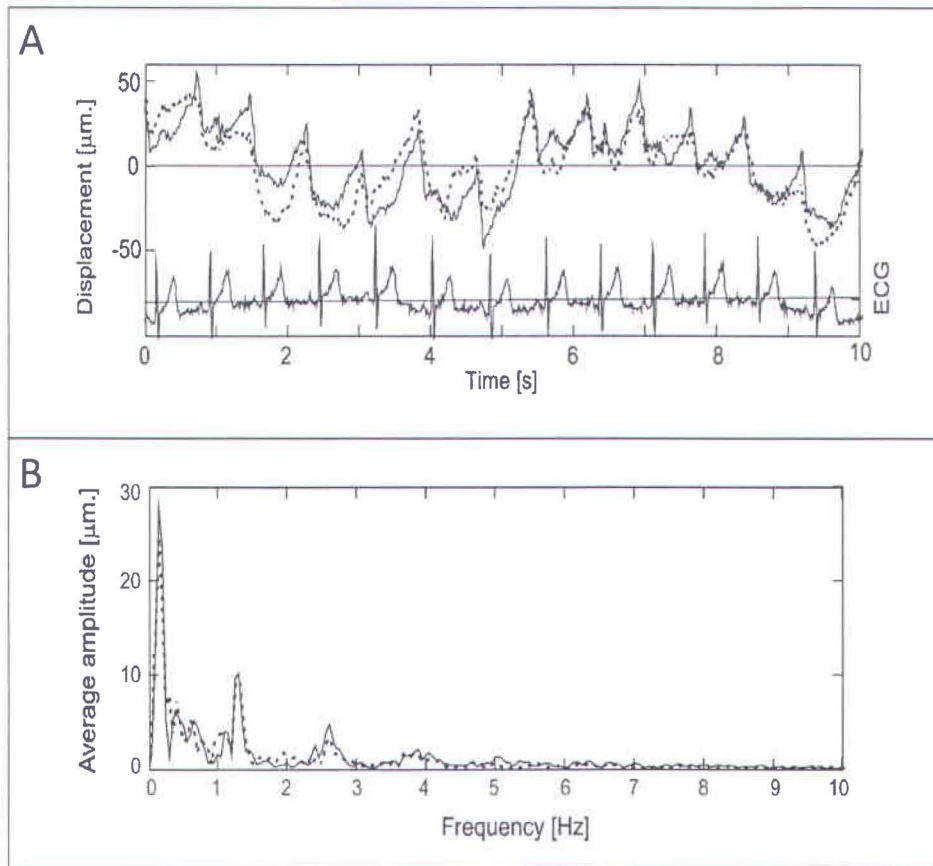
Figure 12. Axial movemet of the cornea (A) measured in both eyes simultaneously along with the electro cardiogram (ECG) signal. (B) Fourier spectrum of the recorded corneal movements. Figures modified from reference [56].

Using this technique, corneal displacements as small as 2 μm sampling at 100 Hz have been reported [54]. One such recording for the axial corneal displacement is shown in Figure 12. In this study, the axial displacement of the cornea in both eyes was simultaneously measured with two transducers. The cardiac signal was also recorded using electro cardiogram (ECG). The cardiac signal is represented by ECG signal in Figure 12(A). The Fourier spectrum of the recorded movement was calculated to investigate the frequencies present in these movements. The calculated Fourier spectrum is shown in Figure 12(B). It can be seen from the Fourier spectrum that the axial displacement of the cornea is composed of frequencies close 1.5 Hz and its harmonics which were attributed to the cardiac

Although efficient in measuring the corneal displacement, this technique cannot measure the movements of inner ocular tissues, such as the ocular lens and the retina.

2.3 Laser Interferometry

The first ever experimental demonstration of light interferometry dates back to 1801 when Dr. Thomas Young established the wave nature of light through his famous double slit experiment. The light source used in those experiments was natural sunlight, which limited the applications of interferometry. After the first operational ruby laser (Light Amplification by Stimulated Emission of Radiation) in 1960, interferometry has found wide spread applications in material inspection, biological imaging and accurate measurement of very small (few picometers) to a fairly large (about 100 meter) displacement measurements. Light signals interfere due to their wave like nature. Light sources based on Laser have large spatial and temporal coherence.

Laser interferometry can be divided into two sub-categories, namely homodyne interferometry and heterodyne interferometry.

2.3.1 Homodyne Interferometry

Homodyne interferometry uses only single frequencies from the laser and hence its name homodyne. The simple outline of a homodyne interferometry system is shown in Figure 13. The light from a laser source is divided into a reference and a sample beam using a beam splitter. The reflected signals from the reference surface and the sample surface interfere at the detector, which is normally a photodiode.
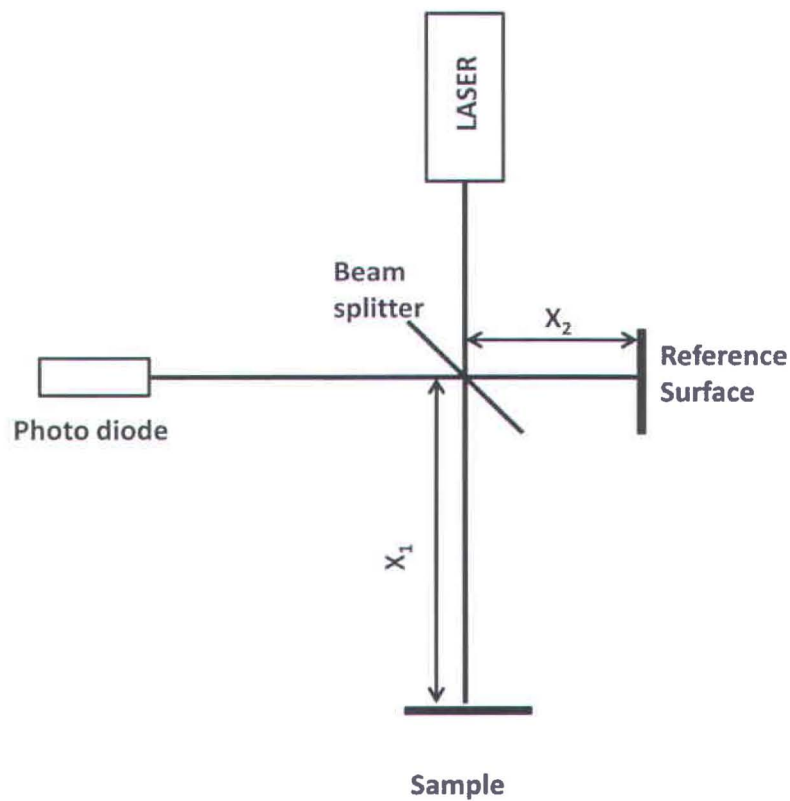
Figure 13. Schematic of the homodyne Michelson interferometer.

The intensity $I_R(k)$ of the interference signal at the detector can be represented as

$$I(k) = I_R(k) + I_S(k) + 2\sqrt{I_R(k)I_S(k)}\cos(2kd + \theta_0),$$ (2.1)

where $I_R(k)$, $I_S(k)$ are the intensities reaching the detector from the reference surface and the sample surface, respectively, k is the wave number, $d = X_1 - X_2$ is the optical path difference (OPD) between the sample and the reference surface and θ_0 is a constant phase difference. If the OPD between the sample and the reference surface changes, then due to the presence of the cosine term in Eq. (2.1), the intensity at the detector varies accordingly. Thus the movement of the sample relative to a fixed reference surface can be measured by monitoring the intensity at the detector. The limitation of homodyne interferometric techniques is that they do not provide the direction of the movement, and the measured phase is intensity dependent. Any fluctuation in the source intensity is measured as phase change leading to error in the measurement.

In some of the previous studies, [49, 52] modified homodyne interferometry was used to measure the ocular tissue movements. The scheme for such an interferometry is shown in Figure 14.
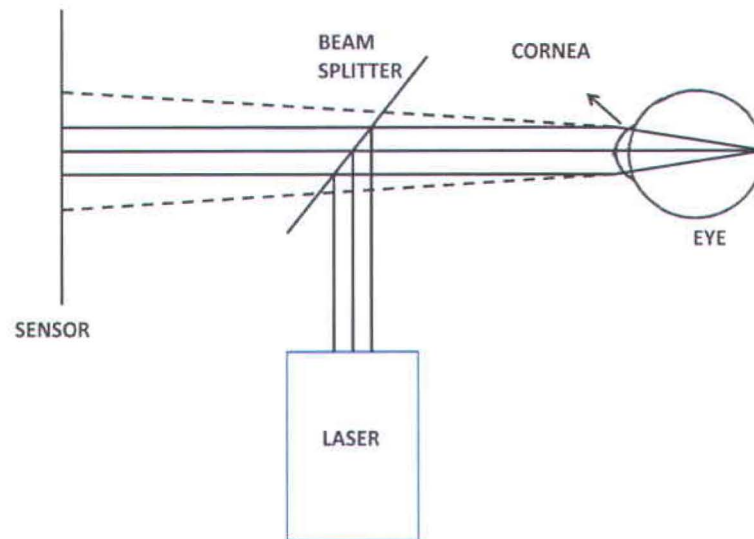
Figure 14. Modified homodyne interferometry to measure the fundus pulsations.

In those studies, the eye was illuminated with a laser beam of high coherence length, which is reflected at the front surface of the cornea as well as at the retina. The signal reflected from the cornea and received at the detector has a spherical wavefront (the beam is diverging) due to corneal curvature. On the other hand, the signal received by the detector after reflection from the retina has almost plane wavefront. The reflected signals from the cornea and the retina interfere with each other to produce an interference pattern with concentric bright and dark circles. This interference pattern is recorded over time to extract the relative movement between the cornea and the retina, *i.e.* the ocular pulsation or fundus pulsation [52]. A recording of such an interference pattern is shown in Figure 15.
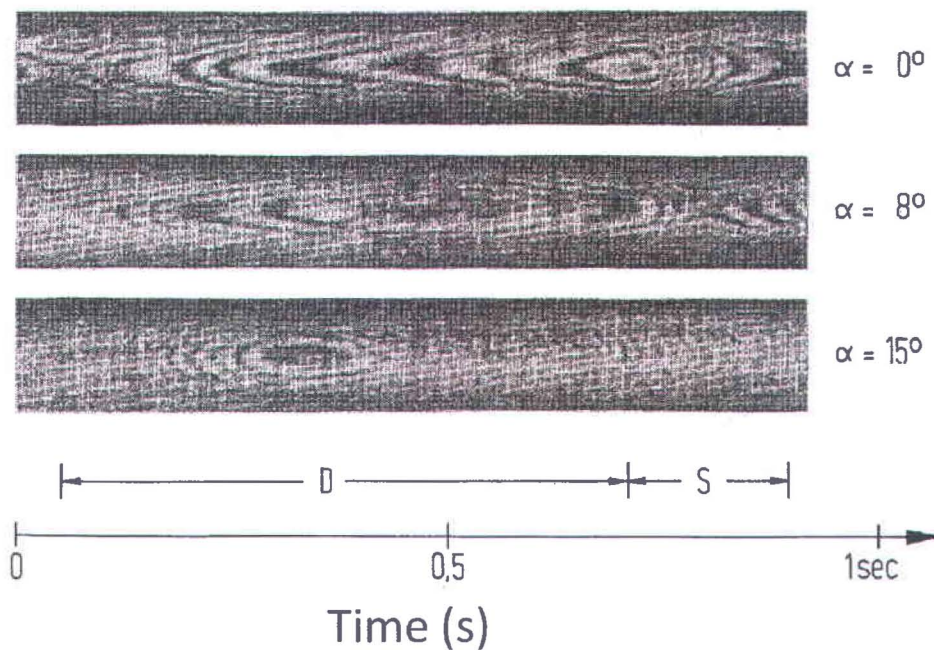
Figure 15. Fundus pulsations measured with modified homodyne interferometry[52].

The fundus pulsations were measured at three different angles from the visual axis, at 0, 8 and 15 degrees. In Figure 15, data acquired for only 1 second is

shown, which represents one cardiac cycle. In this data, the interference pattern during diastole (D) and systole (S) can be seen. For measuring the relative movement between the cornea and the retina, the number of fringes crossing a fixed point must be counted. Each fringe cross accounts for a relative movement equal to half the wavelength of the light source used divided by the average refractive index of the ocular media.

In this technique, movement of the retina and the cornea cannot be obtained independently; therefore no information about the direction of the movement of the cornea or the retina can be deduced. Also, as the laser source used in this technique has a high coherence length, it is difficult to determine with high certainty the specific eye elements producing the interference pattern.

2.3.2 Heterodyne Interferometry

Heterodyne interferometry overcomes some of the limitations of the homodyne interferometer, such as directionality measurement and intensity dependence of homodyne interferometry by introducing a modulating element in the system. In the initial course of this thesis work, a heterodyne interferometer was built in collaboration with MPB Communications Inc. (Pointe-Claire, Quebec) to measure the ocular movements. Heterodyne interferometry uses two frequencies from the same laser source. A layout of the system developed is shown in Figure 16.

The plane polarized light from a Helium-Neon (HeNe) laser is passed through an acousto-optic cell (AOC), which produces two beams of different frequencies, the 0th order beam at the actual frequency of the HeNe laser, and the 1st order beam with up-shifted frequency. The two signals from the AOC are coupled to polarization-maintaining single mode fibers. The 0th order beam after reflection at the beam splitter BS3 and the 1st order beam after reflection at the beam splitter BS1 interfere at the reference detector. If the electric field of the 0th order and the 1st order beam are assumed to be of the form $E_0 \cos(2\pi f_0 + \theta_0)$ and
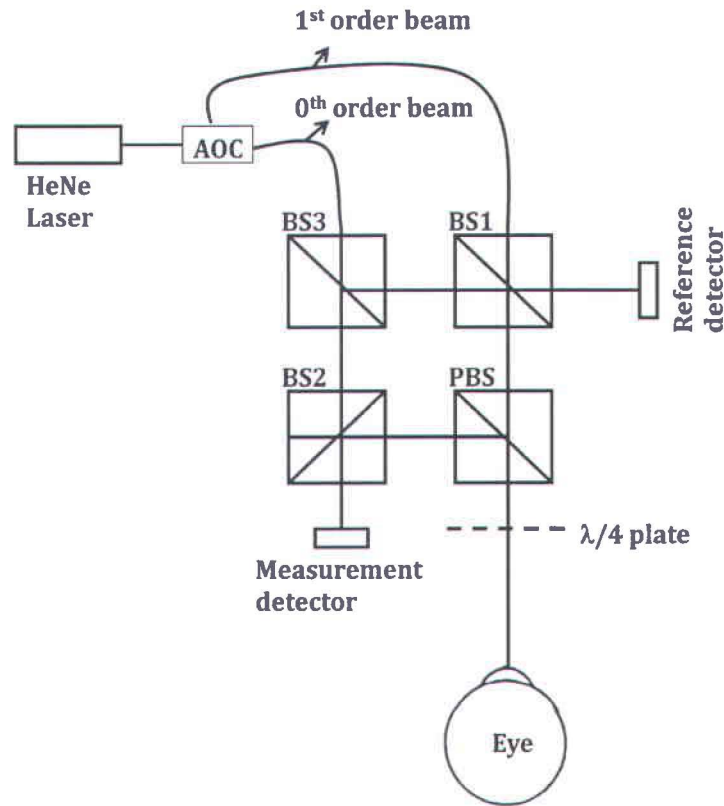
Figure 16. Layout of the heterodyne interferometer.

$E_1 \cos(2\pi f_1 + \theta_1)$, respectively, then the intensity I_r at the reference detector can be expressed as:

$$
\begin{aligned}
I_r &= \left[E_0 \cos(2\pi f_0 + \theta_0) + E_1 \cos(2\pi f_1 + \theta_1) \right]^2 \\
&= \left(\frac{E_0}{\sqrt{2}} \right)^2 + \left(\frac{E_1}{\sqrt{2}} \right)^2 \\
&\quad + \left(\frac{1}{2} \right) \left[E_0^2 \cos\left(4\pi f_0 t + \theta_0 \right) + E_1^2 \cos\left(4\pi f_1 t + \theta_1 \right) \right] \\
&\quad + E_0 E_1 \cos\left[2\pi \left(f_0 + f_1 \right) t + \left(\theta_0 + \theta_1 \right) \right] \\
&\quad + E_0 E_1 \cos\left[2\pi \left(f_0 - f_1 \right) t + \left(\theta_0 - \theta_1 \right) \right]
\end{aligned}
\tag{2.2}
$$

Equation (2.2) suggests that at the reference detector there are signals with frequencies $2f_0, 2f_1, (f_0 + f_1)$ and $(f_0 - f_1)$. Present-day photodetectors have a response time of few nano (10^{-9}) seconds, where as one optical cycle of a visible laser is a few femtosecond (10^{-15}). Thus the current produced in the photodetectors due to optical frequencies does not oscillate at optical frequencies. Rather, photodetectors give a current that is an average of the current produced by many (about 10^6) optical cycles. For this reason, the signals with frequencies $2f_0$, $2f_1$ and $(f_0 + f_1)$ in Eq. (2.2) add up to give a constant intensity term. If we neglect these frequencies in Eq. (2.2) then the signal at the reference detector is given by:

$$I_r = I_0 + I_1 + 2\sqrt{I_0 I_1} \cos\left(2\pi(\Delta f)t + \Delta\theta_r\right), \tag{2.3}$$

where $\Delta f = f_0 - f$ and $\Delta\theta_r = \theta_0 - \theta_1$. This produces an oscillating current of frequency Δf at the reference detector.

On the measurement side, the 1st order beam after passing through polarizing beam splitter and quarter wave ($\lambda/4$) plate falls on the eye. A fraction of this beam is reflected back by different ocular elements. The phase of the reflected signal is modulated on reflection by the reflective elements of the eye. The reflected signal on passing back through the $\lambda/4$ plate changes its polarization and is reflected at the PBS. This signal finally interferes with the 0th order beam at the measurement detector. Similar to Eq. (2.3) it can be shown that the signal at the measurement detector is given by:

$$I_m = I_0 + I_1 + 2\sqrt{I_0 I_1} \cos\left(2\pi(\Delta f)t + \Delta\theta_m + 2kd\right), \tag{2.4}$$

where k is the wave number, $\Delta\theta_m$ is a constant phase difference and d is the optical path difference introduced due to displacement of ocular elements. It can be seen from Eq. (2.4) that the intensity at the measurement detector is alternating at frequency Δf with a phase shift that is proportional to the displacement.
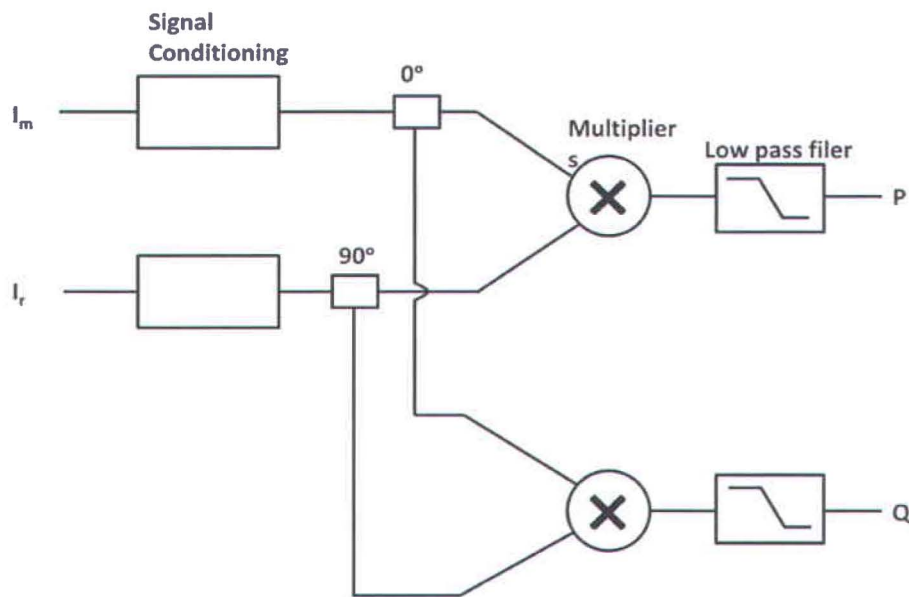
Figure 17. Demodulation technique used in heterodyne interferometer system.

In order to measure the relative displacement between the reference surface and the sample surface, the relative phase difference between the signals produced by the reference detector and the measurement detector must be measured. To measure such phase, a demodulation technique can be applied, and the one applied in the developed system is depicted in Figure 17.

The signal from the reference detector and measurement detector are signal conditioned. This involves conversion of current signal from the detectors to voltage signal and then making their amplitudes equal, preserving the phase of the original signal. The conditioned signals are fed to the splitters creating two signals for both the reference and the measurement signal. Further, the phase of one of the reference signals is shifted by 90°. These signals after passing through

multipliers are low pass filtered to remove the Δf components giving the output as

$$P = V \cos\left[\left(\Delta\theta_m - \Delta\theta_r\right) + 2kd\right] \tag{2.5}$$

$$Q = V \sin\left[\left(\Delta\theta_m - \Delta\theta_r\right) + 2kd\right], \tag{2.6}$$

where V is the maximum voltage signal.

The optical components such as PBS, BS1, BS2, BS3 and detectors of the developed system were fixed and thus the dependence of Eq. (2.5) and Eq. (2.6) on $\Delta\theta_m$ and $\Delta\theta_r$ can be neglected. Thus the optical path difference d introduced due to movement of ocular tissues can be measured from the relation

$$d = \frac{1}{2k} \tan^{-1}\left(\frac{Q}{P}\right) \tag{2.7}$$

It is clear from Eq. (2.7) that the measured optical path difference d does not depend on the intensity of the laser sources, thus free from any error due to fluctuations in the source intensity.

Using this system, the movement of the eye of live rabbits and rats was measured. To measure the movement of the eye, the animal was anesthetised and the measurement beam was focused on the cornea. One such recorded movements and its corresponding frequency spectrum in a live anesthetised rabbit is shown in Figure 18 (A) and Figure 18 (B), respectively.

From the frequency spectrum of the movement, it is clear that the eye movement is pulsatile in nature and is composed of the movements due to the cardiac cycle (2.92 Hz) and its harmonics (5.85 Hz). The pulsatile nature of the movement can also be seen from the actual movement of the eye in Figure 18(A).

38
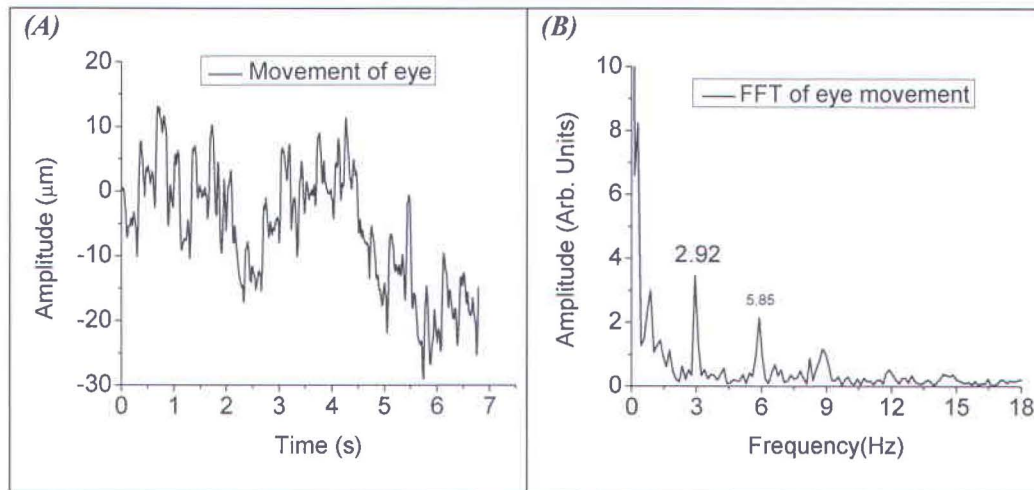
Figure 18. Movement of the cornea and the corresponding frequency components in a live rabbit.

With this technique, it was possible to measure the axial movement, but it could not be established with certainty whether the movements originated at the cornea or at the underlying ocular tissues. This is due to the same reason mentioned previously, *i.e.* the long coherence length of the laser source allows interference from all the ocular tissues. The measurement of the axial movement of the retina is even more difficult, since to reach the retina the beam has to pass through all the ocular element that are reflective. Thus, in the presence of all the reflections from the ocular tissues, it is impractical to determine the movement of any individual element.

To circumvent this problem, instruments based on low-coherence interferometry (LCI) were used. The details of the LCI are discussed further in the next section.

2.4 Low-coherence interferometry (LCI)

The low-coherence interferometry (LCI) technique is a laser interferometry technique using a broadband source, *i.e.* of low coherence length. An interferometric system based on LCI for the measurement of ocular dynamics was first demonstrated by Dragostinoff *et al.* [50].
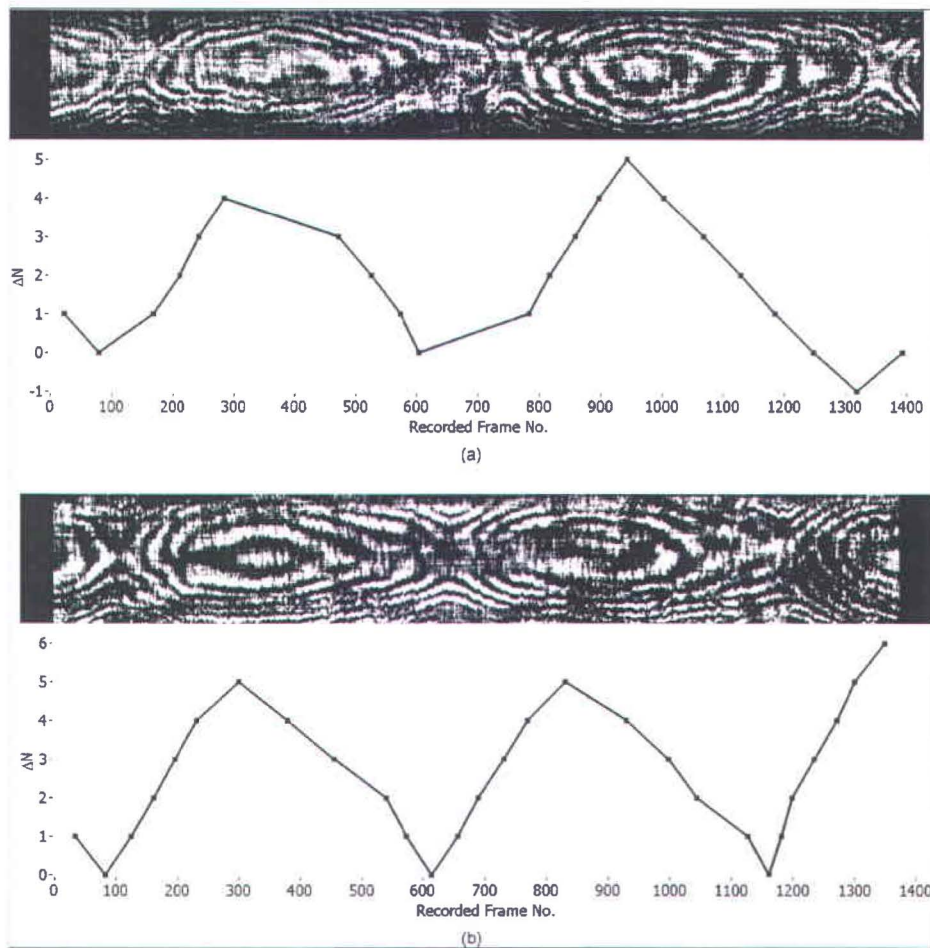
Figure 19. Ocular fundus pulsations measured with low coherence interferometry. Image taken from reference [50].

They used two beams derived from the same light source such that the optical path difference (OPD) between them could be varied. Instead of a fixed reflective surface such as mirror, the reflected signal from the cornea was used as a reference signal. The OPD between the two beams was set such that it was equal to the optical length between the cornea and one of the retina layers. Under these conditions, the signals reflected from the cornea and from a particular layer of the retina interfere with each other, producing circular fringes at the detector. A recording of the fringe pattern close to 7° of the visual axis towards nasal side obtained using this system is shown in Figure 19.

The measured ΔN, which represents the change in the fringe count for each successive frame, is also plotted below the fringe pattern. The two fringed patterns shown are the recordings for the two different layers of the retina. By observing the changes in the fringe pattern, the change in the eye length usually referred to as axial length was estimated. This technique is efficient in measuring the change in the eye length but cannot be used to measure the absolute movement of individual ocular tissues. Moreover, we could only record at a time the pulsations of only one layer of the retina relative to the cornea and the directionality of the movement could not be recovered.

The limitations of the LCI can be addressed using a variant of the LCI called Fourier-domain low-coherence interferometry (FD LCI). The details and application of FD LCI are discussed in the next chapter.

Chapter 3

Spectral-domain low-coherence interferometry

3.1 Introduction

Kasprzak *et al.* demonstrated a system based on spectral-domain optical coherence tomography (SD-OCT) [53], a variant of the LCI to measure individually the movement of different ocular tissues. In the SD-OCT technique, cross-sectional images of the different eye elements are obtained from a series of laterally adjacent depth-scans. The depth-scans are obtained from the spectrally resolved interferograms obtained at the exit of an interferometer, which combines the low-coherent light reflected by a reference mirror and the eye. Video-rate imaging allows the extraction of the movement of individual eye tissues such as the cornea, the crystalline lens, and the retina [53]. This technology thus provides the ability to evaluate the movement of individual eye elements.

Although Kasprzak *et al.* were able to measure the movement of individual ocular tissues, the displacement resolution of their system was approximately 10 μm.

However, earlier works of Schmetterer *et al.* [52] and Dragostinoff *et al.* [50] suggest that the typical eye length change is of the order of few microns. To measure movements of the various eye structures and to avoid aliasing of the data, the technique employed should at least provide an axial displacement resolution of 1 μm and sampling rate of 100 Hz.

In the initial part of this thesis work, a novel non-invasive instrument based on spectral-domain low-coherence interferometry (SD-LCI) was developed, which extracts movement information from sequential axial scans. The device was tested in the laboratory using model materials, as well as *in vivo* using live anesthetized rats. It resulted in better performance than most alternative methods, demonstrating a precision of approximately 200 nm at 100 Hz sampling frequency in displacement measurement of a mirror. Measurements on live animals using this newly developed equipment provided new elements of understanding about the ocular dynamics.

3.2 Theoretical background

Fourier domain low coherence interferometry (FD-LCI) [57] is based on Michelson interferometry, where a broadband light source is used to illuminate a reference surface and a sample (Figure 20). The reflected beams from the sample surface and the reference are recombined, producing interference. Using a diffraction grating that separates angularly the different wavelength components of the light, the spectrum of the interference signal can be observed using a linear CCD array (Figure 20). The intensity distribution along the k-axis (wavenumber-axis) on the linear CCD camera, $I(k)$, can be described as the light source spectrum, $I_0(k)$, with a sinusoidal modulation at the exact frequency of the optical path difference (OPD) between the sample surface and the reference surface. The OPD is the product of the geometric length difference between both

43

arms of the interferometer, d, and the index of refraction of the medium through which it propagates, n,

$$OPD = 2nd. \tag{3.1}$$

The factor of '2' appears in Eq. (3.1), since light has to travel back and forth, doubling the geometrical path difference.

The spectrum intensity distribution along the k-axis can be written as

$$I(k) \sim I_0(k)\big(1 + \alpha \cos(2ndk + \phi)\big), \tag{3.2}$$

where α is a dimensionless parameter related to the visibility of the interference fringes and ϕ is a phase constant.
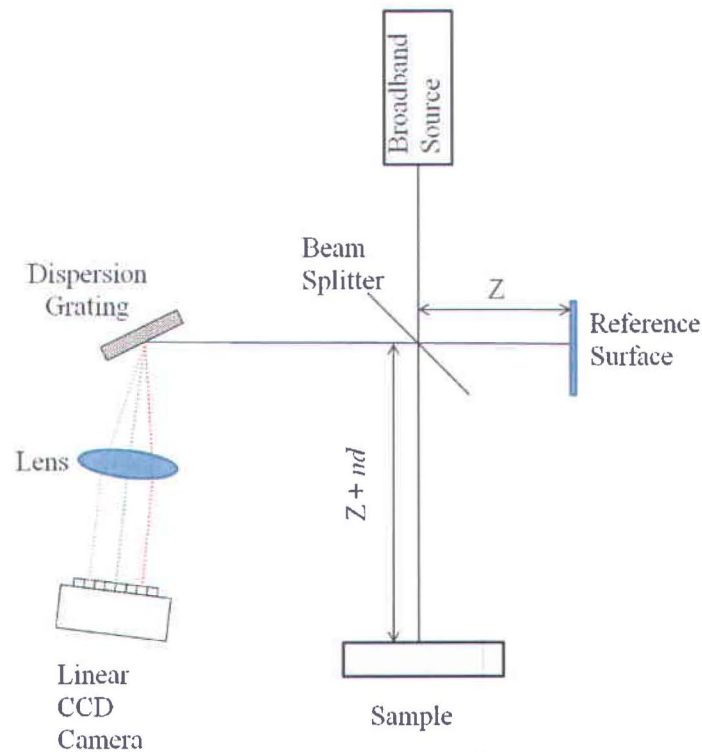
Figure 20. Schematic of the Fourier (Spectral) domain low-coherence interferometric system.

44

In order to use the modulation frequency in the spectrum as a means to extract an accurate measurement of the geometric length, Fourier transformation is performed on the spectrum. Assuming $I_0(k)$ has a Gaussian profile of bandwidth Δk, the Fourier transformation of Eq. (3.2) leads to an analytical solution of the form [58]

$$I(x) \sim \alpha I_0(x - 2nd) + I_0(x), \tag{3.3}$$

where $I_0(x)$ is a Gaussian function of width equal to the coherence length of the source.

From Eq. (3.3) it can be deduced that in the Fourier transformed space, the interference pattern has two peaks: a stationary peak centered at $x = 0$, revealing the light source spectrum, and a second peak of amplitude multiplied by the fringes visibility α, centered at $x = 2nd$. Thus, the center of this second peak is located at the OPD of the interferometer (neglecting the refractive index dependence on wavelength). In the case of samples composed of several partially reflective layers, successive peaks will be observed in the transformed space, and their centers will provide the exact corresponding location with respect to the reference sample.

The Fourier transformation of the spectrum obtained on the CCD providing the reflectivity profile as a function of depth is commonly called an axial scan (A-scan), or depth scan. Thus by observing the change in the position of a reflective structure in the A-Scan, its relative movement with respect to the stationary sample surface can be measured.

The maximum optical path difference (d_{max}) that can be measured following this methodology is limited by the Nyquist criterion. The highest spectrum modulation frequency that the CCD can sample avoiding aliasing corresponds to d_{max}, *i.e.* the high frequency limit after the FFT algorithm. This distance is called the depth range [59] and is given by

$$d_{max} = \frac{1}{n}\frac{\ln 2}{\Delta k}N = \frac{1}{n}\frac{\ln 2}{2\pi}\frac{\lambda_0^{\,2}}{\Delta\lambda}N, \tag{3.4}$$

where Δk is the bandwidth of the light source in k-space, $\Delta\lambda$ is the bandwidth of the light source in wavelength space, λ_0 is the central wavelength, n is the refractive index of the medium and N is the number of pixels of the linear CCD camera. In real experiment, the depth range would also be affected by the attenuation of the light signal in the medium and the Rayleigh range of the focusing optics.

The longitudinal resolution in SD-LCI, defined as the minimum distance between two layers of the sample such that they can be identified separately, is inversely proportional to the bandwidth of the light source and is given by (for a light source with Gaussian shape) [59, 60]

$$\Delta d = \frac{1}{n}\frac{4\ln 2}{\Delta k} = \frac{1}{n}\frac{2\ln 2}{\pi}\frac{\lambda_0^{\,2}}{\Delta\lambda}, \tag{3.5}$$

where $\Delta\lambda$ is the bandwidth of the light source, λ_0 is the central wavelength, n is the medium refractive index and Δk is the bandwidth of the light source in wave number space where the wave number k is defined as $k = \dfrac{2\pi}{\lambda}$. The longitudinal resolution also corresponds to the coherence length of the source.

3.3 Experimental Details

3.3.1 System design

In Figure 21, a schematic of the optical set-up for the SD-LCI is shown, and was developed to measure the retina and cornea movements in a live anaesthetized rat.

A fiber-based Michelson interferometer was used with a superluminescent diode (SLD, Superlum) that has a central wavelength of 844 nm and a bandwidth of 46 nm. Light was split using a 2×2, 80:20 fiber coupler into the reference and sample arms respectively, terminated with fiber collimators.
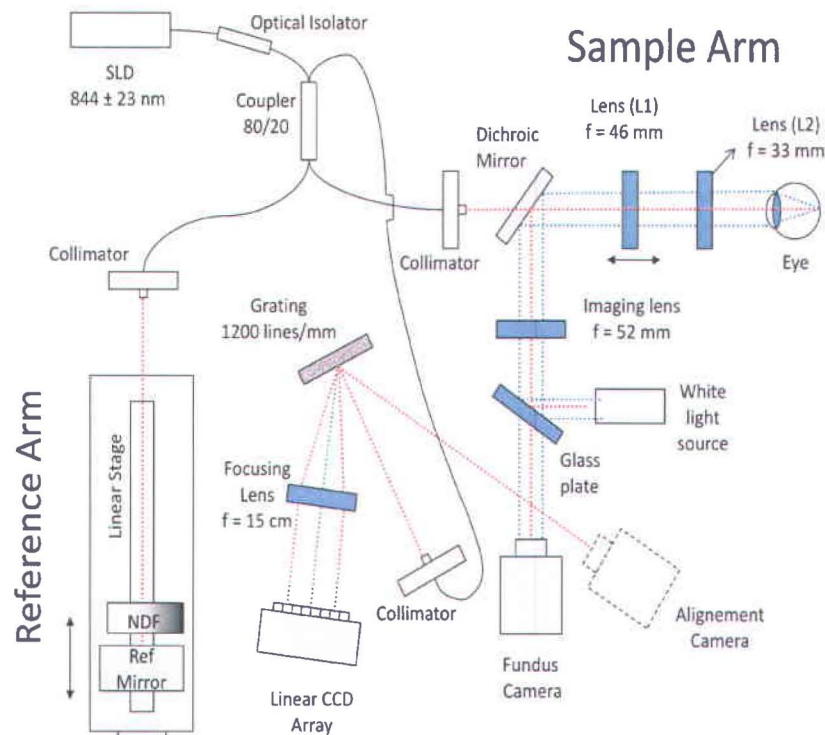
Figure 21. Schematic of the designed system based on Fourier domain low coherence interferometry to measure the ocular dynamics in a rat

At the reference arm, light was reflected by a broadband mirror placed on a motorized translation stage (PI Instrument). The reference arm beam was attenuated by a neutral density filter (NDF) in order to keep its total intensity below the saturation level of the detector. The sample arm was coupled to a fundus camera, which comprised a CCD camera (Pulnix), a white-light source and

47

an imaging lens (focal length $f = 52$mm). In addition, two lenses ($f = 46$mm and $f = 33$mm) were used as a telescope, in front of the sample to correct for myopia or hypermetropia of the eye. The collimated sample beam was focused by the eye optics on to the fundus, or by a focusing lens L1 ($f = 46$mm) onto the cornea. The SLD power incident onto the eye was 700 µW, which is safe for continuous illumination of the human eye according to ANSI safety standards [61]. The two reflected beams (one reflected from the eye layer of interest and the other from the reference mirror) were recombined in the fiber coupler, then dispersed using a diffraction grating (1200 lines/mm) and focused by a lens ($f = 150$ mm) on to a linear CCD camera (Gerhard Stresing).

The camera exposure time was set to 400 µs. Overall, the total data acquisition time of the CCD camera and the oximeter signals provided a sampling rate of 100 Hz. The interference spectra and oximeter signal were both recorded during series of 5 seconds.

To establish a relationship between the eye movements and the cardiac pulsations, heartbeats were simultaneously recorded using a custom-made oximeter [62]. The oximeter is a non-invasive device that measures the oxygen saturation in blood. It measures the oxygen saturation by measuring the transmission of the light through the blood flowing in vascular tissue such as fingers or ear lobes. The oximeter developed used an infrared light-emitting diode facing a photodiode connected to an amplification circuit that was digitized with the computer. The infrared light-emitting diode and the photodiode were placed on a clip. For both the cornea and the retina recordings, the oximeter was located at the exact same position, *i.e.* at the tail of the rat. The signal from the linear CCD camera and oximeter were processed using a 2.0 GHz computer using custom software (LabView; National Instruments Inc.) and saved to the hard disk.

3.3.2 System characterization

3.3.2.1 System calibration

The first step in system characterization was to calibrate the system in order to measure the displacements of the objects. The data acquired by the linear CCD camera has intensity values for each pixel. The complete intensity profile for all the pixels gives the interference spectrum for the reference and the sample signal. The interference signal recorded at the linear CCD camera is linearly spaced in wavelength space. Before performing the fast Fourier transform (FFT) of the measured interference spectrum (which gives the axial scan of the sample), the data was rescaled linearly into the wave number k-space [59]. The exact knowledge of the wavelength for each pixel requires additional calibration of the camera, which was not done in this work. Thus the distance axis or the x-axis of the FFT spectrum was in arbitrary units (pixels) and required calibration to obtain the exact distance per pixel in the FFT spectrum.

To obtain the calibration factor for the system, a mirror was placed on a motorized stage as a sample and linearly displaced in steps of 100 μm. The corresponding pixel number of the maxima of the FFT scan was recorded. These pixels values were plotted with respect to the displacement of the mirror. A linear fit to this data gives the displacement calibration factor per pixel. One such calibration curve is given in Figure 22. The calibration factor obtained was 3.39 μm per pixel of the FFT spectrum. Thus the pixel index of the FFT spectrum along the distance axis has to be multiplied with this value in order to obtain the true distance of the sample structure with respect to the stationary sample mirror. With a position precision of 1 μm in the sample mirror position placed on the motorized stage, the calibration can be obtained with 10^{-4} accuracy [63]. However, it should be kept in mind that the calibration obtained depends on the wavelength of the light source, the dispersion grating and optics used between the dispersion grating and the linear CCD camera (Figure 21). Therefore, it is necessary to perform the calibration every time the system is modified.

49
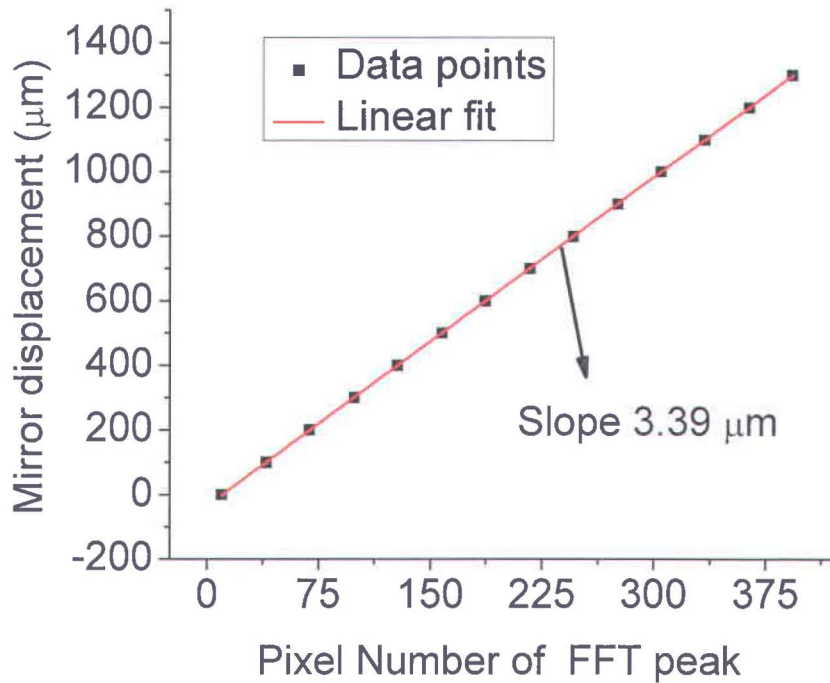
Figure 22. System calibration curve.

3.3.2.2 Axial resolution

The axial resolution (Δd) is the longitudinal resolution of a system, defined as the ability of the system to resolve two closely spaced objects, and is given by $\Delta d = \dfrac{2\ln 2}{\pi}\dfrac{\lambda_0^2}{\Delta\lambda}$. The light source used in work was a super luminescent diode with central wavelength $\lambda_0 = 844.4nm$ and bandwidth defined as full width half maxima (FWHM) of $\Delta\lambda = 46 \pm 3nm$. This gives the theoretical axial resolution of $\sim 6.8 \pm 0.5$ µm in air. Considering an average refractive index of 1.4 for the retina, the theoretical axial resolution of the system in retina will be approximately 5 µm. In order to determine the axial resolution experimentally, a broadband reflective mirror was used as a sample.
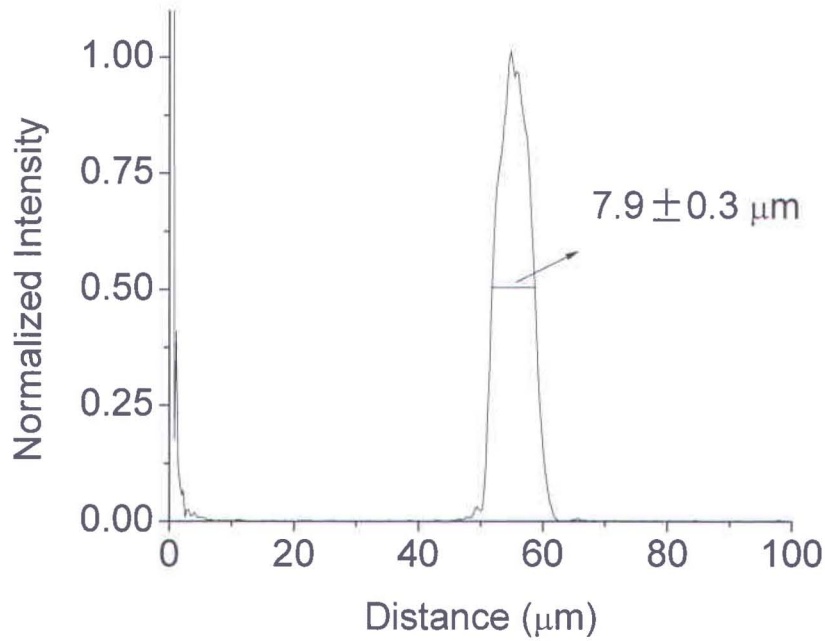
Figure 23. Axial scan of a broadband mirror used as sample.

A typical axial scan of the sample mirror is shown in Figure 23, where the intense peak was attributed to the air/mirror interface. The experimentally obtained axial resolution (FWHM of the axial scan) was found to be ~7.9 ± 0.3 µm in air. This is slightly higher than the theoretically predicated value of ~6.8 ± 0.5 µm.

3.3.2.3 Depth Range

Depth range, defined previously by Eq. (3.4), is the maximum optical path length that can be measured with the system. As given by Eq. (3.4), $d_{max} = \dfrac{1}{n}\dfrac{\ln 2}{2\pi}\dfrac{\lambda_0^{\,2}}{\Delta\lambda}N$ depends on the number of pixels (N) of the camera, the wavelength, the bandwidth of the light source and refractive index of the medium. For a linear CCD camera with N=2048 pixels, a light source with central wavelength $\lambda_0 = 844.4nm$ and bandwidth of $\Delta\lambda = 46 \pm 3nm$, the theoretical depth range in air

that can be achieved is 3.50 ± 0.25 mm. Experimentally, this value was measured to be 3.47 ± 0.2 mm.

3.3.2.4 Resolution and accuracy in displacement measurement

The displacement resolution of a system is defined as the smallest displacement increment that can be measured with the system. However, the accuracy of the system is defined as the actual smallest displacement that the system can measure in the presence of the noises. In FD-LCI, the displacement increment can be measured by tracking the position of the maximum peak FFT value. Thus, the displacement resolution, *i.e.* the minimum change in the position that can be measured, is determined by the position increment between two points of the axial scan, which depends on the light source bandwidth and the total number of pixels of the camera, in our case yielding a displacement resolution of ~3.39 μm. This is the technique that was adopted by Kasprzak *et al.* for the measurement of the movement of ocular tissues [53]. Nevertheless, a shift in the position of a sample can be extracted with much higher accuracy by locating the central position of the Fast Fourier Transform (FFT) peak from curve fitting [64] or centroid location [58]. Accordingly, centroid of the FFT peak was calculated using the relation

$$\frac{\sum X_n I_n}{\sum I_n}, \tag{3.6}$$

where X is the position, I is the intensity and n is the index of the nth point in the FFT spectrum.

Eq. (3.6) does not put any limit on the smallest displacement that can be measured. But the presence of noises from the light source, from the camera and the environmental noises limit the smallest measurable displacement increment. The displacement accuracy of the SD-LCI was evaluated by tracking the centroid of the FFT peak in the axial scan produced by a sample mirror placed on a piezoelectric stage (Piezosystem Jena), which itself was fixed on a motorized translation stage (PI Instrument). It was verified by inducing a periodic movement

to the mirror sample using a piezoelectric crystal, which had a characteristic movement resolution of 0.9 nm. The voltage applied to the piezoelectric stage was used as a reference signal for filtering. Figure 24 (A) and (B) show the measured positions of the sample mirror as a function of time for a sinusoidal movement of amplitude 200 nm and 300 nm.
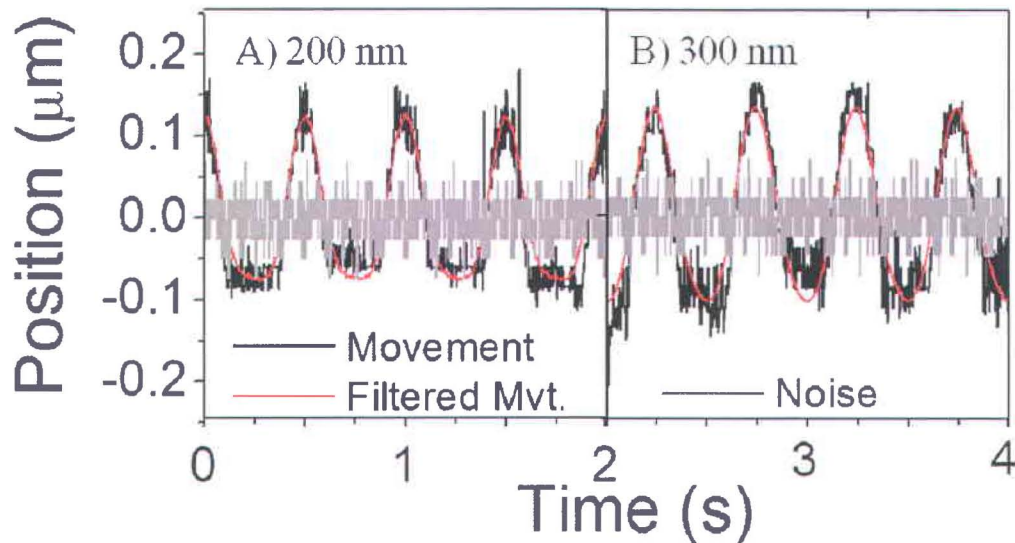
Figure 24. Small movements measured with FD-LCI system.

In the Figure 24, negative (positive) positions correspond to the movement in the forward (backward) direction relative to the sample surface position. By optimizing the interference contrast, a displacement as small as 200 nm could be measured. The standard deviation of the noise when the sample mirror was stationary with respect to the reference mirror was found to be 48 nm. Thus, it is safe to conclude that the developed system based on SD-LCI can measure a displacement increment with an accuracy of about 200 nm.

In actual *in vivo* experiments, the recorded movement will contain unwanted movements, such as head movement and movements due to respiration or

environmental noise. Thus, it is necessary to filter the recorded movement to decouple the movement due to cardiac pulsations. In order to retrieve the amplitude of the displacement due to the cardiac rhythm, the recovered movement was filtered using the oximeter signal as a reference. The oximeter signal was used to design a band pass filter and the frequencies lower than the cardiac frequency and higher than its 5th harmonic were removed.

3.3.3 Animal manipulations

For *in vivo* experiments, live anaesthetized rats were used. The rats were anaesthetized with intraperitoneal injections of ketamine and xylazine mixture (0.1 mL per 100 g of body weight). After anesthesia, animals were placed on a custom-made fixation platform that allowed three axes of head rotation, which facilitated careful alignment of the eye and the sample beam. All animal care was performed under protocols compliant with the Canadian Council on Animal Care with the approval of the Animal Care and Use Committee at the Maisonneuve-Rosemont Hospital.

3.4 Results

The developed SD-LCI system was used to measure the longitudinal movement of the retina and the cornea in live rats. To measure retinal movements, the experimental setup shown in Figure 21 was used, and a collimated sample beam was focused on to the fundus by the eye. A typical axial profile of the retinal layers is shown in Figure 25. The multiple lines were assigned to the various retinal tissue layers after comparing them with the OCT images available in the literature [65]. The retinal tissue layers that can be seen in the A-Scan are nerve fiber layer (NFL), outer nuclear layer (ONL), photoreceptor's inner segment (PR-IS), photoreceptor's outer segment (PR-OS), retinal pigment epithelium (RPE) and choroid (CH). For each scan, the central position of the FFT spectrum was precisely determined using the centroid calculation method described previously

in the section titled "Resolution and accuracy on displacement measurement". When Eq. (3.6) is used to calculate the centroid, it gives a single point that is representative of the position of all the layers in the A-Scan. Such a point for the given A-Scan of the retina in Figure 25(a) is plotted as a star. This point is traced over sequential A-Scans to measure the relative position of the retina. The geometric position of the retina was determined from Eq. (3.6) and Eq. (3.1) using the average refractive index of 1.415 for the rat eye [66, 67].
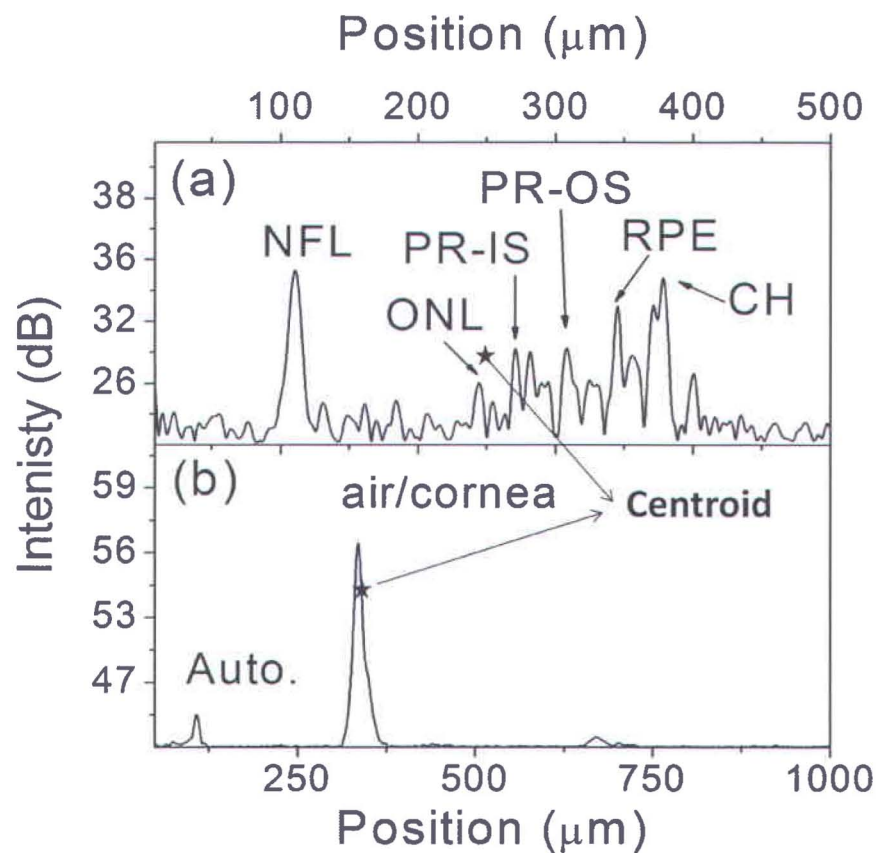
Figure 25. Axial scan (A-Scan) of the rat (a) retina and (b) cornea where different retinal layers are identified as nerve fiber layer (NFL), outer nuclear layer (ONL), photoreceptor's inner segment (PR-IS), photoreceptor's outer segment (PR-OS), retinal pigment epithelium (RPE) and choroid (CH). The star symbol represents the centroid of the cornea and the retina in their respective A-Scans.

For measuring the corneal displacement, the set up shown in Figure 21 was used without the lens L2, so that the sample beam was directly focused on to the cornea by the lens L1. A typical axial profile of the cornea is shown in Figure 25(b), where the intense peak observed is attributed to the air/cornea interface. The peak near the zero position can be attributed to auto-interference within the sample, as this peak does not change in position when the reference mirror is moved. The last visible peak is the second harmonic of the air/cornea peak. The position of the air/cornea peak was also determined using the centroid calculation method, and sequential recordings were obtained to extract the movement.
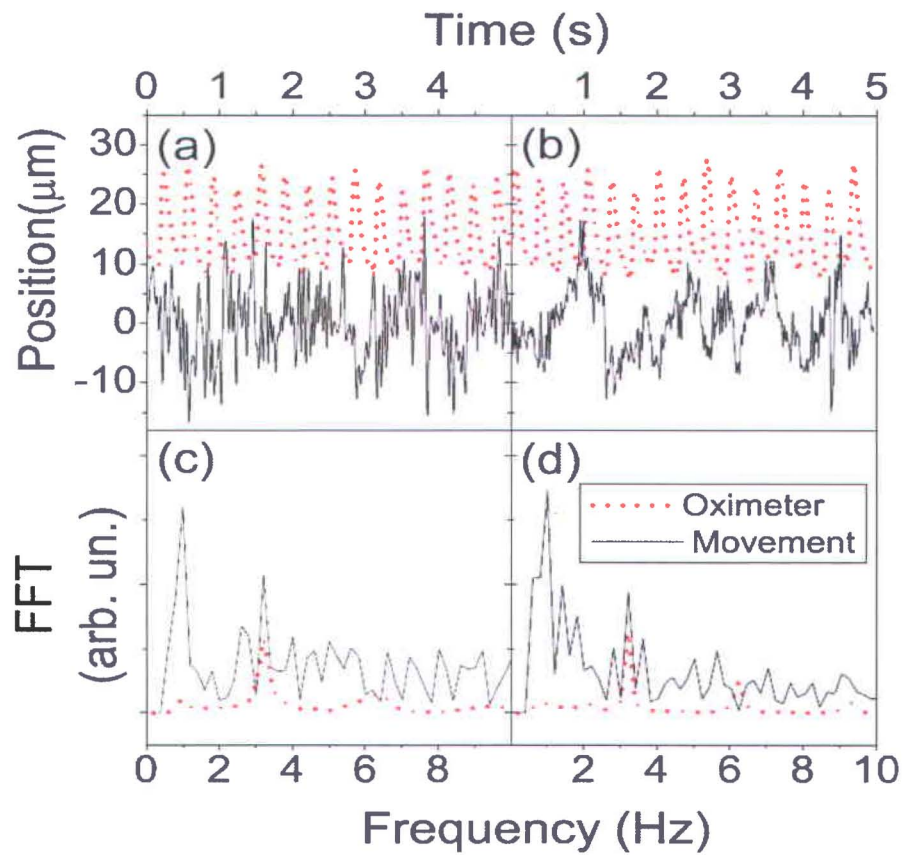
Figure 26. Recorded axial movement of (a) retina and (b) cornea along with the corresponding frequency components in (c) and (d). The oximeter signal is also plotted on dotted red.

56

The displacements obtained using the procedure described above are shown in Figure 26 (a) and (b) for the retina and the cornea, respectively. To investigate the spectral components of such displacements, FFT was performed on the data, whose results are shown in Figure 26(c) and (d). Two main frequency components are present in the retinal and corneal movements: one at 1.0 Hz, which is due to respiration, and the other at 3.5 Hz, which is due to cardiovascular rhythm. To confirm the latter, the FFT of the oximeter signal is also plotted in Figure 26 (c) and (d), which also reveals a frequency at 3.5 Hz.
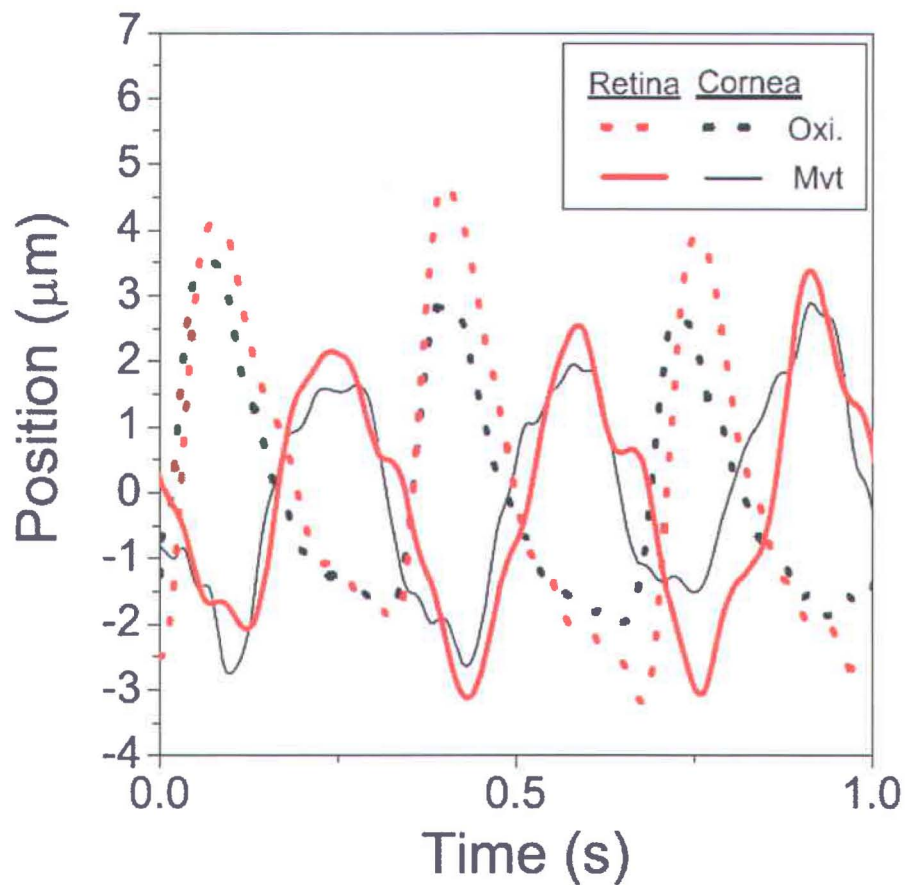
Figure 27. Filtered movement of retina and cornea plotted by matching respective oximeter signal.

To retrieve the relative movement of the retina and the cornea induced by the blood pulsatility, the oximeter signal was used as a common clock. These movements are shown along with the oximeter signals in Figure 27. We shall recall that corneal and retinal movements were recorded from different measurements. Therefore, the reference oximeter signals were matched to compare the two movements. One can see in Figure 27 that, for a similar oximeter signal, the retinal and the corneal movement of the eye are nearly in phase. As a result, we can conclude that the direction of the movement is the same for both tissues; during systole, the layers are pushed forward, whereas during diastole, the layers move backward. This information was not known previously and these results provided the first conclusive evidence to support this theory[58].

For both tissues, the peak-to-peak amplitude was estimated over 30 cycles by locating the two extreme positions (maximum and minimum peaks) for every cycle. The mean of the peak-to-peak values are (3.7 ± 0.6) µm and (3.1 ± 0.7) µm for the retina and cornea, respectively, where the error corresponds to the standard deviation of the data. In order to compare our measurements with the literature [53, 54], we also calculated the effective amplitude of the movements, defined as the root-mean-square amplitude of the movement. The effective amplitude of the retinal and corneal movements due to cardiac pulsation was measured to be 1.10 µm and 1.37 µm, respectively. Given the small size of the rat eye (axial length ≈ 6 mm) and the accuracy of the system (≈ 200 nm), it was difficult to comment on the difference between the amplitude of the cornea and the retina movement.

Chapter 4

Axial movements of the eye for human subjects

4.1 Axial eye movements

The origin of axial eye movements is believed to be related to the ocular blood flow (OBF), which makes them particularly important in diagnosing blood-flow related diseases.

Several ocular pathologies have been associated with the irregularities in the pulsatile ocular blood flow (POBF): exudative age related macular degeneration [68], carotid artery stenosis [69-71], normal tension glaucoma, [32, 72] and giant cell arteritis [73]. In addition, the relationship between the pulsatility of the eye and the prevalence of glaucoma[74], diabetes mellitus [75] and central serous chorioretinopathy [76, 77] has also been investigated.

Typically, ocular pulsatility is indirectly estimated by the ocular pulse amplitude (OPA), defined as the difference between the minimum and the maximum

intraocular pressure measured over the cardiac cycle. Tonometer-based technologies, such as pneumotonometry [78, 79], modified Goldmann applanation tonometry [69], and dynamic contour tonometery [80, 81] are used to measure the OPA. A brief overview of these technologies was provided in the Chapter 1.

Since most techniques used to assess the ocular pulsatility actually measure pulsatile changes of IOP and require contact with the ocular surface, various alternative methods based on the measurement of longitudinal movements of ocular structures have been proposed. These methods measure a different aspect of the eye's response to pulsatile blood flow since they measure pulsatile anatomical changes rather than tonometric changes, and they may provide new insights into the physiology of sight and the pathophysiology of eye disease. Furthermore, they also have the advantage of not requiring contact with the eye.

The non-contact methods to measure the axial movements of the ocular tissues are based on ultrasonic transducers [70], laser interferometers [82] and low coherence interferometers (LCI) [50, 53]. Out of these techniques, the LCI technique can measure the axial movements of almost all the ocular tissues. This is distinct from ultrasound transducers, which can only measure corneal movements, or laser interferometers, where the origin of the movements is ambiguous. Nevertheless, in previous attempts, the movements of the ocular tissues have only been measured separately and never simultaneously. In the present thesis work, one of the objectives was to measure the corneal and the retinal movements simultaneously, so that the eye stretching could be measured. If the simultaneous movements of the cornea and the retina are available, then one can measure the eye stretching by considering the two movements. In this thesis work, such an instrument was developed, which could simultaneously measure *in vivo*, the corneal and the retinal movements.

4.2 Experimental design

In the previous chapter, an instrument based on Fourier-domain low-coherence interferometry was described. The designed system was used to measure the movements of the cornea and the retina, but separately. The recorded heart signal using an oximeter was used as an external reference to demonstrate that the cornea and the retina are displaced together axially during the cardiac cycle. But such measurements cannot be used to measure the fundus pulse amplitude (eye stretching). To measure the eye stretching, it is required that both the cornea and the retina movements are recorded simultaneously. In order to do so, the system described in the previous chapter was modified and the details of the modified system are discussed further.

A schematic diagram of the optical system designed in order to measure the corneal and the retinal movements simultaneously, is shown in Figure 28. A superluminescent diode (SLD, Superlum) with 844 nm central wavelength and 46 nm bandwidth was coupled to a fiber-based Michelson interferometer. A 2×2, 80:20 fiber coupler was used to split the light into the reference and sample arms. The sample arm was terminated using a collimator that produced a 3 mm wide beam. The total power of the sample beam at the exit of the collimator was fixed to 500 μW, which is well below the prescribed ANSI limit of 750 μW for continuous viewing around 844 nm. The sample beam passed through a lens (f=100 mm) with a central hole of 2 mm in diameter. After the lens, the central part of the sample beam remained collimated, but the outer part was refracted. A scanning system was set up so that the outer part of the sample beam was stationary and focused on the cornea, whereas the collimated central part was scanned and focused at the retina. Thus, using this optical scheme, the reflected signals from the corneal apex and the retina were simultaneously acquired. A 2×1, 50:50 fiber coupler was used to obtain two reference signals reflected by mirrors mounted on separate motorized translation stages (Zaber Technology, Vancouver, Canada). The reference signals were attenuated using neutral density filters in

order to keep their total intensity below saturation level. The reflected signals from the sample and reference arms were dispersed using a reflective diffraction grating (1200 lines/mm) and focused by an achromatic lens ($f = 200$ mm) on a linear CCD camera (Spyder 3, Dalsa Technology, Canada).
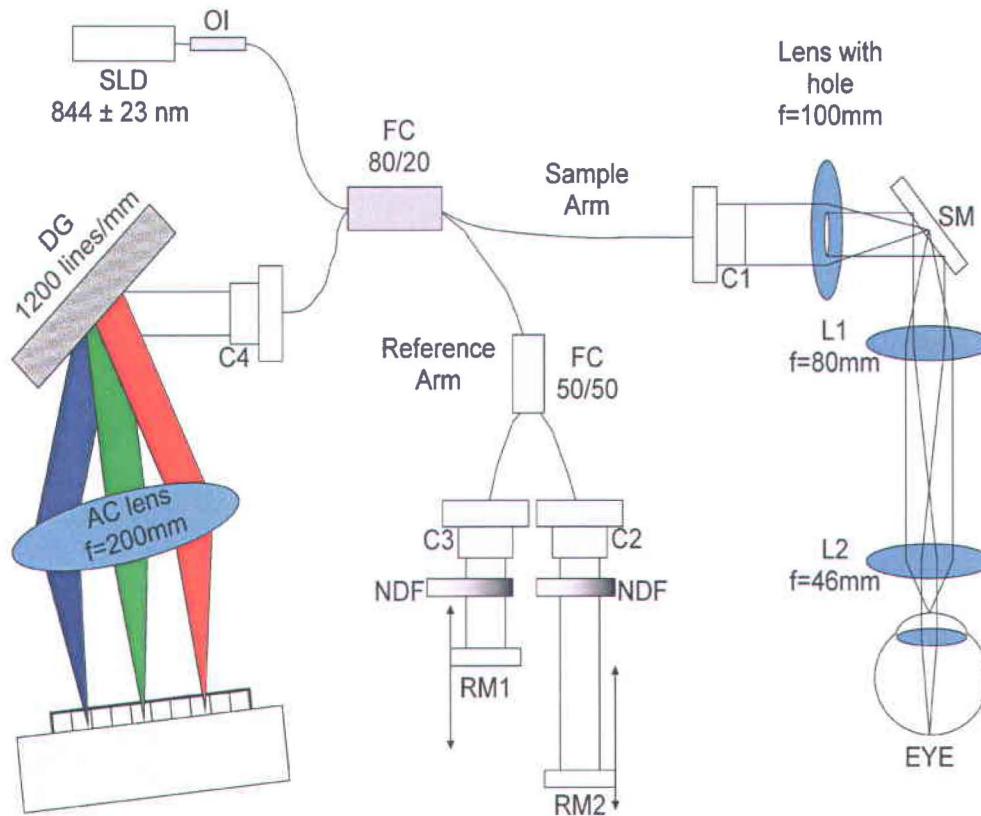
Figure 28. Schematic of the optical system developed to measure the corneal and retinal movements simultaneously.

A custom-made oximeter was placed on the ear lobe during measurements to simultaneously record the heartbeat of the subjects using a data acquisition card (Labjack, Lakewood, CO). The signals from the linear CCD camera and the

oximeter were acquired using a dual core 2.0 GHz computer with custom software (LabView, National Instruments, TX). Data was acquired for 20 seconds and stored for later processing.

4.3 Data processing

In post processing, the data was analyzed using custom made software in LabView. One B-Scan containing signals from the cornea and the retina, obtained with the developed instrument is shown in Figure 29(A). A B-Scan is simply a collection of adjacent axial scans of the sample. The A-Scan along the visual axis in the foveal region is shown in Figure 29(B). The different ocular interfaces that can be identified after comparing with the standard optical coherence tomography (OCT) [59, 83] images are, the corneal epithelium (CEp) and endothelium (CEn), the nerve fiber layer (NFL), the inner-outer segment (IS-OS), the retinal pigment epithelium (RPE), and choriocapillaris (CC).

For data processing, each recorded frame (B-Scan) is loaded in to the computer via our analysis software. Out of this B-Scan, a reference B-Scan is subtracted. The reference B-Scan is a scan recorded at the beginning of the experiment without the signal from the eye. This procedure removes constant noise coming from the source spectrum or interference within the system. From the reference removed B-Scan, one of the A-Scan that corresponds to the region of the interest where the movement has to be measured was selected manually.
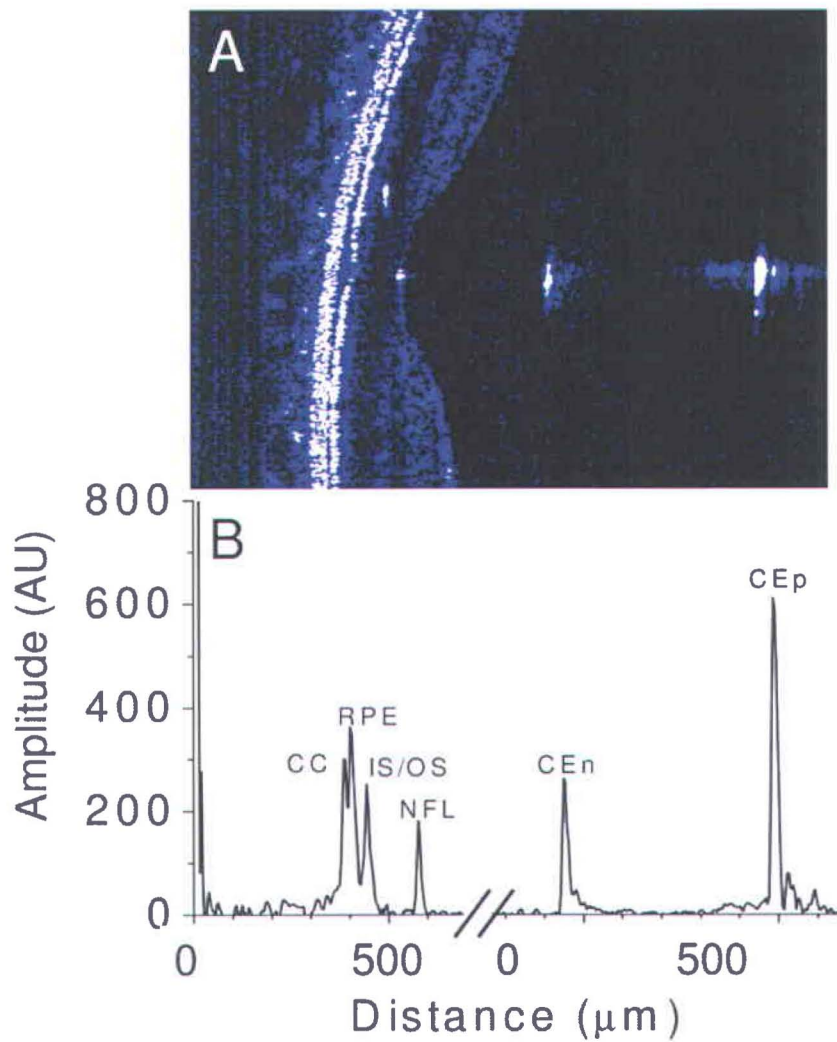
Figure 29. B-Scan of the cornea and the retina.

On each selected A-Scan, a Savitzky-Golay filter is applied to smooth the data, which is then squared to reduce the effect of noise around the ocular tissue signal. From the smoothened A-Scan, a window containing the axial profile of the desired ocular tissue, *i.e.* either cornea or retina, is selected for which the centroid is calculated using the relation, $\dfrac{\sum X_n I_n}{\sum I_n}$, where X is the position, I is the

intensity and n is the index of the nth pixel in the A-Scan. This procedure is performed on all the subsequent B-Scans to obtain a time trace of the centroid, which gives the axial shift of the ocular tissues.

Finally, in order to retrieve the FPA, the difference between the positions of the cornea and the retina were calculated and further Fourier transformed to study their harmonic components relative to those of the cardiac cycle. Signals were processed by applying a band-pass frequency filter between the heartbeat and its 5th harmonic. For statistical data analysis, a t-test model was used and p-values less than 0.05 were considered statistically significant.

4.4 System performance

The performance of the developed system was evaluated for parameters such as axial resolution and depth range, which were found to be comparable with the values obtained in Chapter 3. The system was further evaluated for its performance in terms of speed and displacement resolution.

Setting the camera exposure time to 30 µs, the total frame rate (or B-Scan rate) achieved was 40 frames per second. Each B-Scan consisted of 720 A-Scans with 1024 pixels per A-Scan. For scanning, a 2-dimensional scanner (Nutfield Technology, Inc. USA) was used, but only one of the mirrors was moved to acquire the B-Scans of the retina along a line.

In FD-LCI based systems, the displacement resolution (*i.e.* the smallest position change that can be measured for a well resolved peak) depends on the SNR of the system [84] and is basically limited by the shot noise [85, 86]. To experimentally estimate such displacement resolution of our system, a human cadaver eye was used as a sample. The eye was mounted on a piezoelectric stage (Piezosystem, Jena, Germany), which was moved sinusoidally with variable amplitude at 1 Hz. For filtering out the noise, frequencies lower than 0.75 Hz and higher than 5 Hz

were removed. The piezoelectric stage was driven by a sine wave voltage and moved with amplitudes of 500 nm, 1 μm and 2 μm. The standard deviation (SD) of the noise, after subtracting the measured movement from the perfect sine wave fit, was approximately 100 nm.

4.5 Results

4.5.1 Testing of the system on the normal subjects

To test the developed system, 21 healthy individuals aged between 25 to 35 years, including 11 males and 10 females were recruited. All the subjects had good cardiovascular health with no ocular pathologies other than myopia. Each subject was asked to position his or her head on the headrest and was asked to fixate on a target and blink normally. The eyes were not dilated before the procedure. These experiments were approved by the ethics committee of the Maisonneuve-Rosemont Hospital. The procedure and the consequences were described to all the individuals and informed consent was obtained. The procedure adheres to the Declaration of Helsinki. Although, previous studies have demonstrated that the axial length and refractive error are major factors influencing ocular blood flow measurements[34, 87], for this work such data was not collected as this study was not a clinical trial.

From each recorded B-Scan, the position of the front surface of the cornea and an averaged position of a point on the retina were located, and their displacement in time was traced. An averaged position of a point on the fundus including all retinal layers (ILM to Bruch's membrane) and not the exact position of a particular retinal layer was calculated as the reflected signal from a layer is more prone to noise over A-Scans in time. For calculating the averaged position, Savitzky-Golay filter was applied over the retina A-Scan, as explained in the data processing section. In Figure 30, a fraction of one recording of the cornea and the retina movements, along with the oximeter signal measured in a 30-year-old male

is shown. The recording was done for 20 seconds but for illustration purposes, only the first three seconds of data is shown. To investigate the frequency components present in the movement, in the lower panel of Figure 30 the corresponding computed Fourier power spectrum is shown.
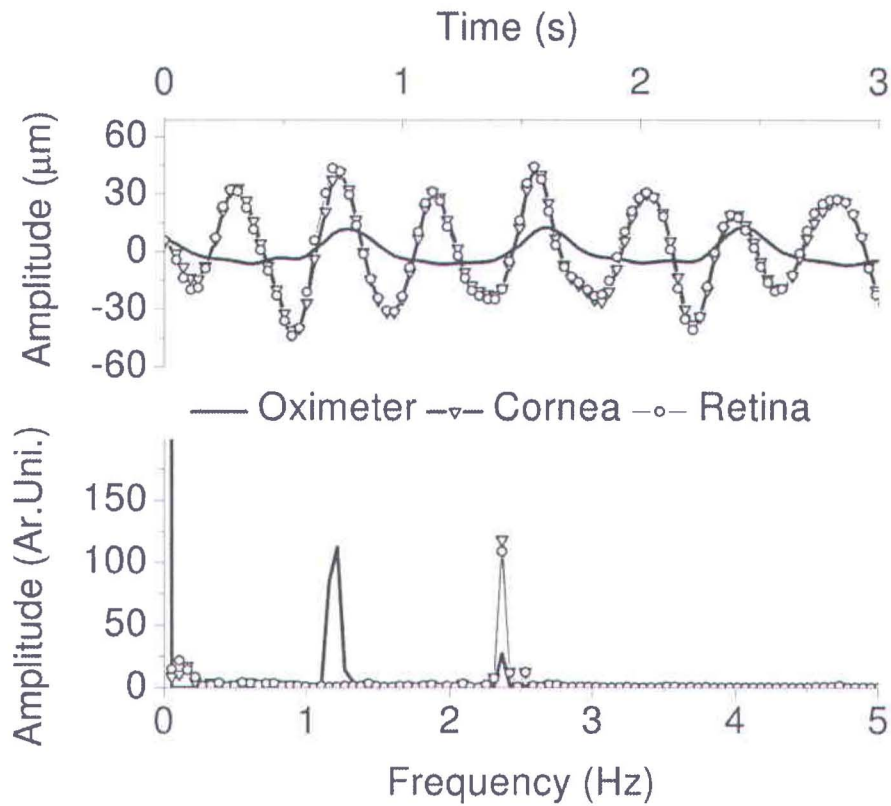
Figure 30. (TOP) The axial displacement of the retina and the cornea along with oximeter signal in time. (Bottom) Corresponding frequency spectrum.
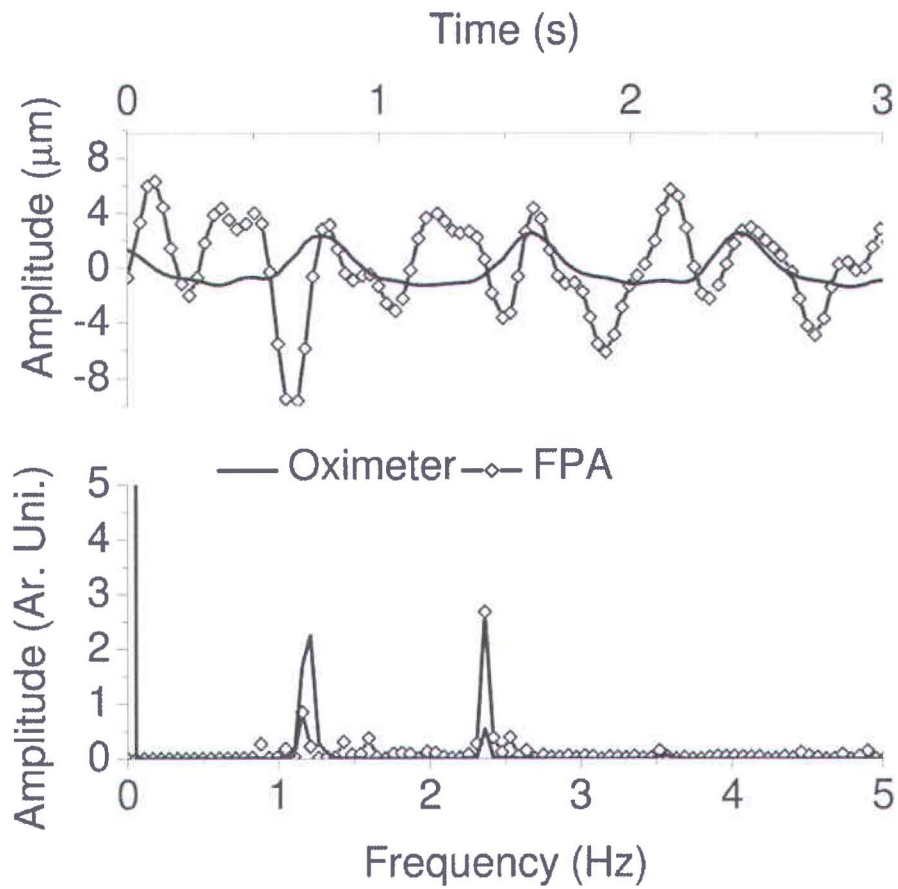
Figure 31. (TOP) Fundus pulse amplitude and oximeter signal along with (Bottom) frequency spectrum.

In Figure 31, the difference between the cornea and the retina movement, *i.e.* the FPA, and the corresponding frequency analysis are plotted. Both, Figure 30 and Figure 31 demonstrate the presence of harmonics in addition to the fundamental frequency of the heartbeat. It can also be observed in Figure 31 that FPA does not follow a perfectly regular pattern.

In order to validate this irregular pattern, the FPA for 20 consecutive A-Scans (covering 100 μm approximately) was measured. The FPA measured at each location was subtracted from the neighbor position, with a distance of

approximately 5 μm. Assuming that adjacent positions in the retina should exhibit equal FPA, the difference obtained provides an estimate of the error in the measurement.
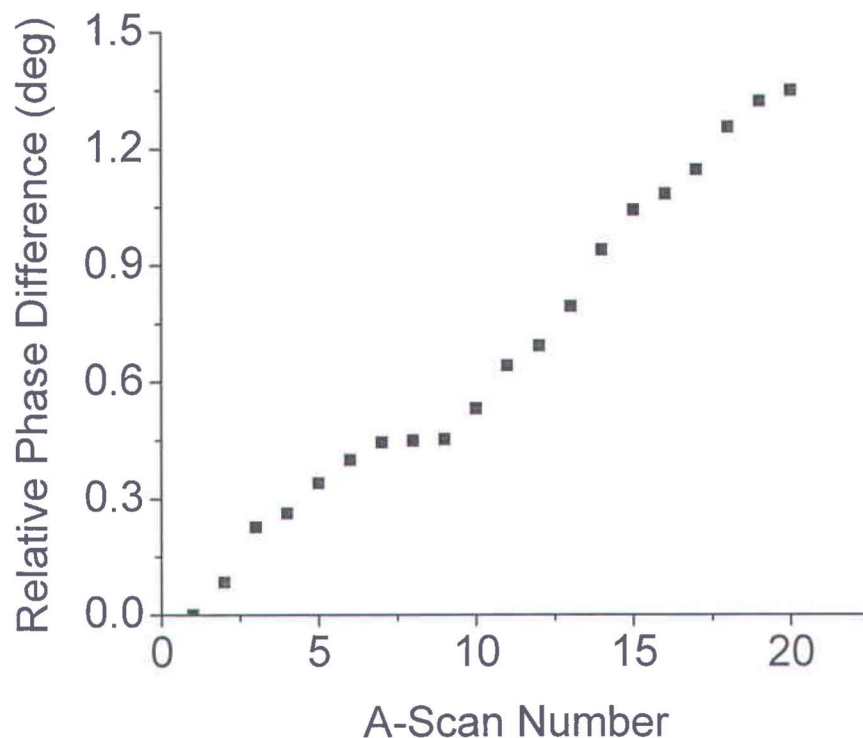
Figure 32. Phase difference of the movement at different A-Scans relative to the 1st A-Scan. The 1st A-Scan was chosen to be the center of the macula and then 20 consecutive A-Scans were taken on the temporal side.

The maximum measured peak-to-peak value of such difference in the FPA was 1.5 μm and SD was 0.7 μm. These values, after applying a band pass filter between 1 Hz and 5 Hz, are reduced to 1μm and 0.3 μm, respectively. This filter minimizes errors in the measurement, induced by lateral and axial eye shifts caused by head movements [88] and fixational eye movements. The phase of the

movements at these 20 consecutive locations was measured and it was found that the phase increased almost linearly with a phase difference of 1.4° between the 1st and the 20th A-Scan (Figure 32).

In Figure 33, the frequency components that describe the movements of the cornea, the retina and the FPA for all individuals as box plots, for the first 4 harmonics only are shown. After applying a t-test, the distributions obtained show significantly higher second harmonic components for both the retina (p=0.019) and the cornea (p=0.015), but a reduced contribution of this frequency for the FPA (p=0.707).
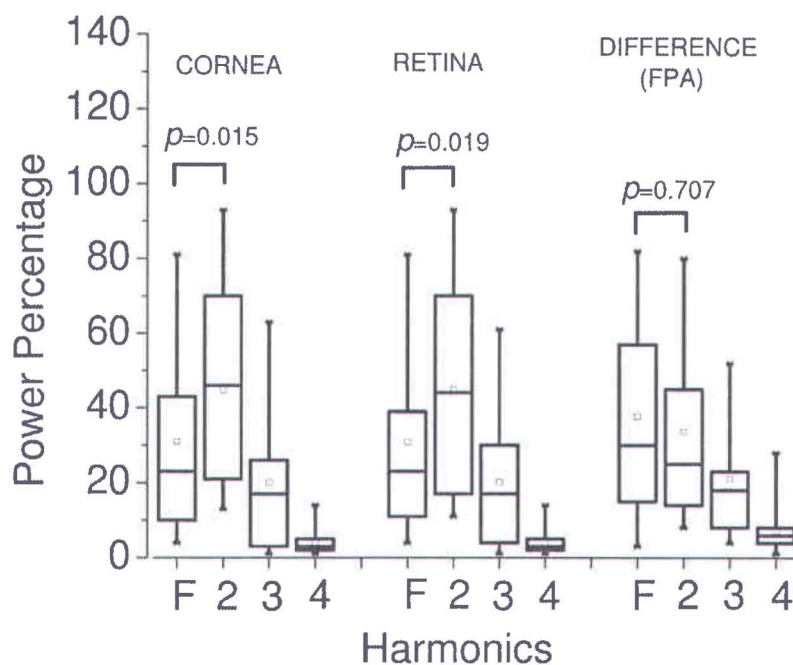
Figure 33. The movement of each ocular element was decomposed in frequencies and the amplitudes corresponding to each harmonic are compared. The results show that the second harmonic of the cardiac pulsation is the principal frequency of both the corneal and the retinal movement. The horizontal segments in the boxes indicate 95th, 75th, 50th, 25th and 5th percentiles (from top to bottom), the square inside the boxes represents the mean of the distribution, and the star symbols show the minima and maxima of the distributions. (Please see the Appendix 1 for detailed description of the box plots).

70

Finally, the root mean square (RMS) for these movements, which represent the effective movement amplitude, was calculated. For every measurement on a patient, at least 10 seconds of data was considered, corresponding to approximately 10 heart cycles. The computed mean ± SD for the RMS of the cohort, yielded 28±9 μm, 29±9μm and 4±2μm for cornea, retina and FPA, respectively (see Figure 34A).
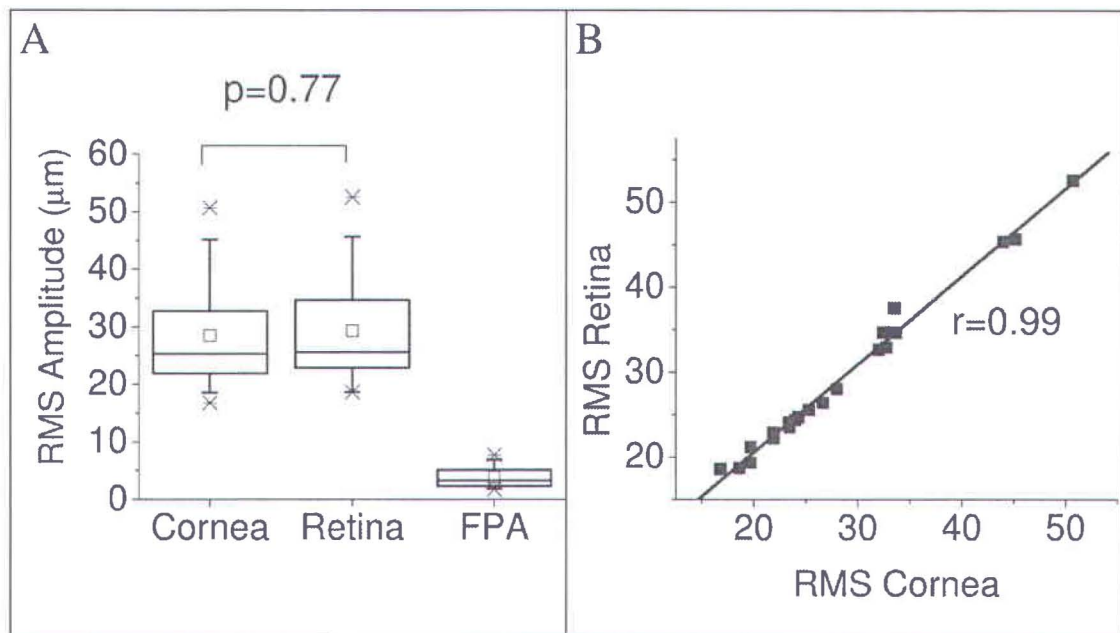
Figure 34. (A) Root mean square (RMS) values of the cornea, the retina and fundus pulse amplitude (FPA) movements. The horizontal segments in the boxes indicate 95th, 75th, 50th, 25th and 5th percentiles (from top to bottom), the square inside the boxes represents the mean of the distribution, and the star symbols show the minima and maxima of the distributions. (B) Cornea movement plotted with respect to the retina movement for each individual to show the correlation between the two.

Also, in Figure 34B, the RMS values of the retina movement with respect to the cornea movement for each individual are plotted. It was found that the cornea and the retina movements were highly correlated with each other (r=0.99). In all 21 subjects, after removing the data acquired during eye blinking, at least 10 cardiac

71

cycles in each measurement were analyzed. These results indicate that given the size of the sample cohort, there is no significant difference (p=0.77) between the amplitudes of the displacements of cornea and retina.

Nevertheless, FPA can be measured by subtracting the absolute positions of the cornea and the retina. The observation of FPA can be attributed to two facts, the difference between the amplitudes of the movement and the phase difference between the two movements. One such recording in which the phase delay between the cornea and the retina movement can be seen is shown in Figure 35.
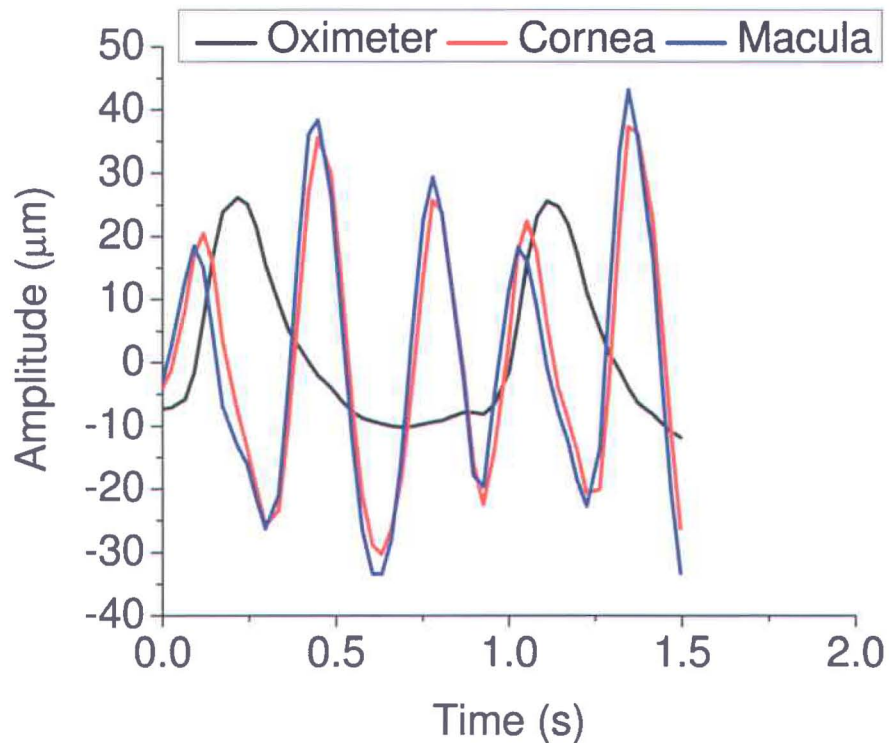
Figure 35. The movement of the cornea and the retina along with the oximeter signal. The movement of the retina precedes the movement of the macula.

Among all the individuals, the phase difference between the cornea and the macula movements varied between 1° and 20° for the fundamental frequency.

Such measured phase difference between the two tissues for all the individuals is shown in Figure 36 as box plots. The phase differences between the cornea and the retina movement, up to the third harmonic of the heartbeat were also calculated and were found to be 7°±3°, 6°±4° and 8°±4° for the fundamental, 2nd and 3rd harmonics, respectively.
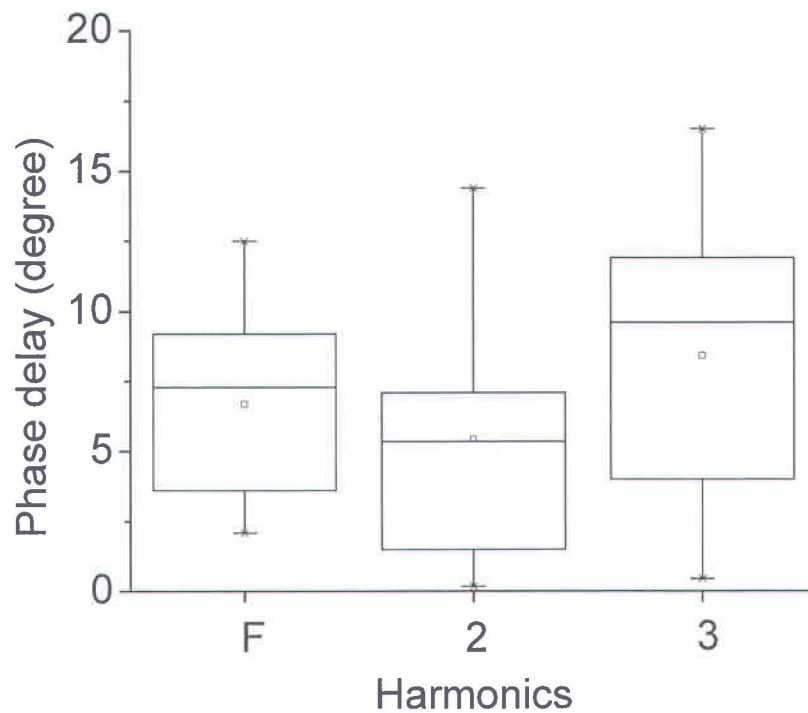
Figure 36. Phase delay between the cornea and the retina calculated for the first three harmonics of the axial shift.

4.5.2 Glaucoma verses non glaucoma subjects

The final objective of this thesis work was to measure the axial eye movements in glaucoma patients and compare it with the axial eye movements in normal

subjects. For this, 12 glaucoma patients and 10 age matched normal subjects were recruited at the Ophthalmology Department of the Maisonneuve-Rosemont Hospital in Montreal. The experiments were approved by the ethics committee of the Maisonneuve-Rosemont Hospital. All volunteers were informed about the procedure and the consequences and a written consent was obtained. Before the measurements were taken, all the subjects underwent a standard eye tests. The measurements for the IOP, axial length and the blood pressure were taken. Subjects with any sign of heart condition were excluded from this study.

Using the system described in the "Experimental design" section, B-Scans of the cornea at the apex and the retina across the optic disk were acquired for 20 consecutive seconds. Line scan or B-Scan on the retinal surface was estimated to be about 4.7 mm wide. Out of these B-Scans, the longitudinal movement of the cornea at apex, and the retina at the optic disc, peripapillary retina nasal side and peripapillary retina temporal side were measured. The location of these measurement points is shown in Figure 37.
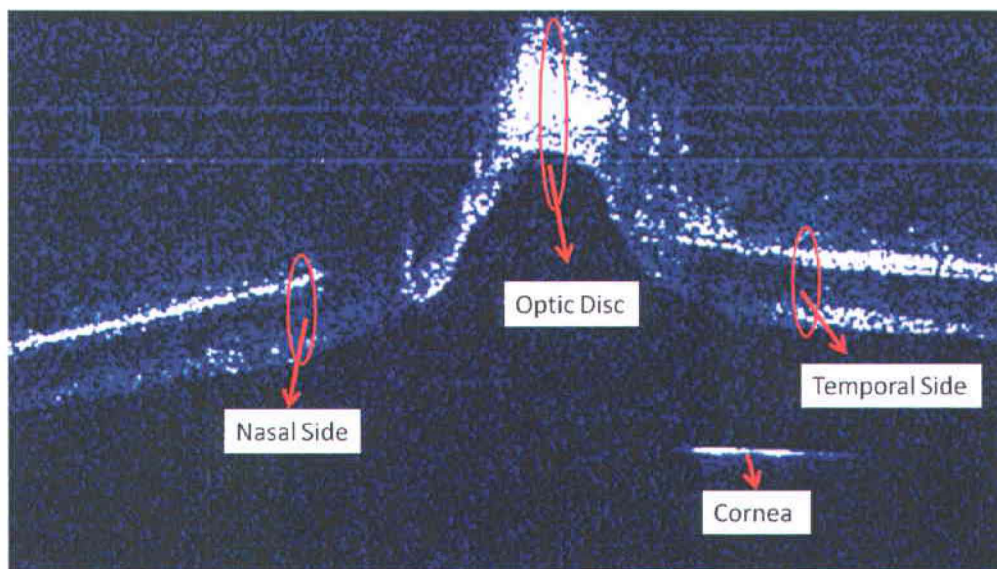
Figure 37. Different measurement points in the B-scan of the eye are shown. The optical path length of the reference mirrors were adjusted in order to bring the B-scan or the cornea and the retina in the same scan.

A typical recording of the measured movement is shown in Figure 38. From Figure 38, it can be seen that the different regions of the fundus and the cornea move with slightly different amplitude and phase. The root-mean-square value of the movements of the different ocular regions is shown in Figure 39. In normal subjects, the mean±SD of the RMS value of the movement was found to be
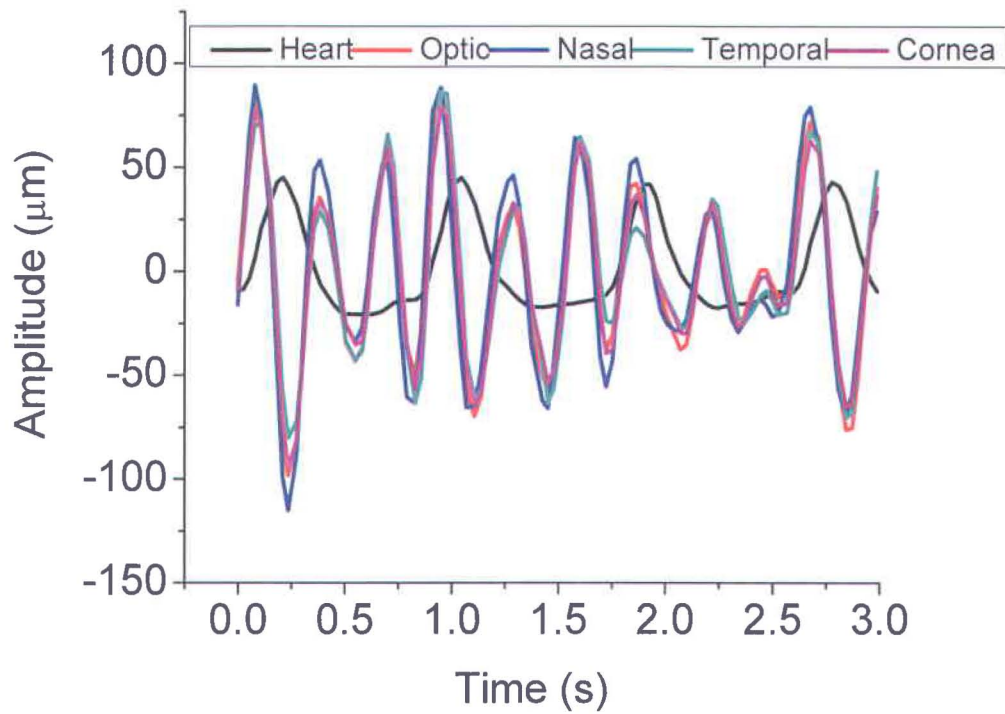
Figure 38. The axial movement of the different ocular elements along with the heart cycle.
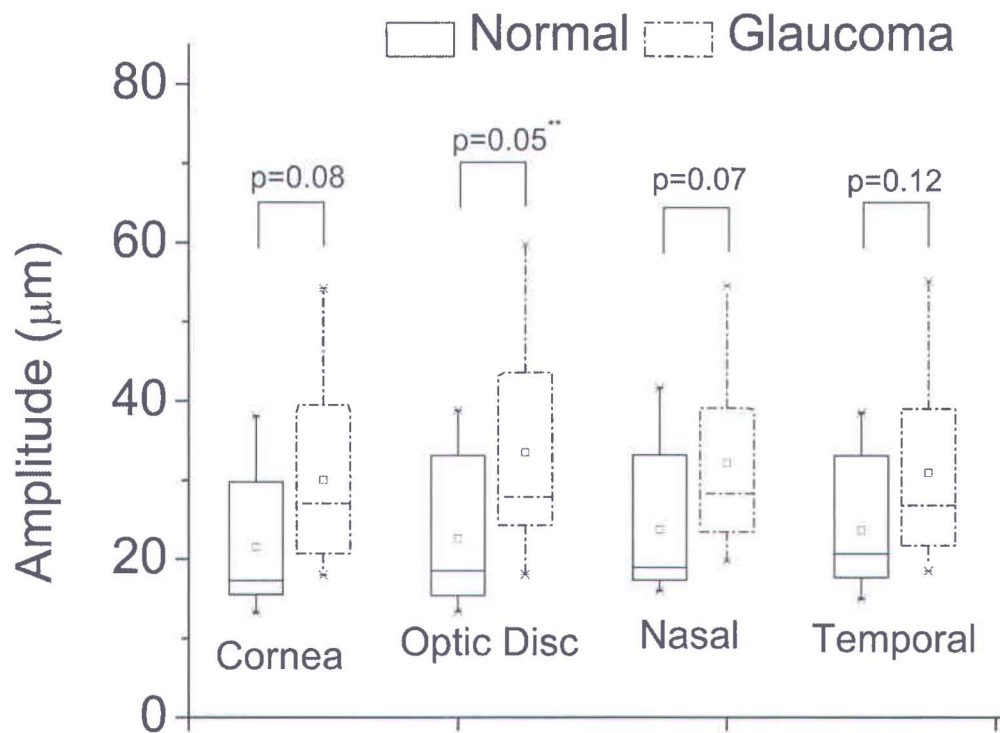
Figure 39. The root mean square (RMS) values of the axial movement of different ocular regions are shown as box plot.

21.5±9.1 μm, 22.5±9.9 μm 23.7±9.4 μm and 23.6±8.5 μm for the cornea, the optic disc, the nasal side and the temporal side, respectively. These readings in the glaucoma patients were found to be 29.9±11.8 μm, 33.5±13.9 μm, 32.2±11.1 μm and 30.9±11.5μm for the cornea, the optic disc, the nasal side and the temporal side, respectively. The mean values of the axial movement for different ocular regions were found to be higher in the glaucoma patients as compared to the normal patients and this difference was statistically significant for the optic disc with a *p*-value of 0.05.

Further, it was particularly desirable to estimate the local change in the tissue length in the optic disc area. This stretching over a period of time can be obtained

by subtracting of absolute position of the peripapillary retina from the position of the base of the optic disc cup. A typical recording of the tissue length change measured in a healthy volunteer is shown in Figure 40.
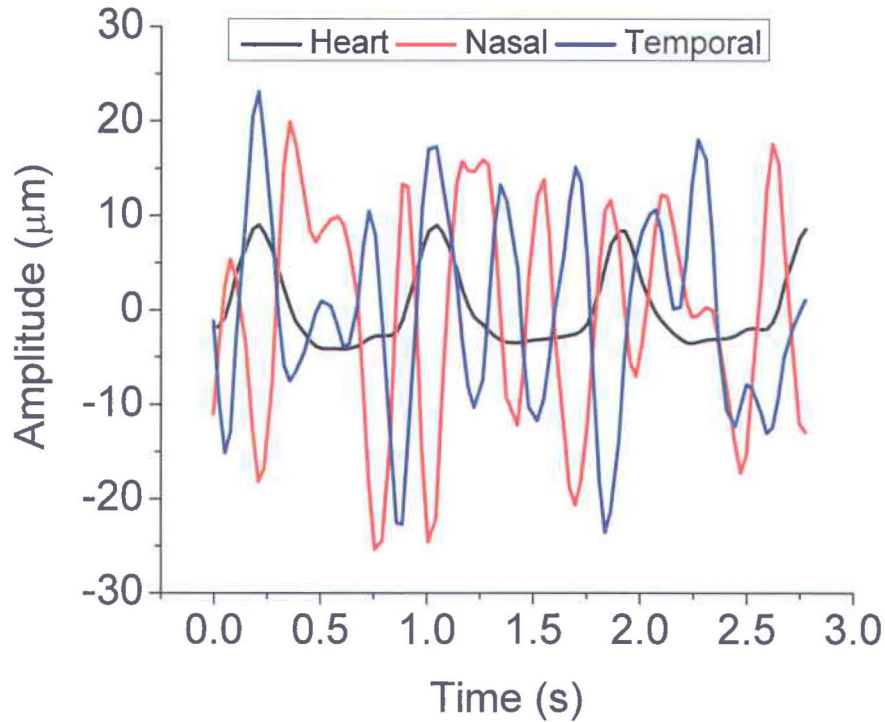
Figure 40. Local stretching of the ocular tissue measured on the temporal and nasal side of the optic disc. The stretching was calculated by subtracting the absolute position of the optic disc from the position of the temporal and the nasal peripapillary retina.

It can be seen from Figure 40, that there is local stretching in both the nasal and the temporal side of the optic disc. The stretching measured for all the subjects is shown in Figure 41. In normal subjects, the mean±SD RMS values were found to be 10.4±2.4 µm and 10.3±2.5 µm for the nasal and temporal side of optic disc, respectively. In the glaucoma patients, these values were found to be 13.4±5.7 µm

77

and 13.2±6.4 μm for the nasal and the temporal side of the optic disc, respectively. Similar to the individual ocular tissue movements, the mean values of the local tissue stretching around the optic disc is higher in glaucoma patients but the difference between the glaucoma patients and the normal subjects is not statistically significant. The standard deviations of our measurements were much larger in the glaucoma patients than in the normal subjects with a skew towards large deviations, so it is conceivable that a subgroup of glaucoma patients have a much larger tissue elongation than found in the normal group.
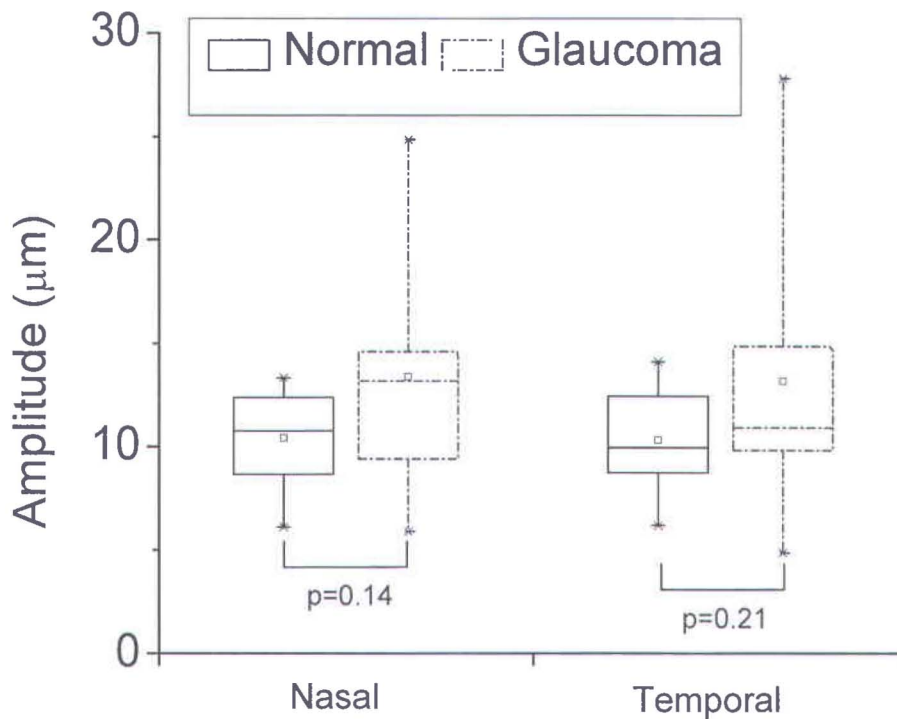
Figure 41. Root mean square (RMS) value of the tissue stretching. For each box different segments from top to bottom give 95th, 75th, 50th, 25th and 5th percentiles, the square in the box represents mean and stars at top and bottom shows the maxima and minima of the distribution.

Finally, the eye globe stretching i.e. change in the axial length was compared between the glaucoma and the non-glaucoma subjects. Such a comparison is shown in Figure 42.
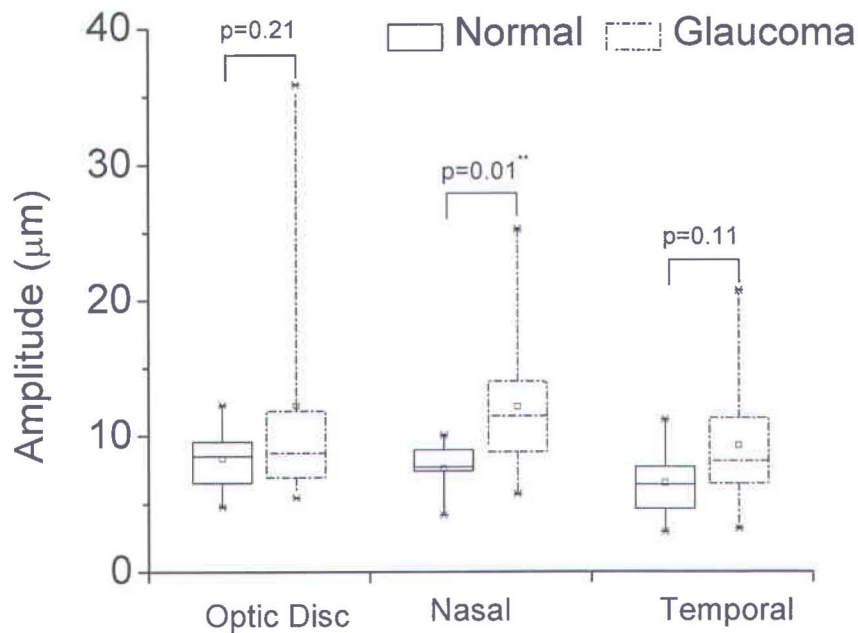
Figure 42. Eye globe stretching at different locations.

The mean±SD RMS values of the eye globe stretching at the optic disc, the nasal peripapillary retina and the temporal peripapillary retina were found to be 8.3±2.3 μm, 7.6±1.8 μm and 6.5±2.8 μm, respectively for the normal subjects, where as in glaucoma patients these values were 12.2±9.3 μm, 12.2±5.0 μm and 9.2±4.5 μm, respectively. The mean eye globe stretching values, found for the glaucoma patients were higher than the normal subjects and even significantly different on the nasal side with a p value of 0.01.

These results suggest that the ocular movements in the glaucoma patients are generally higher than the normal subjects. But given the size of the sample cohort, which included only 12 glaucoma and 10 normal subjects, a bigger clinical study is required to validate these results.

Chapter 5

Conclusion and discussion

During the course of this thesis work, different technologies were developed and tested with the aim to measure the axial ocular tissue movements. In the introductory chapter, it was hypothesized that such movements play an important role in the development of the glaucoma. In order to measure such movements, a technique, which could measure simultaneously the movement of the cornea and the different regions of the retina, with a resolution of at least 1 μm was required.

A review of the previous work related to the measurement of the ocular tissue movements suggested that, no such technology existed prior to this thesis work. Techniques based on ultrasonic transducers were limited to the measurement of the corneal movements only. The resolution of the ultrasound transducers in measuring such movements was shown to be about 2 μm. Laser interferometry was demonstrated to have displacement resolution of approximately 500 nm in ocular tissue displacement measurement. However, owing to the large coherence

length of the light source used in laser interferometry, axial movements of the retina or the cornea cannot be measured separately.

In the initial stages of this thesis work, a heterodyne laser interferometer was developed. This interferometer was tested on live rabbits and live rats. Similar to laser interferometry, with the heterodyne laser interferometer, the individual movements of the cornea or the retina could not be measured simultaneously. Different variants of laser interferometry were used to measure the fundus pulse amplitude, which is a term used to define the variation between the cornea and the retina distance. In these studies also, the origin of the fundus pulsations was ambiguous.

The ability of the low coherence interferometry, to measure the ocular tissue movements, separately from each other, was demonstrated by some groups. For example, Dragostinoff *et al.* [50] used low coherence interferometry to measure the FPA between the cornea and a particular layer of the retina with approximately 500 nm resolution. Although this technology had a sufficiently good displacement resolution, the individual movements of the cornea or the retina could not be recovered. Kasprzak *et al.* [53] demonstrated the use of Fourier domain optical coherence tomography, a variant of the low coherence interferometry, to measure the axial movements of the cornea, the ocular lens and the retina with a resolution of approximately 10 µm. Due to the limited measurement (depth) range of the technique, the movements of the ocular tissues could not be measured simultaneously. Hence no relation could be established between these movements. Also, the displacement resolution achieved by Kasperzak *et al.* was not sufficient to measure the FPA, which is of the order of few microns as demonstrated by Dragostinoff *et al.* [50]

5.1 Initial results on the rat eye

In order to circumvent the problems associated with the previous technologies, a system based on Spectral (Fourier) domain low coherence interferometry (SD-LCI) was developed. Longitudinal retinal and corneal displacements were successfully measured in live rats with SD–LCI, working at an acquisition speed of 100 Hz with displacement precision of 400 nm. This instrument showed a significant improvement in terms of the precision and the acquisition speed, compared with the previous works [53, 89]. Along with these works, the results presented in the study showed a correlation between the kinematics of the eye and the cardiovascular system.

Further, this work provided a new finding in understanding the ocular hemodynamics. Since the oximeter signal could be used as an external reference, the retinal and corneal movements were compared directly. It became clear from the results that the predominant direction of the retinal and the corneal movement relative to the systole and diastole is the same, and the phase of the two movements is approximately similar. Therefore, the results showed that with every heartbeat, the retina and the cornea are both moving together, forward and backward. The results thus provided elements of answer to the hypothesis formulated by Kasprzak *et al.* [53, 89] from previous results, which mentioned that the cornea and the retina were either moving in the same or the opposite direction. Based on the results, it could certainly be confirmed that the cornea and the retina move in the same direction. However, it was not clear if the retina and the cornea were moving with different amplitudes, thus generating the ocular pulsation.

Because measurements were made at different time points, the initially developed system only allowed the measurement of the mean ocular pulsation using the mean movement amplitude of each individual layer. In the present experiment, the mean peak-to-peak amplitudes of 3.7 ± 0.6 μm and 3.1 ± 0.7 μm for the retina and

83

the cornea, respectively, were obtained, which were essentially identical considering the standard deviation of the data. Furthermore, the effective amplitudes of 1.10 μm and 1.36 μm found respectively for the retina and the cornea did not show significant differences, considering the standard deviation of the data and the precision of the instrument (400 nm). Therefore, it was difficult to comment on the rat eye deformation from the experiment achieved with the system. Nevertheless, as the ocular pulsatility in humans was found to be about 2 μm to 8 μm [50], it was expected that the SD-LCI system would be able to measure it in humans with a precision of 400 nm.

It should also be noted that the initially developed equipment required two different measurements (one at the retina, and the other at the cornea) that were performed at different times. Therefore, this could also complicate the understanding of the exact relationship between the two movements. It was of great interest to modify the SD-LCI and measure simultaneously the retinal and the corneal movement. In addition to the phase of the relative movement between the retina and the cornea, this revised equipment was also expected to determine the magnitude of the FPA. As such, it was demonstrated that the SD-OCT technique is promising for measuring ocular pulsation, but further improvement was necessary.

5.2 Results on the Human eye

With the initially developed equipment, the ability of the FD-LCI to measure the ocular tissue movements with submicron displacement resolution was demonstrated in live animals. In order to measure the corneal and the retinal movements simultaneously in human subjects, the SD-LCI system was modified by adding two reference arms and a lens with a hole in the center. The system was tested on normal subjects, recruited from the Research Center of the

Maisonneuve-Rosemont Hospital, and then a comparative study between the glaucoma and the normal subjects was performed.

The developed system could successfully measure the longitudinal movements of the cornea and the retina simultaneously with micron accuracy at video rates. The results that were obtained with this system allowed for the first time and with a high degree of certainty the conclusion that the cornea and retina move with a small phase difference and almost equal amplitudes during the cardiac pulsations.

A comparison of the ocular movements between the glaucoma and the non-glaucoma subjects suggest that the axial movements of the individual ocular tissues (such as corneal and retinal movements) in glaucoma patients are greater than in normal although the difference was statistically significant only for the optic disc in our pilot study.

The tissue elongation between two points, one on the peripapillary retina and the other on the base of the cup of the optic disk was measured. It was found that the mean elongation during systole was of the order of 10 μm. This data suggests, for the first time, that the nerve fibre layer, which runs just under the retinal internal limiting membrane, may actually be stretching over the course of the cardiac cycle. These measurements were made in normal subjects as well as in glaucoma patients. The data suggests that the mean tissue stretching is higher in glaucoma patients as compared to normal subjects, but no statistically significant difference was yet observed.

Although it would be interesting to measure the phase of the axial movement at different locations of the retina, such measurements were not done in this work. It has been shown previously that movements of the ocular tissues consist of heart frequency and its harmonics. This makes it difficult to give a value to the phase of the movement unless a phase value for each of the frequency component is given. The quantity of interest was the local ocular tissue stretching. For measuring such stretching, phase values are not required as it can be obtained by subtracting the instantaneous values of the movement of the different ocular regions.

The data on the eye globe stretching, also known as fundus pulse amplitude (FPA), suggests that the mean value of the FPA is higher in glaucoma patients as compared to the age matched normal people. The FPA on the nasal side was found to be significantly higher in glaucoma patients. Given the size of the sample population, which included only 12 glaucoma and 10 normal subjects, it remains to be established whether this elongation contributes to axonal damage in glaucoma. Nevertheless, in our pilot study, the standard deviations of the measurements were much larger in the glaucoma patients than in the normal subjects, suggesting that glaucoma patients have a much larger tissue elongation than found in the normal group.

Most of the literature on axonal stretching in the optic nerve relates to acute traumatic injury. The effect of smaller changes that repeat tens of thousands of times per day and tens of millions of times per year is unknown. Previous studies [90, 91] indicate that neural axons can sustain stretching up to 30% of their original length without being damaged. One might argue then: Is the tissue stretching of approximately 10 μm observed in this work, sufficient enough to cause axonal damage in glaucoma? Given the number of occurrences of such small movements in a 40 to 50 year of life span of a person when the glaucoma starts to show its signs, the answer is, maybe such movements do play a role in glaucoma. If such stretching does play a role, it could be either by a greater amplitude being present or by a greater susceptibility to stretch in certain individuals. The fact that ocular pulsatility increases with increasing intra ocular pressure (IOP) [92] as well as with decreasing ocular perfusion pressure [44], two of the major risk factors for glaucoma [93] suggests that this mechanism is worthy of further investigation.

The developed system was able to measure the corneal and retinal movements as well as the FPA. Frequency components up to the 7th harmonic of the cardiac cycle were observed in the axial movements of the ocular tissues. The dominant frequency component for both the cornea and the retina movements was found to be the second harmonic; while there was almost equal contribution from the

fundamental and the second harmonic frequencies to the FPA. This is in agreement with previous results of Kasprzak *et al.* [53], where the dominant frequency component was found to be the second harmonic of the heart beat for both the cornea and the retina. One possible explanation for why the second harmonic is less dominant in the FPA is that for the cornea and the retina, there is a pulse with the choroidal pulse and another with the orbital pulse, therefore two movements per heartbeat, but for the FPA, there is only the choroidal pulse, because when the orbital pulse occurs the cornea and the retina move together. Regarding a previous study[50] that showed that the FPA occurs at the fundamental frequency of the heartbeat, the results indicate that it is not just the fundamental frequency that contributes to the FPA, but other frequencies are also present and can be dominant.

So far, the mechanical properties of the ocular elements that move at harmonic frequencies of the heartbeat have not been addressed. Some studies, which were related to the pulsatile blood flow measured in the arteries close to the heart, attributed the presence of frequency harmonics to the tissue properties such as stiffness [94-96]. The technology that was developed in this work provides a straightforward manner to characterize these movements and to build physical models that explain the dynamics observed in the eye. It will allow a better understanding of the mechanical forces that interact within the eye during the cardiac cycle, and their relevance to ocular pathology. For instance, the system can be used to study the eye length, which is of particular importance in myopia studies [97]. The FPA measured with the system could also help in diagnosis of age related macular degeneration [98]. Furthermore, by tuning the wavelength of the laser source to improve penetration, the device could accurately describe the pulsatility of the choroid.

5.3 Limitations

There are few limitations of the developed system. For example, the data acquisition performed by the system is only along a line. Although the movements of the eye along the scanning line can be corrected using this scanning pattern, the movements of the eye along the non-scanning axis will introduce errors in the measurement. Such error can only be corrected if the data is acquired over an area and not along a single line. Such measurements were not feasible with the present system due to technical limitations, such as slow acquisition speed of the camera and requirement of high data sample rate.

Further, the signal to noise ratio of the developed system was not adequate enough to identify all the layers of the ocular structure such as retina. Thus in this study, the average movement of the ocular tissues was measured. Any relative movement between the different layers of the ocular structure such as between the lamina cribrosa and the prelaminar tissue was not taken into account. No such study on the relative movement between the layers of the ocular tissues has been done yet. Improved signal to noise ratio and a layer segmentation technique along with the designed instrument in this work might help in acquiring such data.

5.4 Conclusion

In conclusion, with a custom-designed FD-OCT system, simultaneous measurement of the cornea and the retina position, with high accuracy and for long periods of time was achieved, allowing for the first time a precise description of the eye's pulsatility. The elongation of the neuroretinal tissue at and around the optic nerve head was measured for the first time and there was evidence that there was some stretching of this tissue coincident with the ocular pulse. The developed device also provides means of studying a whole new aspect of glaucoma, which is the role of the biomechanical properties of the eye in the

glaucoma. Although the number of the subjects used for glaucoma study was still limited, the results give the first indication that the biomechanical properties have at least some role to play in glaucoma. A more extensive ongoing clinical study will provide more conclusive evidences on this hypothesis.

References

1. Perruccio AV, Badley EM, Trope GE: **Self-reported glaucoma in Canada: findings from population-based surveys, 1994-2003**. *Can J Opthalmol-J Can Opthalmol* 2007, **42**(2):219-226.
2. Quigley HA, Broman AT: **The number of people with glaucoma worldwide in 2010 and 2020**. *British Journal of Ophthalmology* 2006, **90**(3):262-267.
3. Iskedjian M, Walker J, Vicente C, Trope GE, Buys Y, Einarson TR, Covert D: **Cost of glaucoma in Canada: Analyses based on visual field and physician's assessment**. *J Glaucoma* 2003, **12**(6):456-462.
4. Brubaker R: **Adler's Physiology of the Eye**. *Arch Ophthalmol* 1976, **94**(7):1239-a-1240.
5. Lavanya R, Teo L, Friedman DS, Aung HT, Baskaran M, Gao H, Alfred T, Seah SK, Kashiwagi K, Foster PJ *et al*: **Comparison of anterior chamber depth measurements using the IOLMaster, scanning peripheral anterior chamber depth analyser, and anterior segment optical coherence tomography**. *British Journal of Ophthalmology* 2007, **91**(8):1023-1026.
6. Lee Ann R: **Chapter 4 - Retina**. In: *Clinical Anatomy of the Visual System (Second Edition)*. edn. Saint Louis: Butterworth-Heinemann; 2005: 55-86.
7. Quigley HA: **Open-Angle Glaucoma**. *New England Journal of Medicine* 1993, **328**(15):1097-1106.
8. Plange N, Kaup M, Weber A, Harris A, Arend KO, Remky A: **Performance of colour Doppler imaging discriminating normal tension glaucoma from healthy eyes**. *Eye* 2009, **23**(1):164-170.
9. Butt Z, Obrien C, McKillop G, Aspinall P, Allan P: **Color Doppler imaging in untreated high- and normal-pressure open-angle glaucoma**. *Invest Ophthalmol Vis Sci* 1997, **38**(3):690-696.
10. Harris A, Sergott RC, Spaeth GL, Katz JL, Shoemaker JA, Martin BJ: **COLOR DOPPLER ANALYSIS OF OCULAR VESSEL BLOOD VELOCITY IN NORMAL-TENSION GLAUCOMA**. *Am J Ophthalmol* 1994, **118**(5):642-649.
11. Hollows FC, Graham PA: **Intra-ocular pressure, glaucoma, and glaucoma suspects in a defined population**. *Br J Ophthalmol* 1966, **50**:570-586.
12. Goldmann H, Schmidt T: **Ueber Applanationstonometrie**. *Ophthalmologica* 1957:134:221–142.
13. Kniestedt C, Nee M, Stamper RL: **Dynamic contour tonometry: a comparative study on human cadaver eyes**. *Arch Ophthalmol* 2004, **122**(9):1287-1293.

14. Yagci R, Eksioglu U, Midillioglu I, Yalvac I, Altiparmak E, Duman S: **Central corneal thickness in primary open angle glaucoma, pseudoexfoliative glaucoma, ocular hypertension, and normal population**. *Eur J Ophthalmol* 2005, **15**(3):324-328.

15. Schneider E, Kanngiesser HE, Kniestedt C: **Dynamic Contour Tonometry, Glaucoma**. In., edn. Edited by Grehn F, Stamper R: Springer Berlin Heidelberg; 2006: 47-63.

16. Kotecha A, White ET, Shewry JM, Garway-Heath DF: **The relative effects of corneal thickness and age on Goldmann applanation tonometry and dynamic contour tonometry**. *British Journal of Ophthalmology* 2005, **89**(12):1572-1575.

17. Jorge J, Diaz-Rey JA, Gonzalez-Meijome JM, Almeida JB, Parafita MA: **Clinical performance of the Reichert AT550: a new non-contact tonometer**. *Ophthalmic Physiol Opt* 2002, **22**(6):560-564.

18. Jorge J, Gonzalez-Meijome JM, Diaz-Rey JA, Almeida JB, Ribeiro P, Parafita MA: **Clinical performance of non-contact tonometry by Reichert AT550 (R) in glaucomatous patients**. *Ophthalmic Physiol Opt* 2003, **23**(6):503-506.

19. Langham ME, McCarthy E: **A Rapid Pneumatic Applanation Tonometer: Comparative Findings and Evaluation**. *Arch Ophthalmol* 1968, **79**(4):389-399.

20. Chauhan BC, McCormick TA, Nicolela MT, LeBlanc RP: **Optic Disc and Visual Field Changes in a Prospective Longitudinal Study of Patients With Glaucoma: Comparison of Scanning Laser Tomography With Conventional Perimetry and Optic Disc Photography**. *Arch Ophthalmol* 2001, **119**(10):1492-1499.

21. Huang D, Swanson E, Lin C, Schuman J, Stinson W, Chang W, Hee M, Flotte T, Gregory K, Puliafito C *et al*: **Optical coherence tomography**. *Science* 1991, **254**(5035):1178-1181.

22. Jonas JB, Mardin CY, Gründler AE: **Comparison of measurements of neuroretinal rim area between confocal laser scanning tomography and planimetry of photographs**. *British Journal of Ophthalmology* 1998, **82**(4):362-366.

23. Klein BE, Klein R, Sponsel WE, Franke T, Cantor LB, Martone J, Menage MJ: **Prevalence of glaucoma. The Beaver Dam Eye Study**. *Ophthalmology* 1992, **99**(10):1499-1504.

24. MITCHELL P, SMITH W, ATTEBO K, HEALEY PR: **Prevalence of open-angle glaucoma in Australia : The blue mountains eye study**, vol. 103. New York, NY, ETATS-UNIS: Elsevier; 1996.

25. Kamal DS, Garway-Heath DF, Hitchings RA, Fitzke FW: **Use of sequential Heidelberg retina tomograph images to identify changes at the optic disc in ocular hypertensive patients at risk of developing glaucoma**. *British Journal of Ophthalmology* 2000, **84**(9):993-998.

26. Grieshaber MC, Mozaffarieh M, Flammer J: **What Is the Link Between Vascular Dysregulation and Glaucoma?** *Survey of Ophthalmology* 2007, **52**(6, Supplement 1):S144-S154.

27. Harris A, Rechtman E, Siesky B, Jonescu-Cuypers C, McCranor L, Garzozi HJ: **The role of optic nerve blood flow in the pathogenesis of glaucoma**. *Ophthalmology clinics of North America* 2005, **18**(3):345-353, v.

28. Delaey C, Van De Voorde J: **Regulatory mechanisms in the retinal and choroidal circulation**. *Ophthalmic research* 2000, **32**(6):249-256.

29. Quigley HA, Nickells RW, Kerrigan LA, Pease ME, Thibault DJ, Zack DJ: **Retinal ganglion cell death in experimental glaucoma and after axotomy occurs by apoptosis**. *Invest Ophthalmol Vis Sci* 1995, **36**(5):774-786.

30. Nickells RW: **Apoptosis of Retinal Ganglion Cells in Glaucoma: An Update of the Molecular Pathways Involved in Cell Death**. *Survey of Ophthalmology* 1999, **43**(Supplement 1):S151-S161.

31. Trew DR, Smith SE: **Postural studies in pulsatile ocular blood flow: II. Chronic open angle glaucoma**. *Br J Ophthalmol* 1991, **75**(2):71-75.

32. Schwenn O, Troost R, Vogel A, Grus F, Beck S, Pfeiffer N: **Ocular pulse amplitude in patients with open angle glaucoma, normal tension glaucoma, and ocular hypertension**. *British Journal of Ophthalmology* 2002, **86**(9):981-984.

33. Ravalico G, Pastori G, Toffoli G, Crocé M: **Visual and blood flow responses in low-tension glaucoma**. *Survey of Ophthalmology* 1994, **38**(Supplement 1):S173-S176.

34. James CB, Smith SE: **Pulsatile ocular blood flow in patients with low tension glaucoma**. *British Journal of Ophthalmology* 1991, **75**(8):466-470.

35. Butt Z, McKillop G, Obrien C, Allan P, Aspinall P: **MEASUREMENT OF OCULAR BLOOD-FLOW VELOCITY USING COLOR DOPPLER IMAGING IN LOW-TENSION GLAUCOMA**. *Eye* 1995, **9**:29-33.

36. Johnson CA, Adams AJ, Casson EJ, Brandt JD: **Blue-on-Yellow Perimetry Can Predict the Development of Glaucomatous Visual Field Loss**. *Arch Ophthalmol* 1993, **111**(5):645-650.

37. Albon J, Purslow PP, Karwatowski WSS, Easty DL: **Age related compliance of the lamina cribrosa in human eyes**. *British Journal of Ophthalmology* 2000, **84**(3):318-323.

38. Levy NS, Crapps EE, Bonney RC: **Displacement of the Optic Nerve Head: Response to Acute Intraocular Pressure Elevation in Primate Eyes**. *Arch Ophthalmol* 1981, **99**(12):2166-2174.

39. Lesk MR, Spaeth GL, Azuara-Blanco A, Araujo SV, Katz LJ, Terebuh AK, Wilson RP, Moster MR, Schmidt CM: **Reversal of optic disc cupping after glaucoma surgery analyzed with a scanning laser tomograph**. *Ophthalmology* 1999, **106**(5):1013-1018.

40. Raitta C, Tomita G, Vesti E, Harju M, Nakao H: **Optic disc topography before and after trabeculectomy in advanced glaucoma**. *Ophthalmic Surg Lasers* 1996, **27**(5):349-354.

41. Burgoyne CF, Quigley HA, Thompson HW, Vitale S, Varma R: **Early changes in optic disc compliance and surface position in experimental glaucoma**. *Ophthalmology* 1995, **102**(12):1800-1809.

42. Lesk MR, Hafez AS, Descovich D: **Relationship between central corneal thickness and changes of optic nerve head topography and blood flow after intraocular pressure reduction in open-angle glaucoma and ocular hypertension**. *Archives of Ophthalmology* 2006, **124**(11):1568-1572.

43. Yan DB, Flanagan JG, Farra T, Trope GE, Ethier CR: **Study of regional deformation of the optic nerve head using scanning laser tomography**. *Curr Eye Res* 1998, **17**(9):903-916.

44. Kiss B, Dallinger S, Polak K, Findl O, Eichler H-G, Schmetterer L: **Ocular Hemodynamics during Isometric Exercise**. *Microvascular Research* 2001, **61**(1):1-13.

45. Silver DM, Farrell RA: **Validity of pulsatile ocular blood flow measurements**. *Surv Ophthalmol* 1994, **38 Suppl**:S72-80.

46. Hommer A, Fuchsjager-Mayrl G, Resch H, Vass C, Garhofer G, Schmetterer L: **Estimation of ocular rigidity based on measurement of pulse amplitude using pneumotonometry and fundus pulse using laser interferometry in glaucoma**. *Invest Ophthalmol Vis Sci* 2008, **49**(9):4046-4050.

47. Friedenwald J: **Contribution to the theory and practice of tonometry**. *Am J Ophthalmol* 1937, **20**:985-1024.

48. Zuckerman JL, Taylor KD, Grossman HJ: **Noncontact detection of ocular pulse--correlation with carotid stenosis**. *Invest Ophthalmol Vis Sci* 1977, **16**(11):1018-1024.

49. Fercher AF: **Invivo Measurement of Fundus Pulsations by Laser Interferometry**. *IEEE Journal of Quantum Electronics* 1984, **20**(12):1469-1471.

50. Dragostinoff N, Werkmeister RM, Groschl M, Schmetterer L: **Depth-resolved measurement of ocular fundus pulsations by low-coherence tissue interferometry**. *J Biomed Opt* 2009, **14**(5):054047.

51. Fercher AF, Mengedoht K, Werner W: **Eye-length measurement by interferometry with partially coherent light**. *Optics Letters* 1988, **13**(3):186-188.

52. Schmetterer LF, Lexer F, Unfried CJ, Sattmann H, Fercher AF: **Topical Measurement of Fundus Pulsations**. *Optical Engineering* 1995, **34**(3):711-716.

53. Kasprzak H, Iskander DR, Bajraszewski T, Kowalczyk A, Nowak-Szczepanowska W: **High accuracy measurement of spectral characteristics of movements of the eye elements**. *Optica Pura Y Aplicada* 2007, **70**(1):7-11.

54. Kowalska MA, Kasprzak HT, Iskander DR: **Comparison of high-speed videokeratoscopy and ultrasound distance sensing for measuring the longitudinal corneal apex movements**. *Ophthalmic Physiol Opt* 2009, **29**(3):227-234.

55. Kowalska MA, Kasprzak HT, Iskander DR, Danielewska M, Mas D: **Ultrasonic in vivo measurement of ocular surface expansion**. *IEEE transactions on bio-medical engineering* 2011, **58**(3):674-680.

56. Kowalska MA, Kasprzak HT, Iskander DR: **Ultrasonic measurement of binocular longitudinal corneal apex movements and their correlation to cardiopulmonary system**. *Biocybernetics and Biomedical Engineering* 2008, **28**(3):35-43.

57. Fercher AF, Hitzenberger CK, Kamp G, El-Zaiat SY: **Measurement of intraocular distances by backscattering spectral interferometry**. *Optics Communications* 1995, **117**(1-2):43-48.

58. Singh K, Dion C, Costantino S, Wajszilber M, Lesk MR, Ozaki T: **Development of a novel instrument to measure the pulsatile movement of ocular tissues**. *Experimental Eye Research* 2010, **91**(1):63-68.

59. Wojtkowski M, Srinivasan VJ, Ko TH, Fujimoto JG, Kowalczyk A, Duker JS: **Ultrahigh-resolution, high-speed, Fourier domain optical coherence tomography and methods for dispersion compensation**. *Optics Express* 2004, **12**(11):2404-2422.

60. Izatt JA, Kulkarni MD, Wang H-W, Kobayashi K, Jr. MVS: **Optical Coherence Tomography and Microscopy in Gastrointenstinal Tissues**. *IEEE Journal of Selected Topics In Quantum Electronics* 1996, **2**(4):1017-1028.

61. Delori FC, Webb RH, Sliney DH: **Maximum permissible exposures for ocular safety (ANSI 2000), with emphasis on ophthalmic devices**. *J Opt Soc Am A-Opt Image Sci Vis* 2007, **24**(5):1250-1265.

62. Wukitsch MW, Petterson MT, Tobler DR, Pologe JA: **Pulse oximetry: Analysis of theory, technology, and practice**. *Journal of Clinical Monitoring and Computing* 1987, **4**(4):290-301.

63. Grecco HE, Martínez OE: **Calibration of Subnanometer Motion with Picometer Accuracy**. *Appl Opt* 2002, **41**(31):6646-6650.

64. Costantino S, Martinez OE, Torga JR: **Wide band interferometry for thickness measurement**. *Optics Express* 2003, **11**(8):952-957.

65. Srinivasan VJ, Ko TH, Wojtkowski M, Carvalho M, Clermont A, Bursell SE, Song QH, Lem J, Duker JS, Schuman JS *et al*: **Noninvasive volumetric Imaging and morphometry of the rodent retina with high-speed, ultrahigh-resolution optical coherence tomography**. *Invest Ophthalmol Vis Sci* 2006, **47**(12):5522-5528.

66. Schmucker C, Schaeffel F: **A paraxial schematic eye model for the growing C57BL/6 mouse**. *Vision Research* 2004, **44**(16):1857-1867.

67. Remtulla S, Hallett PE: **A schematic eye for the mouse, and comparisons with the rat**. *Vision Research* 1985, **25**(1):21-31.

68. Mori F, Konno S, Hikichi T, Yamaguchi Y, Ishiko S, Yoshida A: **Pulsatile ocular blood flow study: decreases in exudative age related macular degeneration**. *British Journal of Ophthalmology* 2001, **85**(5):531-533.

69. Perkins ES: **The ocular pulse and intraocular pressure as a screening test for carotid artery stenosis**. *British Journal of Ophthalmology* 1985, **69**(9):676-680.

70. Zuckerman JL, Taylor KD, Grossman HJ: **Noncontact detection of ocular pulse--correlation with carotid stenosis**. *Investigative Ophthalmology & Visual Science* 1977, **16**(11):1018-1024.

71. McDonald PT, Rich NM, Collins GJJ, Kozloff L, Andersen CA: **Ocular Pneumoplethysmography: Detection of Carotid Occlusive Disease**. *Annals of Surgery* 1979, **189**(1):44-48.

72. Fontana L, Poinoosawmy D, Bunce CV, O'Brien C, Hitchings RA: **Pulsatile ocular blood flow investigation in asymmetric normal tension glaucoma and normal subjects**. *British Journal of Ophthalmology* 1998, **82**(7):731-736.

73. Bosley TM, Savino PJ, Sergott RC, Eagle RC, Sandy R, Gee W: **Ocular Pneumoplethysmography Can Help in the Diagnosis of Giant-Cell Arteritis**. *Arch Ophthalmol* 1989, **107**(3):379-381.

74. Evans D, Hosking S, Embleton S, Morgan A, Bartlett J: **Spectral content of the intraocular pressure pulse wave: glaucoma patients versus normal subjects**. *Graefe's Archive for Clinical and Experimental Ophthalmology* 2002, **240**(6):475-480.

75. Schmidt K-G, von Rückmann A, Kemkes-Matthes B, Hammes H-P: **Ocular pulse amplitude in diabetes mellitus**. *British Journal of Ophthalmology* 2000, **84**(11):1282-1284.

76. Wang M, Munch IC, Hasler PW, Prünte C, Larsen M: **Central serous chorioretinopathy**. *Acta Ophthalmologica* 2008, **86**(2):126-145.

77. Tittl M, Polska E, Kircher K, Kruger A, Maar N, Stur M, Schmetterer L: **Topical Fundus Pulsation Measurement in Patients With Active Central Serous Chorioretinopathy**. *Arch Ophthalmol* 2003, **121**(7):975-978.

78. Silver DM, Farrell RA, Langham ME, O'Brien V, Schilder P: **Estimation of pulsatile ocular blood flow from intraocular pressure**. *Acta Ophthalmologica* 1989, **67**(S191):25-29.

79. Langham ME, To'mey KF: **A clinical procedure for the measurements of the ocular pulse-pressure relationship and the ophthalmic arterial pressure**. *Experimental Eye Research* 1978, **27**(1):17-25.

80. Kniestedt C, Kanngiesser H: **Dynamische Konturtonometrie**. *Der Ophthalmologe* 2006, **103**(8):713-723.

81. Punjabi OS, Kniestedt C, Stamper RL, Lin SC: **Dynamic contour tonometry: principle and use**. *Clinical & Experimental Ophthalmology* 2006, **34**(9):837-840.

82. Schmetterer, L, Dallinger, S, Findl, O, Graselli, U, Eichler, H G *et al*: **A comparison between laser interferometric measurement of fundus pulsation and pneumotonometric measurement of pulsatile ocular blood flow.**, vol. 14. Basingstoke, ROYAUME-UNI: Nature Publishing Group; 2000.

83. Drexler W, Morgner U, Ghanta RK, Kartner FX, Schuman JS, Fujimoto JG: **Ultrahigh-resolution ophthalmic optical coherence tomography**. *Nat Med* 2001, **7**(4):502-507.

84. Singh K, Dion C, Lesk MR, Ozaki T, Costantino S: **Spectral-domain phase microscopy with improved sensitivity using two-dimensional detector arrays**. *Review of Scientific Instruments* 2011, **82**(2):023706-023704.

85. Choma MA, Ellerbee AK, Yang C, Creazzo TL, Izatt JA: **Spectral-domain phase microscopy**. *Opt Lett* 2005, **30**(10):1162-1164.

86. Zhang J, Rao B, Yu L, Chen Z: **High-dynamic-range quantitative phase imaging with spectral domain phase microscopy**. *Opt Lett* 2009, **34**(21):3442-3444.

87. Ravalico G, Pastori G, Croc, egrave M, Toffoli G: **Pulsatile Ocular Blood Flow Variations with Axial Length and Refractive Error**. *Ophthalmologica* 1997, **211**(5):271-273.

88. Keshner FA, Peterson BW: **Mechanisms controlling human head stabilization. I. Head-neck dynamics during random rotations in the horizontal plane**. *Journal of Neurophysiology* 1995, **73**(6):2293-2301.

89. Iskander DR, Kasprzak HT: **Dynamics in longitudinal eye movements and corneal shape**. *Ophthalmic Physiol Opt* 2006, **26**(6):572-579.

90. Smith DH, Wolf JA, Lusardi TA, Lee VM-Y, Meaney DF: **High Tolerance and Delayed Elastic Response of Cultured Axons to Dynamic Stretch Injury**. *The Journal of Neuroscience* 1999, **19**(11):4263-4269.

91. Tang-Schomer MD, Patel AR, Baas PW, Smith DH: **Mechanical breaking of microtubules in axons during dynamic stretch injury underlies delayed elasticity, microtubule disassembly, and axon degeneration**. *The FASEB Journal* 2010, **24**(5):1401-1410.

92. Breusegem C, Fieuws S, Zeyen T, Stalmans I: **The Effect of Trabeculectomy on Ocular Pulse Amplitude**. *Investigative Ophthalmology & Visual Science* 2010, **51**(1):231-235.

93. Schmidl D, Garhofer G, Schmetterer L: **The complex interaction between ocular perfusion pressure and ocular blood flow – Relevance for glaucoma**. *Experimental Eye Research* 2011, **93**(2):141-155.

94. Nichols WW, Conti CR, Walker WE, Milnor WR: **Input impedance of the systemic circulation in man**. *Circ Res* 1977, **40**(5):451-458.

95. Finkelstein SM, Collins VR, Cohn JN: **Arterial vascular compliance response to vasodilators by Fourier and pulse contour analysis**. *Hypertension* 1988, **12**(4):380-387.

96. O'Rourke MF, Taylor MG: **Input Impedance of the Systemic Circulation**. *Circ Res* 1967, **20**(4):365-380.

97. Drexler W, Findl O, Schmetterer L, Hitzenberger CK, Fercher AF: **Eye elongation during accommodation in humans: differences between emmetropes and myopes**. *Invest Ophthalmol Vis Sci* 1998, **39**(11):2140-2147.

98.   Schmetterer L, Kruger A, Findl O, Breiteneder H, Eichler H-G, Wolzt M:
       **Topical fundus pulsation measurements in age-related macular
       degeneration**. *Graefe's Archive for Clinical and Experimental
       Ophthalmology* 1998, **236**(3):160-163.

Appendix A

Box plot
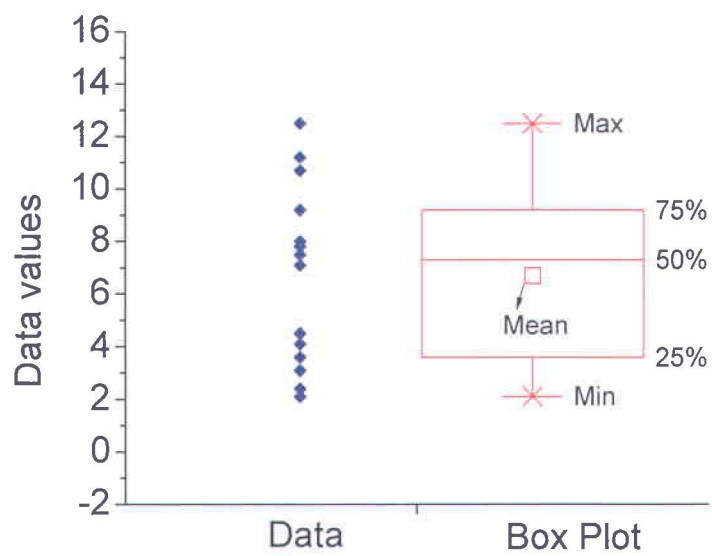
Figure (A) Box plot for statistical representation of the data

In the figure above, a box plot (right side) corresponding to the data set shown on the left of the figure is plotted. In this box plot, there are 6 values that represent the statistics of the data. The horizontal lines along with cross symbol at the top and bottom represents the maximum (Max) and minimum (Min) values of the data. The horizontal lines of the main box from top to bottom represent the 75%, 50 % and 25 % of the percentile. For example, 75% percentile line means that the 75 percent of data values are below this line. Finally, the small rectangular box within the main box represents the mean value of the data value.

Appendix B

Résumé en Français

I. Introduction

Le glaucome est la deuxième plus importante cause de cécité après la cataracte et est prévalent au sein de la population plus âgée. Au Canada, par l'an 2002, plus de 400 000 cas de glaucome avaient déjà été signalés et on s'attend à ce que ce nombre augmente au cours des années à venir [1]. Selon une étude récente [2], nous compterons environ 80 million de personnes à travers le monde atteintes de glaucome.

Dans un cas de glaucome, le nerf optique, qui est chargé de transmettre la vision de l'œil au cerveau, souffre d'un dommage permanent et irréversible. Ce dommage peut être vu comme étant une augmentation de l'excavation papillaire centrale. La papille optique est la région derrière l'œil d'où les vaisseaux sanguins pénètrent et d'où les axones transportant l'information sur la vision quittent l'œil. L'une des plus grandes difficultés que représente cette maladie est que la plupart des personnes atteintes de glaucome ne perçoivent aucun symptôme jusqu'à ce qu'il y ait une importante perte de segments de leur champ visuel. D'un point de vue clinique, sans des années de surveillance, il est impossible d'identifier les

personnes atteintes de glaucome qui en sont au stade initial de la maladie. Si l'on parvient à détecter le glaucome aux stades initiaux de sa progression, bien que les dommages existants ne soient pas réversibles, cette progression pourrait être arrêtée ou ralentie.

Il a été estimé [3] qu'entre 1990 et 2000, le système de santé au Canada a déboursé environ 300 millions de dollars canadiens annuellement en coûts liés directement au glaucome. En raison de la population vieillissante du pays, les incidences de glaucome montent en flèche alors que les baby-boomers atteignent l'âge de 50 et 60 ans. Ainsi, une méthode rentable liée à la détection du glaucome viendrait aider de manière significative à réduire les coûts requis pour son traitement.

II. Anatomie de l'oeil humain

Avant d'aborder les détails quant au glaucome, il est nécessaire de comprendre les éléments de base de la formation d'images et de l'anatomie de l'œil. L'œil est l'un des organes les plus importants du corps humain puisqu'il nous permet de percevoir le monde visuel. La procédure de base de la formation de la vision est décrite dans la Figure 1. Lorsque la lumière se projette sur un objet, elle se disperse et se reflète dans toutes les directions. Une portion de la lumière atteint l'œil, où elle rencontre le premier élément oculaire, soit la cornée. Les rayons lumineux sont réfractés lorsqu'ils traversent la cornée en raison de la courbure cornéenne et de la différence dans l'indice de réfraction entre la cornée et l'air. Ces rayons réfractés sont davantage réfractés par les lentilles oculaires pour former une image inversée de l'objet sur la rétine, soit la membrane photosensible de l'œil. La lumière reçue par la rétine est convertie en des signaux électriques par les nombreuses cellules se trouvant dans la rétine. Ces signaux de la rétine sont alors transférés au cerveau par l'entremise des axones des cellules ganglionnaires qui forment le nerf optique. Les signaux électriques que transfère le nerf optique

sont reçus par le cortex visuel du cerveau, là où ils sont interprétés en tant qu'images.
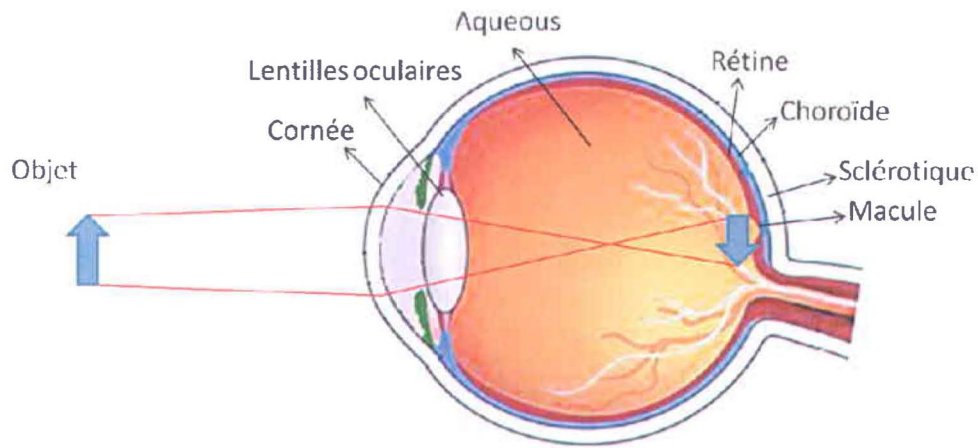
Figure 1. Diagramme de base pour la formation d'images dans l'œil humain.
Source de l'image : http://www.improve-vision-naturally.com

III. Glaucome

Dans un cas de glaucome, les axones des cellules ganglionnaires sont endommagés, empêchant ainsi les signaux de vision d'atteindre le cerveau. Ce type de dommage est irréversible. Plusieurs facteurs de risque pouvant mener au glaucome ont été décelés. L'un des facteurs les plus acceptés est la pression intraoculaire (PIO) élevée. La PIO est la pression de l'humeur aqueuse qui comble l'espace entre la cornée et les lentilles oculaires. Dans un œil normal, la PIO se situe à 15 mmHg. Une pression supérieure à 21 mmHg est considérée comme étant un facteur de risque significatif pouvant mener au glaucome.

Un diagnostic précoce du glaucome représente toujours un défi pour les cliniciens puisqu'il n'existe aucun indicateur défini lié aux premiers stades du glaucome. Il

est estimé que seulement la moitié des personnes aux prises avec le glaucome savent qu'elles en sont atteintes.

Grâce à la recherche continue, de nouveaux facteurs de risque possibles liés au glaucome sont déterminés. Comme marqueur du glaucome, la plupart des études antérieures se fiaient à une pression intraoculaire élevée, soit une condition appelée hypertension oculaire. Une PIO de plus de 21 mmHg était considérée comme étant un facteur de risque important lié au glaucome [12]. La PIO est mesurée par les cliniciens à l'aide d'une technique nommée tonométrie. Un tonomètre est un instrument servant à mesurer la pression de l'œil.

Des changements structuraux chez la tête du nerf optique (TNO) représentent un facteur de risque significatif ainsi qu'un indicateur important de glaucome. Les dommages de la TNO peuvent être visualisés directement en observant l'œil à l'aide d'un ophtalmoscope ou d'une autre technique d'imagerie. L'étude de l'hémodynamique de l'œil est un autre secteur de recherche présentement exploré pour assurer le diagnostic du glaucome [27, 28]. L'approvisionnement sanguin vers l'œil, appelé débit sanguin oculaire (DSO) est pulsatile de nature, et plusieurs mesures de ce débit sanguin oculaire pulsatile (DSOP) peuvent être effectuées. Le DSO a été estimé en mesurant l'amplitude des pulsations oculaires (APO) de l'œil. L'APO est la différence entre le DSO minimal et maximal mesuré sur une certaine période de temps et elle peut être mesurée à l'aide de tonomètres standards, tels que le tonomètre de contour dynamique [14] et le pneumotonographe de Langham.

La périmétrie [37] est une autre technique de diagnostic du glaucome. Il s'agit d'un outil de diagnostic concluant du glaucome, puisqu'il mesure directement chez les patients l'étendue du champ visuel et sa sensibilité à la lumière. Des schémas précis de la perte du champ visuel représentent un diagnostic du glaucome s'ils sont corroborés par des changements structuraux de la tête du nerf optique et de la couche des fibres nerveuses rétiniennes. Le champ visuel sert également à surveiller la progression du glaucome chez une personne.

Une grande partie des études repose sur la mesure de la PIO ou du débit sanguin en lien avec le glaucome. Le rôle des propriétés biomécaniques telles que la rigidité de l'œil dans le cas de glaucome n'a pas beaucoup été étudié.

IV. Le rôle des propriétés biomécaniques de l'œil dans le cas de glaucome

Les axones des cellules ganglionnaires forment la couche interne de la rétine, qui est appelée la couche de fibres nerveuses. La couche de fibres nerveuses, à partir de différents endroits de la rétine, converge à la papille optique pour former la tête du nerf optique. Ces axones quittent alors l'œil en traversant une sclérotique spécialisée connue sous le nom de lame criblée, qui est montrée à la Figure 2.
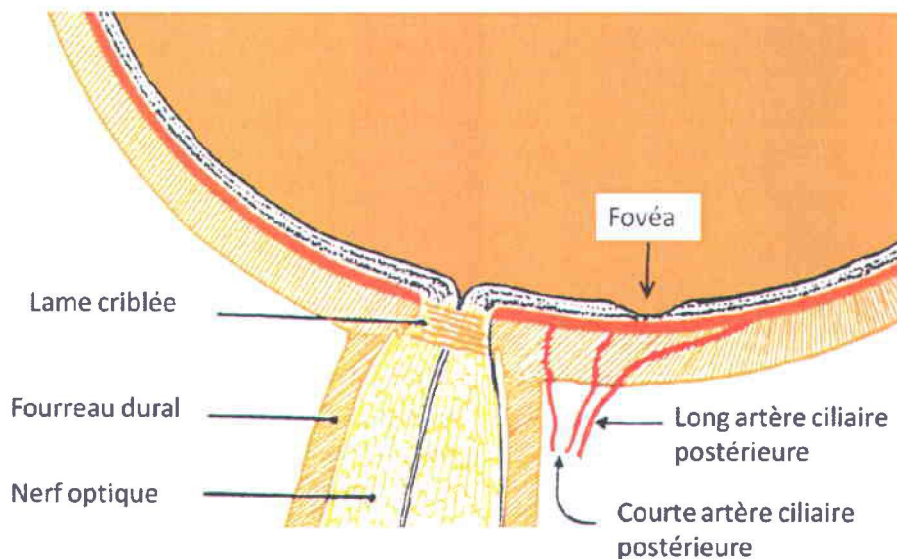
Figure 2. Structure de l'œil postérieure démontrant la lame criblée.

Certaines études suggèrent qu'au stade initial du glaucome, la lame criblée est moins rigide, alors qu'elle est plus rigide aux stades ultérieurs ou avancés du glaucome. Bien qu'il ait été estimé qu'une lame criblée moins rigide mène au

développement du glaucome, le mécanisme exact entre la progression du glaucome et la rigidité de la lame criblée n'est pas connu.

La rigidité de la lame criblée peut être évaluée en étudiant sa conformité à la pression intraoculaire [43]. Pour y parvenir, le changement de la position de la lame criblée relativement à la surface rétinienne est mesuré après le changement de la pression intraoculaire sur une longue période de temps.

Tel que discuté plus tôt, le débit sanguin oculaire joue un rôle important lié au glaucome. Ceci fait de la lame criblée un joueur important en ce qui concerne le glaucome puisque les micros vaisseaux sanguins qui nourrissent la tête du nerf optique pénètrent l'œil à cet endroit. La structure est illustrée à la Figure 3.
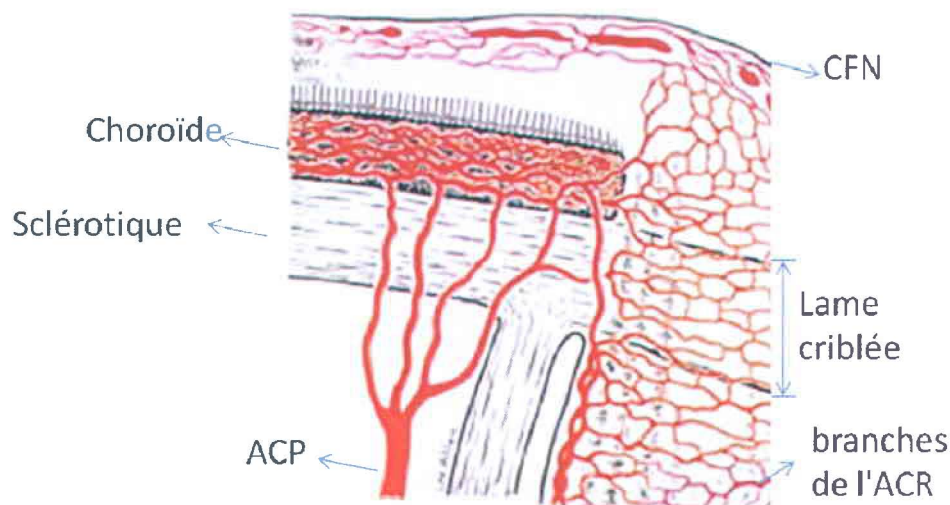
Figure 3. L'approvisionnement sanguin à la tête du nerf optique et à la rétine. Les abréviations sont la couche de fibres nerveuses (CFN), l'artère centrale de la rétine (ACR) et l'artère ciliaire postérieure (ACP).

Lors de la systole du cycle cardiaque, la lame criblée est repoussée vers l'arrière, ce qui suggère que les micros vaisseaux sanguins seront compressés en raison d'un tel mouvement. En fait, lors d'une étude [43], une légère amélioration a été

105

observée au niveau du débit sanguin de la tête du nerf optique au moment de la réduction de la PIO. Chez les patients dont les yeux répondent mieux au traitement ou dont les lames criblées sont moins rigides, les micros vaisseaux sanguins sont soumis à une plus grande compression. En considérant le rôle du débit sanguin dans le glaucome et le rôle de la lame criblée dans le débit sanguin, il devient évident que les propriétés biomécaniques, telles que la rigidité de la lame criblée, peuvent contribuer à la progression du glaucome.

Ci-dessous, nous avons seulement considéré les effets du changement à long terme de la PIO sur le déplacement de la lame criblée afin d'évaluer ses propriétés biomécaniques. Grâce aux recherches précédentes sur le débit sanguin oculaire pulsatile, nous savons que la PIO de l'œil n'est pas une quantité constante; plutôt, elle est aussi pulsatile de nature. La PIO pulsée, telle que mesurée à l'aide de nombreux tonomètres, est synchrone avec le cycle cardiaque. Si un changement à long terme dans la PIO peut déplacer la lame criblée en référence à la surface rétinienne, nous ne pouvons donc pas exclure l'effet du changement pulsatile de la PIO sur la lame criblée. En tenant compte de ce fait, nous émettons l'hypothèse dans ce travail de thèse que « *en raison du changement pulsatile dans la PIO, la lame criblée émet aussi une pulsation de façon synchronisée avec le cycle cardiaque, et ces petits déplacements de la lame criblée contribuent à la progression du glaucome.* »

Ce n'est pas seulement le changement au niveau du débit sanguin causé par le mouvement pulsatile de la lame criblée qui peut contribuer à la progression du glaucome; d'autres mécanismes pourraient aussi y contribuer. Puisque la lame criblée et la rétine péripapillaire sont alimentées de sang provenant de différentes artères, il pourrait y avoir un délai entre les mouvements axiaux des deux zones de tissu. Dans cette situation, il y aurait un mouvement relatif pulsatile entre les deux tissus. Ainsi, les axones des cellules ganglionnaires s'attachant à la lame criblée et à la rétine péripapillaire ressentiraient un étirement pulsatile au fil du temps en raison d'un tel mouvement relatif.

Par conséquent, nous émettons de plus l'hypothèse dans ce travail de thèse « *qu'il existe un mouvement relatif entre la lame criblée et la rétine péripapillaire au cours du cycle cardiaque qui entraîne un étirement chez les axones des cellules ganglionnaires, et qu'un tel étirement peut endommager les axones, ce qui mène au glaucome.* »

V. Objectif

Afin de mesurer les petits mouvements des tissus oculaires, tels que la lame criblée, un nouveau dispositif est requis. *L'objectif de cette thèse est d'élaborer un tel dispositif et de mesurer son rendement auprès de sujets humains en tant qu'un outil possible pour assurer le diagnostic du glaucome.* Il est requis de ce dispositif qu'il soit capable de mesurer le mouvement des tissus oculaires avec une résolution axiale d'environ 1 μm. Le dispositif devrait aussi être en mesure de localiser précisément la position de la mesure de sorte que les mouvements des différentes zones de la rétine puissent avoir lieu. Par dessus tout, il est fortement désirable que le dispositif soit non invasif.

Dans ce travail de thèse, un nouvel instrument non invasif fondé sur l'interférométrie à faible cohérence dans le domaine spectral (IFC-DS) a été conçu et extrait l'information sur le mouvement à partir de balayages axiaux séquentiels.

VI.   Contexte théorique

L'interférométrie à faible cohérence dans le domaine Fourier (IFC-DF) [57] est fondée sur l'interférométrie Michelson où une source de lumière à large bande est utilisée pour illuminer la surface de référence et de l'échantillon. Les faisceaux réfléchis à partir de la surface de l'échantillon et la surface de référence sont recombinés, ce qui produit une interférence. À l'aide d'un réseau de diffraction qui sépare de manière angulaire les différentes composantes de longueur d'onde

de la lumière, le spectre du signal d'interférence peut être observé à l'aide d'un réseau linéaire de CCD (Figure 4).
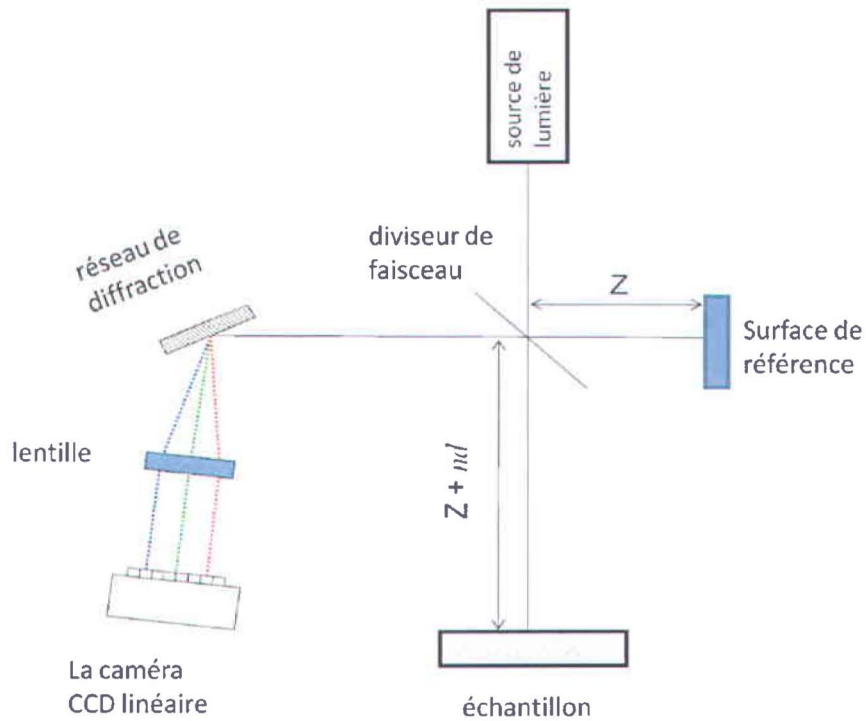
Figure 4. Schéma du système d'interférométrie à faible cohérence dans le domaine Fourier (spectral).

La distribution d'intensité le long de l'axis-k (axis de nombre d'onde) sur la caméra CCD linéaire, $I(k)$, peut être décrite comme étant le spectre de la source de lumière, $I_0(k)$, avec une modulation sinusoïdale à la fréquence exacte de la différence de trajet optique (DTO) entre la surface de l'échantillon et la surface de référence. La DTO est le produit de la différence de longueur géométrique entre les deux bras de l'interféromètre, d, et l'index de réfraction du medium par l'entremise duquel il se propage, n,

$$\text{DTO} = 2^{nd}. \tag{0.1}$$

108

Le facteur de « 2 » apparaît dans l'Éq. (0.1) puisque la lumière doit faire un va-et-vient, doublant ainsi la différence de trajet géométrique.

La distribution d'intensité du spectre le long de l'axis-*k* peut être rédigée ainsi

$$I(k) \sim I_0(k)\left(1+\alpha\cos(2ndk+\phi)\right),\qquad(0.2)$$

où α est un paramètre sans dimension lié à la visibilité des franges d'interférence et où ϕ est une constante de phase.

Afin d'utiliser une fréquence de modulation dans le spectre comme moyen d'extraire une mesure précise de la longueur géométrique, la transformation Fourier est effectuée sur le spectre. En présumant que $I_0(k)$ détient un profil gaussien de bande large Δk, la transformation Fourier d'Éq. (0.2) mène à une solution analytique de la forme

$$I(x) \sim \alpha I_0(x-2nd)+I_0(x),\qquad(0.2)$$

où $I_0(x)$ est une fonction gaussienne d'une largeur égale à la longueur de la source de cohérence.

À partir de l'Éq. (0.3), on peut déduire que dans l'espace avec transformation Fourier, le modèle d'interférence connaît deux pointes : une pointe stationnaire centrée à $x=0$, révélant le spectre de la source de lumière, ainsi qu'une deuxième pointe d'amplitude multipliée par la visibilité des franges α, centrée à $x=2nd$. Ainsi, le centre de cette seconde pointe est placé à la DTO de l'interféromètre (négligeant la dépendance de l'index réfractif sur la longueur d'onde). Dans le cas d'échantillons composés de nombreuses couches partiellement réfléchissantes, des pointes successives seront observées dans l'espace transformé, et leurs centres offriront l'emplacement correspondant exact quant à l'échantillon de référence.

La transformation Fourier du spectre obtenue sur le CCD offrant le profil de réflectivité comme fonction de profondeur, est communément appelée un balayage axial (balayage-A) ou balayage approfondi. Ainsi, en observant le changement dans la position d'une structure réfléchissante dans le balayage-A,

109

son mouvement relatif en ce qui concerne la surface d'échantillon stationnaire peut être mesuré.

VII.   Conception expérimentale

Un diagramme schématique du système optique conçu dans le but de mesurer les mouvements cornéens et rétiniens de façon simultanée est illustré à la Figure 5.
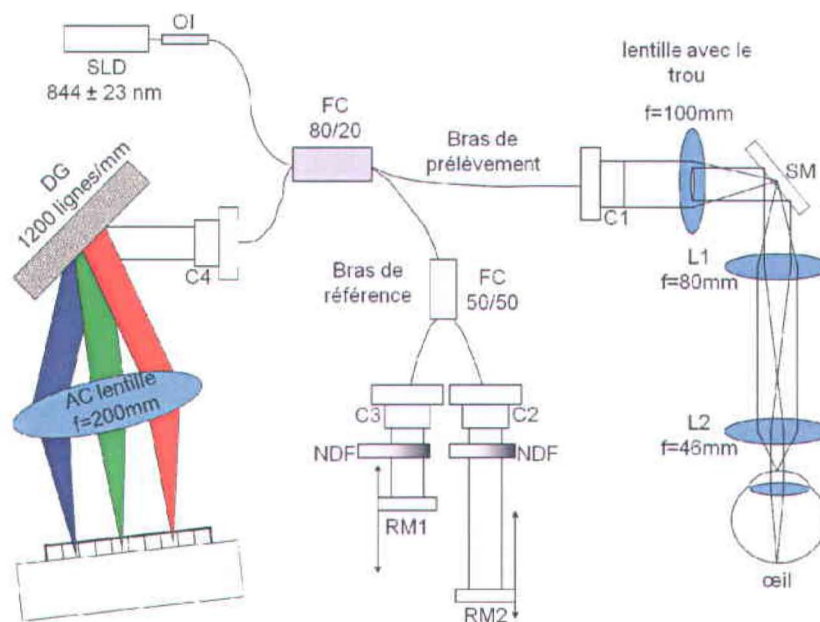
Figure 5. Schéma du système optique conçu pour mesurer les mouvements cornéens et rétiniens simultanément.

Une diode superluminescente (DSL, Superlum) avec une longueur d'onde centrale de 844 nm et une largeur de bande de 46 nm a été jumelée à un interféromètre Michelson à base de fibres. Un coupleur à fibres 2×2, 80:20 a été utilisé pour diviser la lumière en les bras de référence et d'échantillon. Le bras d'échantillon a été éliminé à l'aide d'un collimateur qui produit un faisceau d'une largeur de 3 mm. Le pouvoir total du faisceau d'échantillon à la sortie du

collimateur a été fixé à 500 μW, ce qui est grandement inférieur à la limite prescrite d'ANSI de 750 μW pour une visualisation continue d'environ 844 nm. Le faisceau d'échantillon a traversé une lentille (f=100 mm) munie d'un trou central de 2 mm de diamètre. Après la lentille, la partie centrale du faisceau d'échantillon est demeurée collimatée, mais la partie extérieure a été réfractée. Un système de balayage a été mis sur pied afin que la partie extérieure du faisceau d'échantillon soit stationnaire et qu'elle focalise sur la cornée, tandis que la partie centrale collimatée était balayée et focalisait sur la rétine. Ainsi, à l'aide d'un schéma optique, les signaux réfléchis de l'apex cornéen à la rétine ont été acquis simultanément. Un coupleur à fibres 2×1, 50:50 a été utilisé pour obtenir deux signaux de référence réfléchis à l'aide de miroirs montés sur des platines motorisées séparées (Technologie Zaber, Vancouver, Canada). Les signaux de référence ont été atténués à l'aide de filtres de densité neutres afin de maintenir leur intensité totale au-dessous du niveau de saturation. Les signaux réfléchis des bras d'échantillon et de référence ont été dispersés à l'aide d'un réseau de diffraction réfléchissant (1200 lignes/mm) et focalisés par une lentille achromatique (f = 200 mm) sur une caméra CCD linéaire (Spyder 3, Technologie Dalsa, Canada).

Un oxymètre sur mesure a été placé sur le lobe de l'oreille lors des mesures pour enregistrer en simultané les battements de cœur des sujets à l'aide d'une carte d'acquisition de données (Labjack, Lakewood, CO). Les signaux de la caméra CCD linéaire et de l'oxymètre ont été captés à l'aide d'un ordinateur duo core 2.0 GHz avec logiciel sur mesure (LabView, National Instruments, TX). Les données ont été acquises pendant 20 secondes et ont été emmagasinées afin d'être traitées ultérieurement.

VIII. Traitement des données

Lors du traitement ultérieur, les données ont été analysées à l'aide d'un logiciel sur mesure à LabView. Un balayage-B comprenant des signaux de la cornée et de

111

la rétine, captés à l'aide de l'instrument conçu, est montré à la Figure 6(A). Un balayage-B est simplement une collection de balayages axiaux adjacents de l'échantillon. Le balayage-A le long de l'axis visuel dans la zone fovéale est montré à la Figure 6(B). Les différentes interfaces oculaires pouvant être identifiées après une comparaison avec les images standards de tomographie par cohérence optique (TCO) [59, 83] sont l'épithélium cornéen (CEp) et l'endothélium (CEn), la couche de fibres nerveuses (CFN), le segment interne-externe, l'épithélium rétinien pigmenté (RPE) et les choriocapillaires (CC).
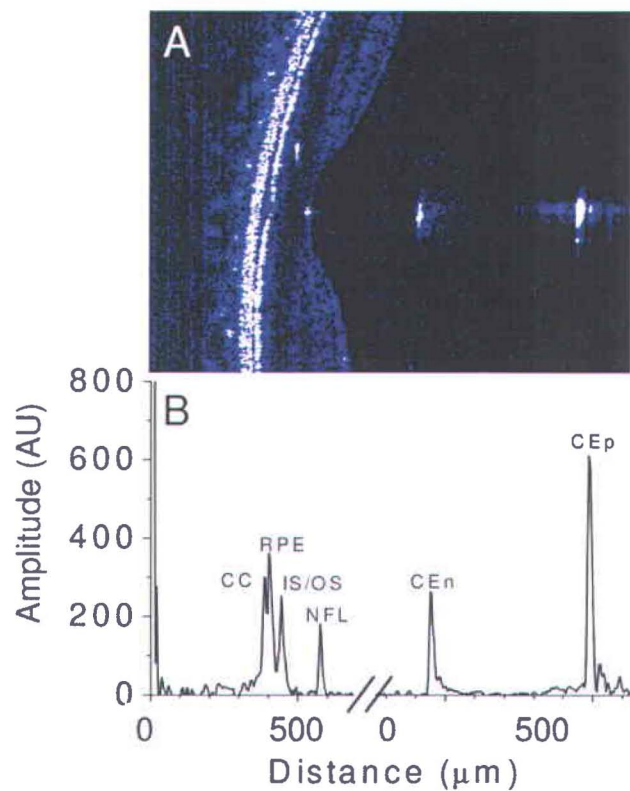
Figure 6. Balayage-B de la cornée et la rétine.

Pour traiter les données, chaque image enregistrée (balayage-B) est chargée dans l'ordinateur par l'entremise de notre logiciel d'analyse. De ce balayage-B, un balayage-B de référence est soustrait. Le balayage-B de référence est un balayage

112

enregistré au début de l'expérimentation sans le signal provenant de l'œil. Cette procédure élimine le bruit constant provenant du spectre ou de l'interférence de source dans le système. Du balayage-B supprimé de la référence, l'un des balayages-A correspondant à la zone de l'intérêt où le mouvement a été mesuré fut sélectionné manuellement.

Sur chaque balayage-A sélectionné, un filtre Savitzky-Golay est appliqué pour lisser les données, qui sont alors cadrées pour réduire l'effet du bruit entourant le signal du tissu oculaire. Du balayage-A lissé, une fenêtre contenant le profil axial du tissu oculaire désiré, c.-à-d. la cornée ou la rétine, est sélectionnée pour laquelle le centroïde est calculé à l'aide de la relation $\dfrac{\sum X_n I_n}{\sum I_n}$, où X est la position, I est l'intensité et n est l'index du n-ième pixel dans le balayage-A. Cette procédure est effectuée sur tous les balayages-B subséquents afin d'obtenir une trace temporelle du centroïde, ce qui fournit le déplacement axial des tissus oculaires.

Finalement, afin de récupérer l'amplitude des pulsations du fond de l'oeil, la différence entre les positions de la cornée et de la rétine a été calculée et transformée davantage selon la transformation Fournier pour étudier leurs composantes harmoniques relatives à celles du cycle cardiaque. Les signaux ont été traités en appliquant un filtre passe-bande de la fréquence entre le battement de cœur et son 5e harmonique. Pour l'analyse des données statistiques, un modèle t-test a été utilisé et des valeurs-p de moins de 0,05 ont été considérées comme étant statistiquement significatives.

IX.   Résultats

L'objectif final de ce travail de thèse était de mesurer les mouvements axiaux de l'œil chez les patients atteints de glaucome et de les comparer avec les mouvements axiaux de l'œil chez les patients normaux. Pour y parvenir, 12 sujets atteints de glaucome et 10 sujets normaux d'âge équivalent ont été recrutés au

département d'ophtalmologie de l'Hôtel Maisonneuve-Rosemont de Montréal. Les expérimentations ont été approuvées par le comité d'éthiques de l'Hôpital Maisonneuve-Rosemont. Tous les bénévoles ont été renseignés quant aux procédures et aux conséquences. Un consentement écrit a été obtenu. Avant que les mesures soient prises, tous les sujets ont subi des examens oculaires standards. Les mesures de la PIO, de la longueur de l'œil et de la pression sanguine ont été notées. Les sujets présentant le moindre indice d'une condition cardiaque ont été exclus de cette recherche.

À l'aide d'un système décrit dans la section « Conception expérimentale », des balayages-B de la cornée à l'apex et de la rétine à la papille optique ont été acquis pendant 20 secondes consécutives. Il est estimé que balayage linéaire ou le balayage-B sur la surface rétinienne avait une largeur d'environ 4,7 mm. De ces balayages-B, le mouvement longitudinal de la cornée à l'apex et de la rétine à la papille optique, le côté nasal de la rétine péripapillaire et le côté temporal de la rétine péripapillaire a été mesuré. L'emplacement des points de mesure est montré à la Figure 7.
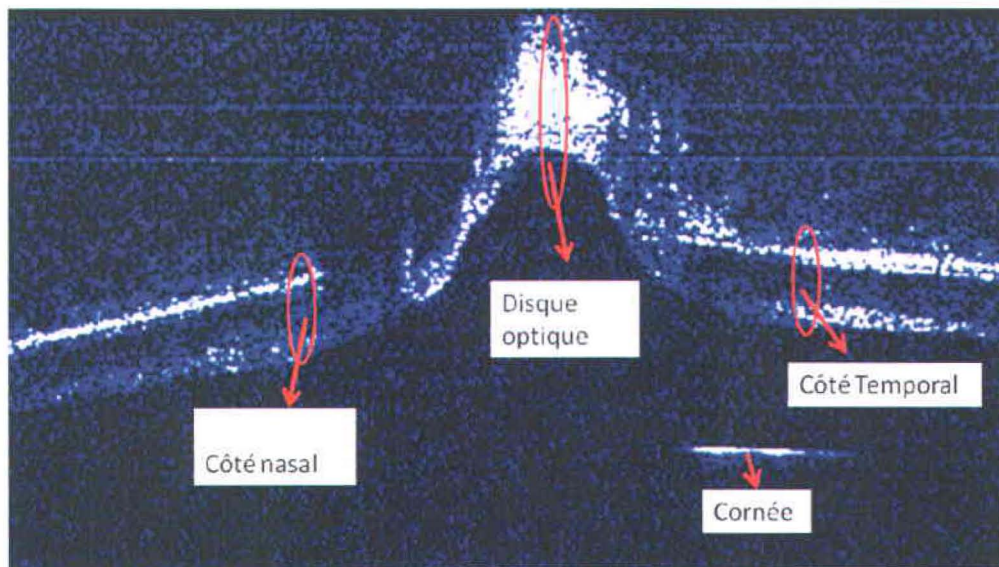
Figure 7. Différents points de mesure du balayage-B de l'oeil sont montrés. La différence de trajet optique des miroirs de référence a été ajustée afin d'incorporer le balayage-B ou la cornée et la rétine dans le même balayage.

Un enregistrement typique du mouvement mesuré est montré à la Figure 8. À partir de la Figure 8, nous pouvons voir que les différentes zones du fond d'œil et de la cornée se déplacent avec une amplitude et une phase légèrement différentes. La valeur quadratique moyenne des mouvements des différentes zones oculaires est montrée à la Figure 9. Chez les sujets normaux, la valeur quadratique moyenne±DS du mouvement a été établie à
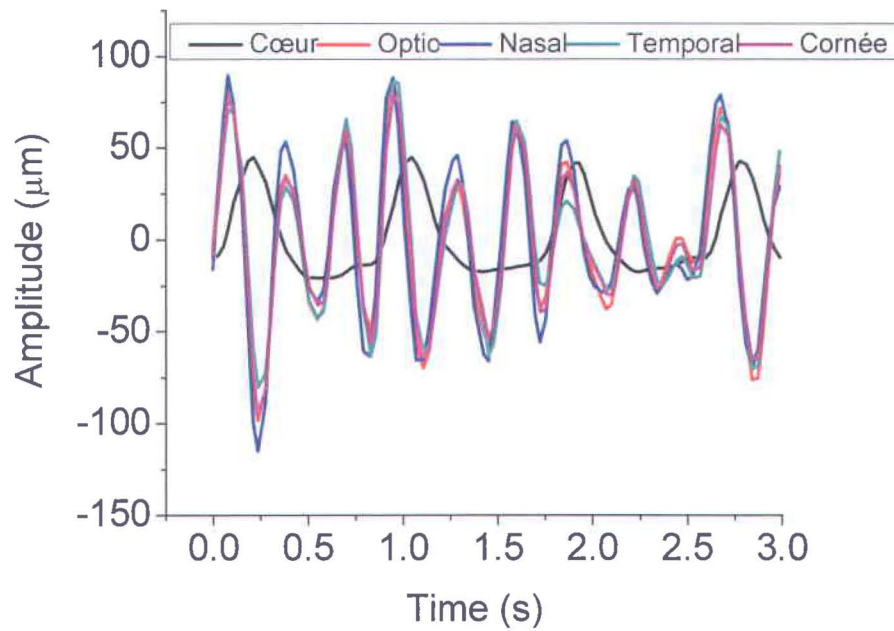
Figure 8. Le mouvement axial des divers éléments oculaires ainsi que le cycle cardiaque. Nous pouvons voir que les différentes zones oculaires se déplacent avec une amplitude et une phase légèrement différentes.
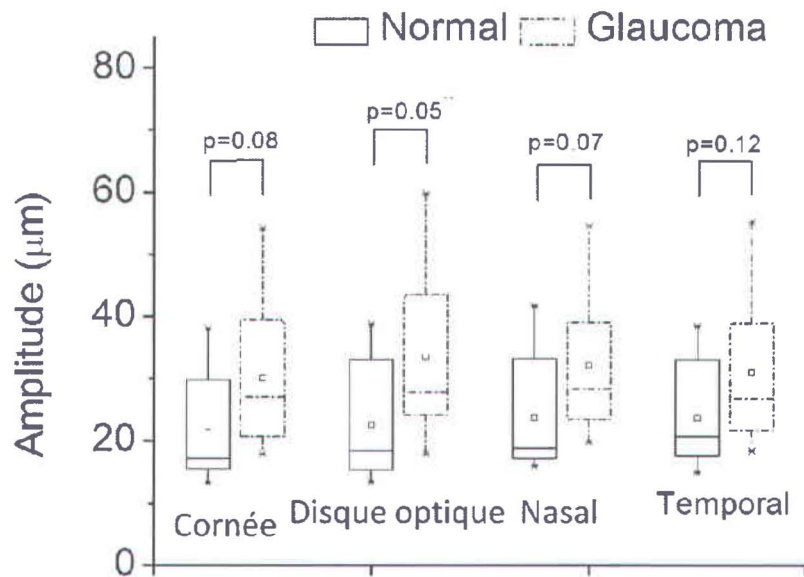
Figure 9. Les valeurs quadratiques moyennes du mouvement axial des différentes zones oculaires sont démontrées en tant que diagramme en boîtes.

21.5±9.1 μm, 22.5±9.9 μm 23.7±9.4 μm et 23.6±8.5 μm pour la cornée, la papille optique, le côté nasal et le côté temporal, respectivement. Ces lectures chez les patients atteints de glaucome indiquaient 29.9±11.8 μm, 33.5±13.9 μm, 32.2±11.1 μm et 30.9±11.5μm pour la cornée, la papille optique, le côté nasal et le côté temporal, respectivement. Les valeurs moyennes du mouvement axial portant sur les différentes zones oculaires se sont avérées supérieures chez les patients atteints de glaucome comparativement aux sujets normaux, et cette différence était statistiquement significative en ce qui a trait à la papille optique.

De plus, il était particulièrement désirable d'estimer le changement local de la longueur du tissu dans la région de la papille optique. Cet étirement sur une certaine période de temps peut être obtenu en soustrayant la position absolue de la rétine péripapillaire de la position de la papille optique. Un enregistrement

116

typique du changement mesuré de la longueur du tissu chez un sujet en santé est montré à la Figure 10.
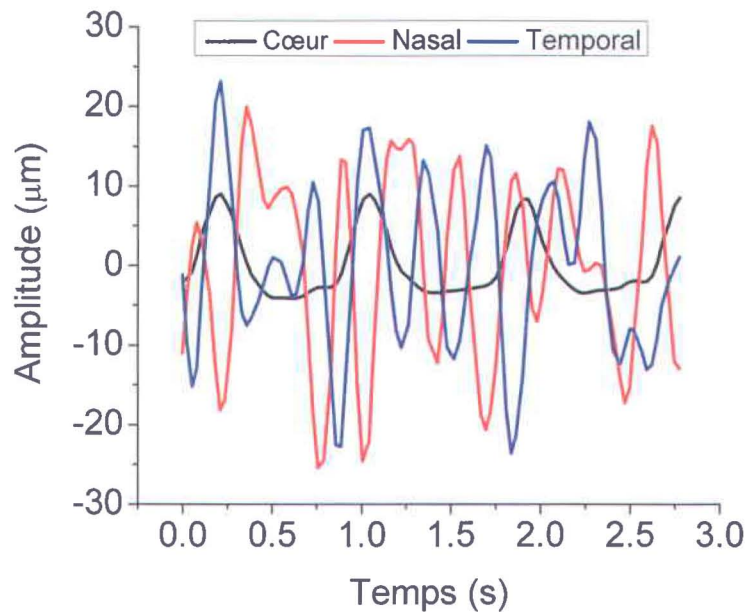
Figure 10. Un étirement local du tissu oculaire mesuré sur le côté temporal et nasal de la papille optique. L'étirement a été calculé en soustrayant la position absolue de la papille optique de la position de la rétine péripapillaire temporale et nasale.

Nous pouvons voir à partir de la Figure 10 qu'il y a un étirement local tant du côté nasal que temporal de la papille optique. L'étirement mesuré chez tous les sujets est montré à la Figure 11. Chez les sujets normaux, les valeurs quadratiques moyennes±SD ont été établies à 10.4±2.4 µm et 10.3±2.5 µm pour le côté nasal et temporal de la papille optique, respectivement. Chez les patients atteints de glaucome, ces valeurs étaient 13.4±5.7 µm et 13.2±6.4 µm pour le côté nasal et temporal de la papille optique, respectivement. Semblables aux mouvements de tissus oculaires individuels, les valeurs moyennes de l'étirement local des tissus autour de la papille optique sont supérieures chez les patients atteints de glaucome, mais la différence entre les patients atteints de glaucome et les sujets normaux n'est pas statistiquement significative.

117
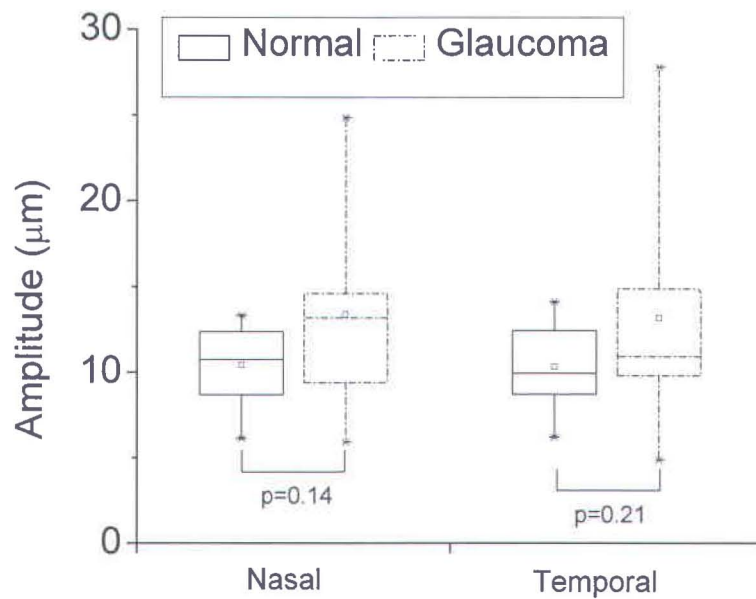
Figure 11. La valeur quadratique moyenne de l'étirement du tissu. Pour chacune des boîtes, des segments différents du haut vers le bas donnent les 95e, 75e, 50e, 25e et 5e centiles, le carré dans la boîte représente la valeur moyenne et les étoiles au haut et au bas démontrent les maxima et les minima de la distribution.

Finalement, l'étirement complet de l'œil, c.-à-d. un changement dans la longueur axiale, a été comparé entre les sujets atteints de glaucome et ceux qui ne le sont pas. Une telle comparaison est montrée à la Figure 12.
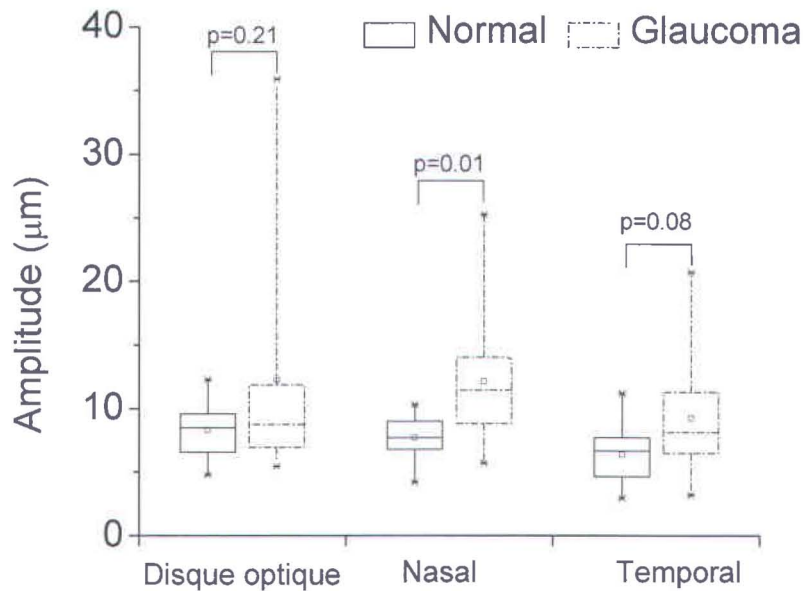
Figure 12. Étirement de l'œil à différents endroits.

Les valeurs quadratiques moyennes±DS de l'étirement de l'œil à la papille optique, au côté nasal et au côté temporal a été établie à 8.3±2.3 µm, 7.6±1.8 µm et 6.5±2.8 µm, respectivement chez les sujets normaux, alors que chez les patients atteints de glaucome, ces valeurs étaient 12.2±9.3 µm, 12.2±5.0 µm et 9.2±4.5 µm, respectivement. Les valeurs moyennes de l'étirement de l'œil, déterminées chez les patients atteints de glaucome, étaient supérieures à celles chez les sujets normaux et même sensiblement différentes du côté nasal avec une valeur p de 0,01.

Ces résultats suggèrent que les mouvements oculaires chez les patients atteints de glaucome sont généralement plus élevés que chez les sujets normaux. Mais compte tenu de la taille de la cohorte échantillonnée, qui comprenait seulement 12 sujets atteints de glaucome et 10 sujets normaux, une étude clinique plus approfondie est requise pour valider ces résultats.

X. Conclusion

Au cours de ce travail de thèse, différentes technologies ont été conçues et mises à l'essai dans le but de mesurer les mouvements axiaux des tissus oculaires. Dans le chapitre d'introduction, *l'hypothèse avait été émise que de tels mouvements jouent un rôle important dans le développement du glaucome. Afin de mesurer de tels mouvements, une technique pouvant mesurer simultanément le mouvement de la cornée et des différentes zones de la rétine et ayant une résolution d'au moins 1 μm a été élaborée.*

Une comparaison des mouvements oculaires entre les sujets atteints de glaucome et les sujets normaux suggère que les mouvements axiaux des tissus oculaires individuels (comme les mouvements coréens et rétiniens) chez les patients atteints de glaucome sont plus élevés que chez les sujets normaux.

Grâce au système personnalisé DF-TCO, la mesure simultanée de la position de la cornée et la rétine, avec une grande précision et sur de longues périodes de temps, a été accomplie, ce qui a permis d'obtenir pour la première fois une description précise de la pulsatilité de l'œil. Le dispositif élaboré fournit des moyens d'étudier un tout nouvel aspect du glaucome, soit le rôle des propriétés biomécaniques de l'œil atteint de glaucome. Bien que le nombre de sujets prenant part à l'étude était limité, les résultats offrent une première indication que les propriétés biomécaniques ont un certain rôle à jouer relativement au glaucome. Une étude clinique plus approfondie pourrait offrir des preuves plus concluantes pour soutenir l'hypothèse.